A STUDY OF THE PRODUCTION AND APPLICATION OF NONLINEAR MATERIALS FOR USE IN FREQUENCY DOUBLED DYE LASERS

Stephen John Bastow

A Thesis Submitted for the Degree of PhD
at the
University of St Andrews

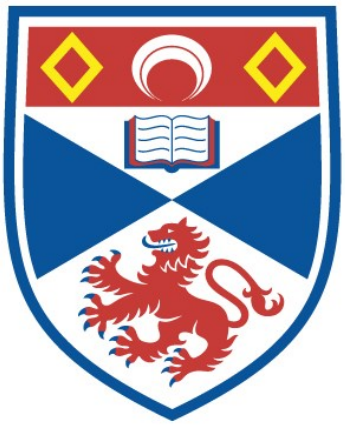

1986

01

A THESIS

entitled

"A study of the production and application of nonlinear materials for use in frequency doubled dye lasers",

in application to the University of St. Andrews

for the Degree of Doctor of Philosophy,

by

Stephen John Bastow, BSc.,

September, 1985.

INTRO2

I, Stephen John Bastow, hereby certify that this thesis, which is approximately 60,000 words in length, has been written by me, that it is a record of work carried out by me and that it has not been submitted in any previous application for a higher degree.

S.J.Bastow.

I hereby certify that the candidate has fulfilled the conditions of the Resolution and Regulations appropriate to the degree of Doctor of Philosophy of the University of St. Andrews, and that he is qualified to submit this thesis in application for that degree.

M.H.Dunn.

I was admitted as a research student under Ordinance No.12 in October 1978 and as a candidate for the degree of PhD in September 1979. The higher study for which this is a record was carried out in the University of St. Andrews between October 1978 and August 1981.

In submitting this thesis to the University of St. Andrews I understand that I am giving permission for it to be made available for use in accordance with the regulations of the University Library for the time being in force, subject to any Copyright vested in the work not being affected thereby. I also understand that the title and abstract will be published, and that a copy of the work may be made and supplied to any bona fide library or research worker.

S.J.Bastow

ABSTRACT

A selection of nonlinear materials for use in various frequency-doubled dye lasers is studied.

Lithium Formate Monohydrate is operated intracavity in a Coumarin 102 dye laser for the first time. A maximum of 70 microwatts of tunable ultraviolet light was generated over the range 237nm to 248nm, representing an improvement of an order of magnitude on previously reported work with this material.

A pulsed xenon ion laser of high efficiency has been built and the design optimised, giving an output power of 185W. The laser is used to pump a Rhodamine 6G dye laser containing a crystal of Ammonium Dihydrogen Arsenate, to generate 280 milliwatts of tunable UV over the range 291nm to 297nm and this is the first time that a detailed study of this type of laser has been reported.

A crystal growing system for water based crystals is described. A crystal of Urea grown in the apparatus has been cut for use in a dye laser and tested with the beam from an argon ion laser. A value of the nonlinear coefficient d_{14} of 0.90pm/V is reported.

INTRO5

Acknowlegements

I would like to record my thanks to the following people who have assisted me over the course of the last few years, with work directly and indirectly connected with this thesis:

Mr. Geoffrey Foxcroft, formerly Senior Science Master at Rugby School, who was directly responsible for my interest in lasers and optics, in teaching, and my choice of University;

Emeritus Professor J.F.Allen for his interest and encouragement during my time as undergraduate;

Professor R.A.Stradling for allowing me to work in his Department as postgraduate;

Messrs. Ron McCraw, Mike Robertson, Fritz Ackerboom and their staff in the various workshops for considerable technical assistance and instruction over the years;

My supervisor, Dr. Malcolm Dunn, and his wife Catherine, for their encouragement and enthusiasm over many years;

And finally to my own wife Catherine, for her calm persuasion, endless cups of coffee, proof-reading at all hours, and for simply being around at times of crisis.

Chapter 1: Laser systems

1-1 Introduction

Shortly after its inception in 1960, the laser was hailed as a "solution in search of a problem". In the intervening quarter of a century it has indeed solved many thousands of problems, and is now in such widespread use that few people in the western world can have failed to experience or benefit from some laser application.

This thesis considers the production and applications of nonlinear materials for use as frequency doubling elements in dye lasers. Such elements allow the production of tunable ultraviolet radiation for spectroscopic applications, and the use of the nonlinear material within the laser cavity means that a very much greater ultraviolet power is then obtained, compared with the case of extracavity generation.

This Chapter considers the laser in general terms, but with specific relevence to the dye lasers discussed later. The application of the laser to spectroscopy is first considered, along with the features of the dye laser which make it suitable as a spectroscopic tool. The design of dye laser cavities containing nonlinear elements is then discussed, together with the techniques for selecting and controlling the frequency of the laser.

Chapter 2 deals exclusively with nonlinear materials. We first discuss the theory of second harmonic generation, as applied to crystals of the type used in laser systems, with particular reference, where appropriate, to three materials used in this work, namely ammonium dihydrogen

arsenate (ADA), lithium formate monohydrate (LFM) and Urea. The various factors affecting the suitability and use of such materials in tunable dye lasers are considered, followed by a detailed discussion of each of the three materials, both within the context of this work and in relation to other nonlinear materials. Tables of refractivity values for LFM and Urea are presented as Appendices.

The third Chapter considers the application of LFM within a Coumarin 102 dye laser, which was built for the purpose of achieving intracavity frequency doubling from 486nm for the first time. A UV power of 70 microwatts was obtained, along with useful information concerning the angular dependence of phasematching within the LFM crystal. The Coumarin 102 dye solution was observed to deteriorate rapidly during laser use, and a technique is proposed for filtering contaminated solution to increase its useful lifetime severalfold. This is then tested successfully and proposals made concerning the nature of the deterioration of the dye. The LFM crystal as used within the dye laser is then tested extracavity, and shown to generate very little UV by comparison.

Chapter 4 deals with a rather different feature of the work. A Xenon ion laser is designed and built for the purpose of pulsed pumping of a Rhodamine 6G dye laser, which itself contains an ADA crystal. Although the ion laser is based on established designs, we attempt to optimise its performance with respect to the firing voltage, capacitors and gas pressure. Two versions have been built and we show that both closely match the

b3a performance of the best xenon lasers so far reported.

Chapter 5 is a logical continuation of the work discussed in the previous Chapter, in that the application of the Xenon ion laser in pumping a Rhodamine 6G dye laser is considered. The dye laser contains a crystal of ADA in order to generate pulses of tunable ultraviolet light at around 295nm, and powers of 100mW were obtained. This represents an improvement of nearly two orders of magnitude in UV power from this type of laser, compared with the case of continuous wave pumping by an argon ion laser. This is also the first occasion on which a detailed study has been reported of long-pulse pumping of a Rhodamine 6G dye laser containing a nonlinear element.

In order to extend the use of second harmonic generation to shorter wavelengths, new materials have to be investigated which will achieve generation at around 240nm, and then suitable crystals must be grown for use within dye lasers. Chapter 6 describes a crystal growing system which we have designed and built for the production of crystals of Urea. These crystals must be sufficiently large and of sufficient clarity for use within a laser cavity, and the problems associated with the growth of such crystals from water based solution are discussed in detail, based on our experience with this system. We have obtained some crystals several centimetres in length, one of which has been cut to achieve optimum phasematched second harmonic generation at around 500nm. This crystal has been tested with the green and blue-green output beams from an argon ion laser, and shown to be of good quality.

1-2 Laser spectroscopy

As a tool for modern spectroscopy, the laser has become almost indispensible. The narrow linewidth of the continuous wave (cw) laser, which can be only a few megahertz, allows far more precise resolutions of fine spectral structure than by any other technique. It is possible to detect very small numbers of atoms and molecules and to observe their behaviour on timescales of a few picoseconds, yielding information about their structure and stability. By scanning the laser frequency through an absorption resonance of the material, the fine and hyperfine structure of the atomic or molecular energy levels can be examined very precisely.

For most spectroscopic applications a laser is required which can be scanned in frequency. Early work with gas lasers was limited in the range of scan to that set by the linewidth of the energy transition which generated the laser output, and so observations were restricted to those absorption lines which, by chance, happened to correspond with the laser wavelength.

From the mid 1960s, lasers became available which could be tuned over very much larger ranges, often tens of nanometres. Such lasers were based on organic dyes, and their tunability was a consequence of the broadening of their energy levels due to the large size of the molecules and frequently the presence of several benzene ring structures. The operation of the dye laser is discussed in more detail later. Since the early 1970s, both pulsed and cw dye lasers have become available commercially, and,

using a large range of dyes, can cover the entire visible and infrared spectrum. However, the ultraviolet (UV) spectrum is still not directly accessible to the dye laser. Other forms of tunable lasers have recently become available, such as the colour centre laser and parametric oscillator, but the range and tunability still does not cover the more interesting parts of the UV spectrum.

Tunable laser output in the near UV can, however, be achieved by nonlinear processes such as second- and third-harmonic generation (SHG, THG), in which the output from a laser is passed through a suitable crystalline material and is partially converted to light at twice or three times the frequency, and thus at half or a third of the wavelength. Such processes are, however, very inefficient, and UV outputs of a few milliwatts normally require visible or infrared input powers of many tens of watts. Chapter 2 deals in detail with the process of second harmonic generation and its application to various materials, and later chapters consider practical laser systems using this technique. Presently the harmonic generation process has a lower limit of around 215nm, though only extremely small powers have been produced. Much better performance is available around 300nm, but in the region of 250nm, which is of growing interest to spectroscopists, there remains much work to be done. The work described in this thesis deals mainly with materials for use in SHG around 250nm.

Spectroscopic applications available to the dye laser are normally based on Doppler-free techniques. In a gas, the

rapidly moving molecules (with speeds of the order of 1km/s) experience a Doppler shift in the frequency of a laser beam passing through. The shift of frequency is small, only a few hundred megahertz, but very much greater than the resolution available from the laser and greater than the fine structure within a set of energy levels. Doppler-free techniques eliminate the first order Doppler effect (due to thermal motion parallel to the beam) by using two counterpropagating beams in which the only atoms to interact with both must be those which experience the same Doppler shift in each case. This can only be so for atoms moving normal to the beams and so the first order Doppler effect is zero. Further refinements have led to the well-proven saturation spectroscopy technique, first introduced in 1971 by Hansch et al [1] and applied to the hyperfine structure of iodine with a resolution of 6MHz. Later work (1972) by Hansch, Shakin and Schawlow [2] applied the technique to the Hydrogen Balmer series and observed the fine structure of the H-alpha line for the first time. Over the years, Doppler-free saturation spectroscopy has been developed to the extent that it now provides some of the highest resolution spectra likely to be seen.

Two-photon spectroscopy is becoming an increasingly popular technique for examining spectra in the middle UV, from 200nm downwards. This technique involves causing a single atom to absorb two photons of the same frequency simultaneously, often from counterpropagating beams so that the results are free of Doppler broadening. This technique was proposed by Vasilenko in 1970 and has now been applied to many atomic species, and the hyperfine

splitting of the energy levels of, for example, hydrogen and deuterium, observed for comparison with theory. The work by Hansch et al [3] on the 1S-2S transitions in hydrogen and deuterium used a pulsed dye laser operating at 486nm, frequency doubled extracavity by a crystal of lithium formate monohydrate, and obtained values of the 1S ground state Lamb shifts to an accuracy of 300MHz. Their pulsed laser had a bandwidth of 120MHz. Very much improved bandwidths, as low as 10MHz, can be obtained with single mode, cw lasers, and by using intracavity frequency doubling, hyperfine structure has been observed with this resolution at around 300nm [4].

There is therefore considerable need for a laser of high resolution, operating at 243nm, to extend the work of Hansch in the realm of two-photon spectroscopy, and also in Doppler-free spectroscopy of other atoms.

1-3 Principles of laser operation

A photon interacting with a group of atoms may have one of two effects upon a member of that group. The photon may either be absorbed and the single atom placed in a higher energy state, or the photon may stimulate an already excited atom to relax to a lower state and release another photon. In both cases, the energy of the incoming photon must equal that of whatever energy transition takes place. These energies are quantised in accordance with the Planck law. Einstein showed that for a single atom in the appropriate state, both processes have an equal probability, and thus for a group of atoms irradiated by

sufficient photons, the ratio of absorptions to stimulated emissions must be the same as the number of atoms in the lower state to the number in the higher.

The process of stimulated emission yields another photon which is not only of the same energy as the incoming photon but is also coherent with it. The whole process produces an amplification of the photon flux in a particular direction. It is this result which gives the laser its name: light amplification by the stimulated emission of radiation.

For there to be a net amplification, the process of stimulated emission must dominate over all losses. The first possible loss is the reabsorption by low energy atoms of the additional photons. This will occur if the population of the lower state exceeds that of the higher, which is always the case in thermal equilibrium. In order to achieve laser action, therefore, the laser medium must be in a non-equilibrium state, to which the Boltzman population distribution does not apply, and there must be at least one high energy state with a greater population than a lower state, a situation known as a "population inversion".

The process of achieving a population inversion can take many forms. All involve pumping low energy atoms to a higher energy at a sufficient rate to obtain and maintain the inversion. Frequently the pumping process involves optical excitation, which must be at a higher energy (shorter wavelength) than that of the laser action sought. Optical excitation can be either by incoherent pumping,

such as by focusing the output from a xenon flashlamp into the entire laser medium, or by coherent pumping using another laser focused into a small region of the medium. The latter is normally used for the dye laser as it is by far the more efficient process.

A detailed analysis of the processes involved in laser operation may be found in specialised textbooks, for example, Tarasov [5] or Shimoda [31].

1-4 Dye laser operation

Dyes are complex organic compounds with a branched system of conjugate bonds, and with strong absorption bands in the visible and near-UV spectrum. Commonly their structure is based on benzene rings or similar groups, which give the molecule a large number of electronic, vibrational and rotational energy states. This gives their energy level diagrams a banded structure, with each individual level further broadened by the proximity of solvent molecules (water, ethanol, ethylene glycol etc.) when in liquid solution.

A simplified energy level diagram for the dye laser process is shown in Fig 1-1. We assume optical pumping of the ground state S_0 mainly to any part of the S_1 band (transition A). Further excitation from S_1 to S_2 or direct pumping of S_2 from the ground state (B,C) will occur, but at a very slow rate. The relaxation time from S_2 is also extremely short compared with other times and so the population of S_2 can be considered negligible. The

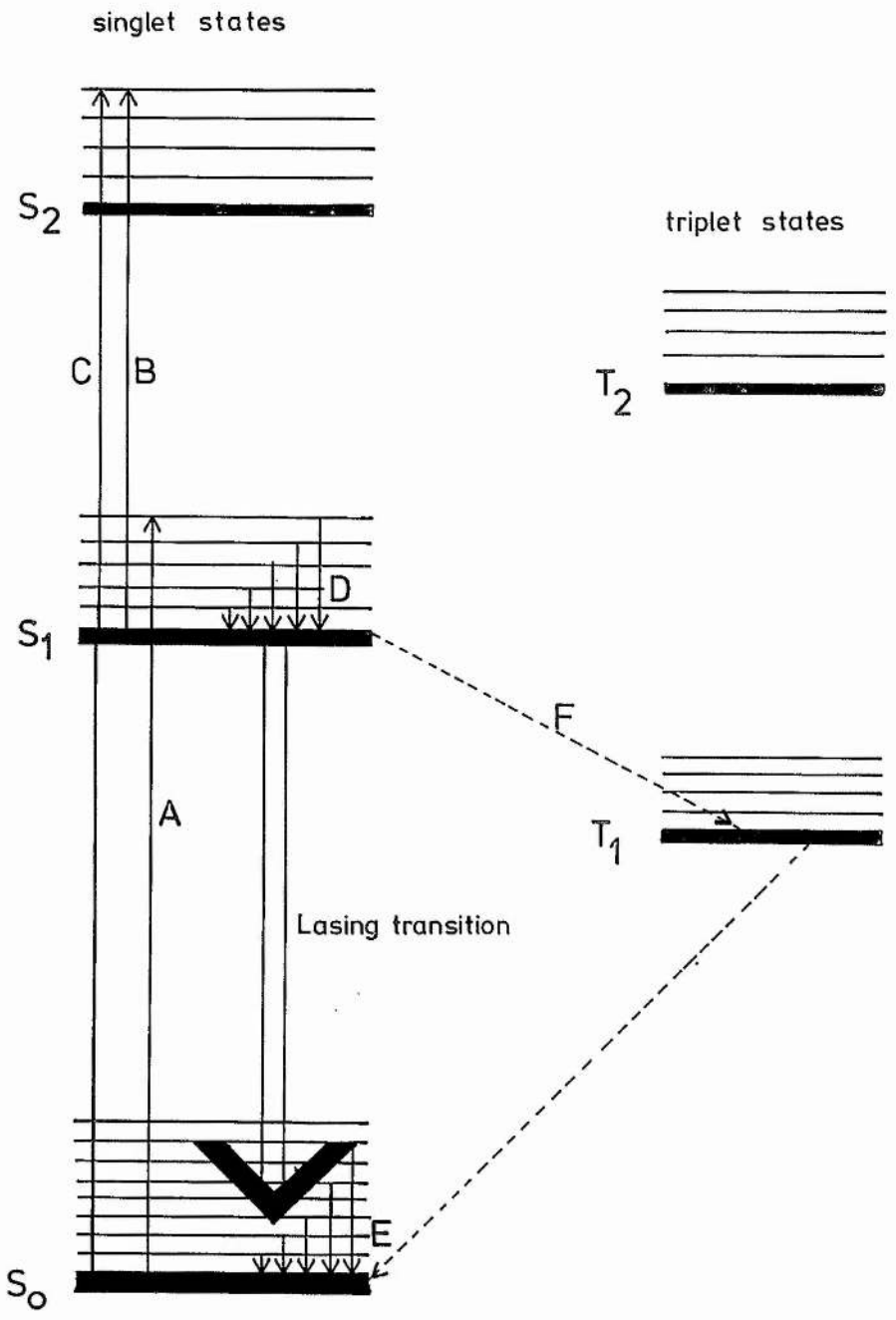

Fig 1-1: Simplified energy level diagram for the dye laser

excited molecule in the S_1 band undergoes a nonradiative transition to the bottom of the band (D), transferring its surplus energy to the solvent. The timescale of this transition is very rapid, of the order of 10ps, so the population of the lower S_1 state rises almost as rapidly as the overall pumping rate.

The laser transition is then from the bottom of the S_1 band to the ground state, but not necessarily to the lowest energy of the ground state band. For the transition to any higher level in the S_0 band, the remaining energy is dissipated nonradiatively (E), as in the S_1 band. Again this process is extremely rapid and the population of the higher energy states of the ground state band remains almost zero. This allows the required population inversion to be maintained between the lowest level of S_1 and almost any non-zero level of S_0

To some extent, there is some depletion of the upper laser level by nonradiative transitions (F) to the triplet state T_1. The effect of this is normally small as the singlet-triplet transition probability is low, due to the electron spin-flip, and the effect can sometimes be reduced by chemical modification of the molecule itself.

The fact that, except very close to the bottom of the S_0 band all non-zero energy states in S_0 have negligible population means that a single atom may radiate at any one of a range of wavelengths. Averaged over all molecules which may be excited at any one time (of the order of 10-100 million) the laser output has now become tunable over this range, which is of the order of 10nm for the

most widely used laser dye, Rhodamine 6G (Rh6G), one of the xanthene group of dyes. The ability of dye lasers to be tuned over this large range while maintaining reasonable power in the beam is the cause of their widespread use in spectroscopy.

Rh6G has a peak absorption around 520nm and much weaker absorptions near 340nm and 250nm in the UV. It is commonly pumped by the green line from an argon ion laser at 514.5nm, or by the UV output from a pulsed nitrogen laser at 337.1nm. The fluorescence has a peak at about 560nm, ranging from 530nm to 620nm.

The coumarin group operate at rather shorter wavelengths. Coumarin 102 absorbs from 300nm to 420nm and is frequently pumped by a krypton ion laser at around 415nm, or by a pulsed xenon ion laser in the UV. In neutral solution, the fluorescence peak is around 480nm.

At the red end of the spectrum the oxazines are normally used, with an absorption peak at 645nm and fluorescence at 715nm for Oxazine 1, for example.

1-5 The laser resonator

For most laser media the gain of the active medium is small, perhaps only 1% (≃0.004dB) per pass, and in order to obtain a net amplification greater than the losses, the beam must be fed back into the active medium many times. This is normally achieved with a pair of mirrors which require very high reflectivities, approaching 100%.

)2

Silver or aluminium coatings are not sufficiently reflecting and also have relatively large absorptions, so multilayer dielectric coatings are employed, which can be tailored to the reflectivity and wavelength required for any situation.

The need for several hundred passes of the beam through the amplifying medium sets very small tolerances on the alignment of the mirrors. Two plane mirrors have an alignment tolerance of 1"arc (or the apparent diameter of a golf ball at 8km), and so curved mirrors are used, which also reduces diffraction losses very considerably. The mirrors may be both of large radius of curvature relative to their separation, as is used in many gas lasers, they may be confocal (their foci coincide, often at the mid-point of the laser), or they may be hemispherical, with one plane mirror and the other with a radius of curvature equal to the separation. Such an hemispherical system is used in most dye lasers, although in a more complex form involving more than two mirrors in a zig-zag arrangement.

It can be shown that for any given laser, there is an optimum transmission value for the mirrors, at which the output power will be a maximum. This optimum coupling depends on the cavity losses and gain of the laser medium, and is discussed in detail later (Sec. 1-6-5). For a low gain system, such as the helium-neon laser, the optimum transmission is only about 1%. For a Neodymium-YAG laser it is about 20%.

Dye lasers are optimised at a transmission of about 5%.

This is of course the total transmission loss, summed over all mirrors. The actual output coupler may have a transmission rather less than this if the loss from the other mirrors is significant.

1-6 Optomechanics of the laser cavity

1-6-1 Cavity design

In order to achieve the minimum pumping requirements of the dye, the pumping beam must be focused into the dye solution, which is either in the form of a free flowing jet or within a thin parallel sided cell. Normally this dye jet (or cell) will be oriented at the Brewster angle to the laser axis to eliminate Fresnel losses for a correctly polarised intracavity beam. However, the process of focusing a beam through an angled interface introduces aberrations which degrade the focus and thus reduce the efficiency of the laser.

This problem was first addressed in detail by Kogelnik et al [6] in 1972. They considered the possibility of using the astigmatism created by off-axis focusing by a curved mirror to compensate for the astigmatism due to focusing through the Brewster surface. It was found that total compensation was possible for a unique combination of jet thickness, refractivity and angle between the beams at the focusing mirror.

Dunn and Ferguson [7] showed that although in this case the whole cavity was astigmatically compensated, this was

only possible after the beam had made one round trip, and that due to the asymmetry, the focus within the jet was not fully compensated. In the case of a very thin dye jet, there is minimal effect on the overall performance.

However, the case of a nonlinear crystal within the cavity must also be considered as such a crystal may well be over 1cm long. In order to increase the efficiency of the nonlinear process within the crystal, the intracavity beam must be focused within it and any antireflection coatings on the crystal surfaces are subject to damage in such a focused beam. Cutting a crystal with Brewster surfaces eliminates this problem but only at the expense of introducing aberrations into the beam. In particular, coma becomes more significant than in the case of the jet, and increases with crystal length and mirror angle (which itself is now much larger than before). The effect of coma on the laser performance is that the focus in the crystal is degraded and further reflective losses are introduced into the cavity.

Accordingly, Dunn and Ferguson designed a cavity which compensated both coma and astigmatism within the crystal and the design was then applied successfully to a frequency doubled Rh6G dye laser [8]. A similar analysis using tilted lenses within the cavity was carried out shortly afterwards by Huffer et al [9]. Later, Wagstaff et al [10] combined the two situations of compensated jet and crystal regions and analysed the general stability of a linear cavity with two interacting foci. The same method was then applied to a ring cavity [11] and later a more general approach was proposed by Dunn and Dunn [12].

This thesis involves the application of this design method only for the case of a standing wave resonator with two focal regions as shown in Fig 1-2. A detailed view of the two regions of interest is shown in Figs 1-3 and 1-4, where the various labels are identified. In the jet region, the requirement for full astigmatism compensation (for the round trip) and ignoring coma is that [6]

$$R_2 \sin(\alpha) \tan(\alpha) = \frac{2t(n^2-1)\sqrt{n^2+1}}{n^4}$$

For a mirror R_2 of radius of curvature of 10cm and a jet thickness of 0.5mm and refractivity 1.4, we get $\alpha = 3.7^\circ$.

In the case of the crystal region, Fig 1-4, there is astigmatism compensation when we have [6,12]:

$$R\sin(\theta) \tan(\theta) = \frac{(n_c^2-1)\, L_c}{n_c^3}$$

For a 1.5cm crystal of refractivity 1.5 and using the same mirrors as before, we get $\theta = 13^\circ$ and thus the Z-arrangement has fold angles of 26°.

From the work of Wagstaff et al [10], the overall stability of a cavity containing both these sections is maximised when the dimensions x, y, d_1 and d_2 (Fig 1-2) are:

$x = 45cm$ $y = 10cm$ $d_1 = 15.4cm$ $d_2 = 10.4cm$

with the jet 9.97cm from R_1 and the centre of the crystal 5.31cm from R_3.

This design of cavity has been successfully used, and

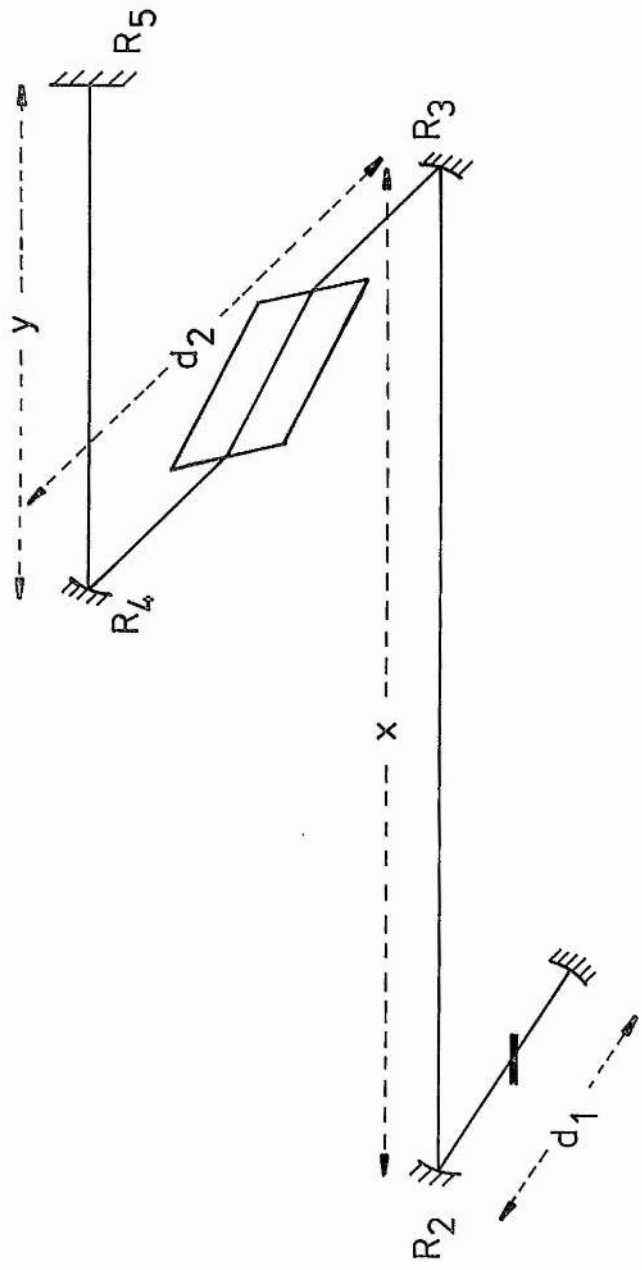

Fig 1-2: General arrangement of the frequency doubling cavity

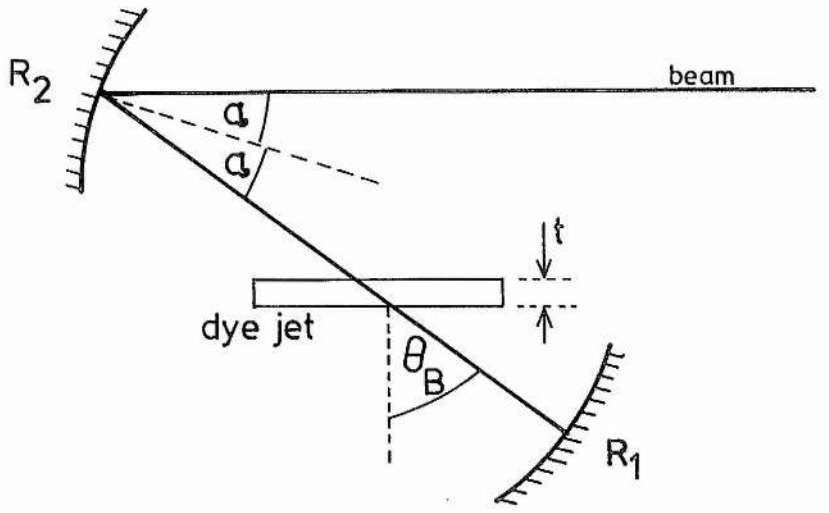

Fig 1-3: Geometry of the jet region

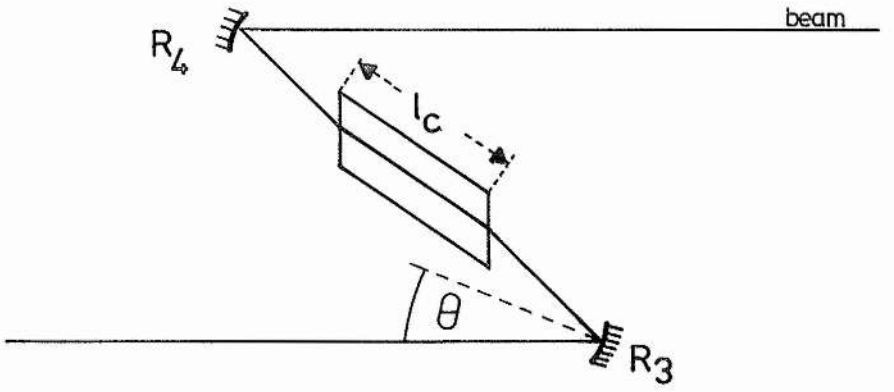

Fig 1-4: Geometry of the crystal region

E1 modified for use as a ring laser by several workers [4,8,11,13,14] for the testing of new materials for second harmonic generation and for atomic spectroscopy.

1-6-2 Frequency selection and control

At any instant a dye laser may lase at any one of a range of wavelengths which satisfy the relation

$$N\lambda/2 = L$$

where L is the length of the cavity and N is an integer, and the output beam will, on average contain all possible wavelengths allowed by the fluorescence and gain. For any spectroscopic application it is necessary to select a narrow band of this output, the spectral width being determined by the resolution required by the particular application. High resolution spectroscopy of the hyperfine structure of atomic energy levels, for example, may require resolutions of the order of a few tens of megahertz ($\simeq 10^{-5}$ nm in the visible), whereas for less critical applications, a resolution of a few gigahertz ($\simeq 10^{-3}$ nm) is sufficient [eg 3,4,8,13]. The various methods of achieving and controlling this resolution in the case of a dye laser must now be considered.

1-6-2-1 Prisms and diffraction gratings

The spatial restrictions placed on an intracavity beam by the stability requirements of the cavity allow the use of spatially dispersive elements for wavelength selection.

E2

In particular, a prism placed within the cavity or a reflection diffraction grating acting as one of the mirrors have both been used to good effect. Capelle and Phillips [15] in 1970, for example, using a nitrogen laser as the pumping source, obtained linewidths of 0.3nm over most of the visible spectrum. This was based on earlier work by Myer et al [16] and later (1972) refined and extended by Hansch [17], whose work has been the basis of pulsed dye laser design ever since. Hansch obtained linewidths of 0.04nm, which allowed study of the sodium D resonance lines by saturation spectroscopy. More refined techniques, for example by Saikan [18], have allowed linewidths of around 10^{-3} nm in certain cases. Examples of the cavity arrangements are shown in Fig 1-5.

The use of prisms as dispersive elements has been largely confined to cw rather than pulsed lasers due to the lower dispersions limiting their selectivity. In cw lasers this is compensated by the beam making many hundreds of passes through the prism before emerging, whereas in pulsed lasers the pulse length is generally short enough only to allow a few passes. Prisms have been used in both standing wave [19,20] and travelling wave [21,22,23] lasers. The bandwidth depends to some extent on the cavity size and geometry, but can sometimes be as low as 20MHz ($\simeq 10^{-5}$ nm) for a cw laser with careful control.

1-6-2-2 The birefringent filter

The main drawback with spatially dispersive elements such as prisms or gratings is that they are spatially

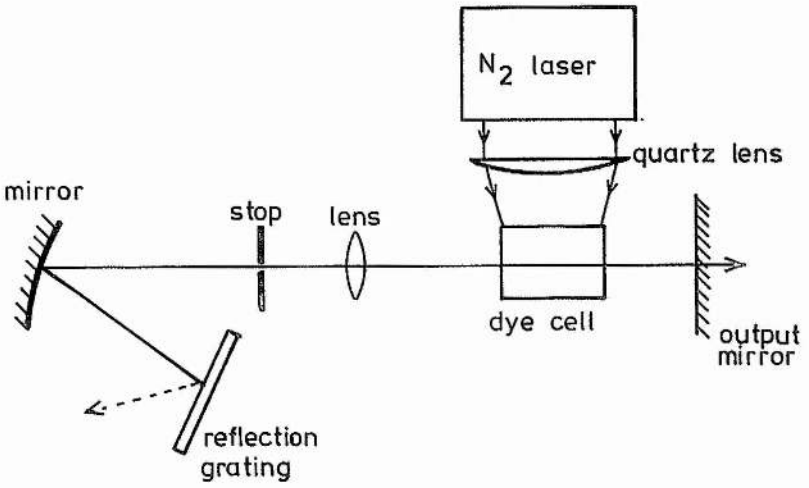

(a) Capelle and Phillips [15]

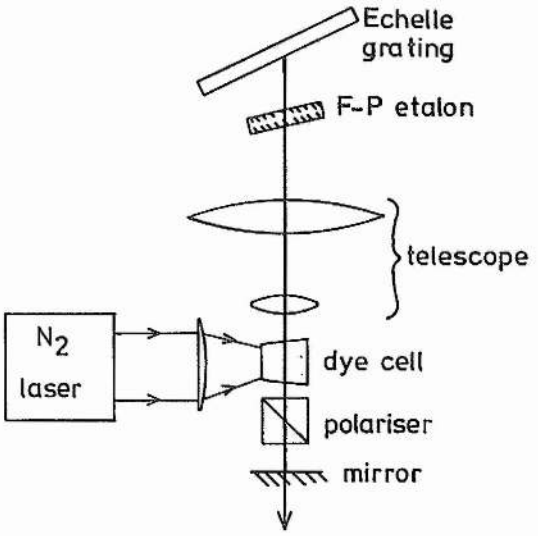

(b) Hansch [17]

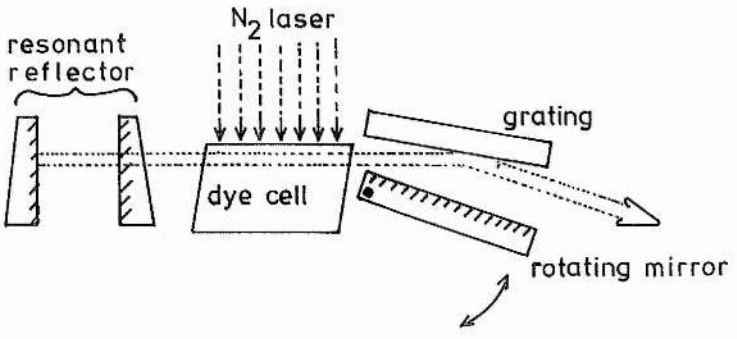

(c) Saikan [18]

Fig 1-5: A selection of short-cavity pulsed dye laser designs

dispersive, and in order to function properly it is necessary to have relatively large beams incident upon them. This creates difficulties in the design of other parts of the laser, by reducing the size of the stability regions for example, and ultimately it is necessary to use some other method of frequency selection. The birefringent filter, proposed for laser use by J.M.Yarborough and later developed in detail by Bloom [24] and others, offers an excellent alternative to the prism or grating and is not spatially dispersive.

A beam of light passing through an isotropic material suffers a retardation due to the refractivity of the material. However, a birefringent material such as crystalline quartz has a refractivity which depends on the polarisation of the light transmitted. Light polarised in a plane parallel to the optic axis of the crystal experiences a different refractivity to that polarised in a plane normal to the axis. Polarised light passing through the material at a general angle θ to the optic axis may be considered as made up of two linearly polarised components, one parallel to and one normal to the axis. In the general case these two polarisations will suffer different retardations, and on emerging from the material the plane of polarisation will be rotated relative to that when the beam entered.

However, if the differential retardation is equal to an integral number of wavelengths, the waves behave as if the material was not there, since the net rotation is an integral multiple of π. In a laser cavity, optical surfaces at the Brewster angle to the cavity axis define a

polarisation for which the Fresnel loss at these surfaces is zero. If a birefringent material is included in the cavity, most wavelengths will suffer a net rotation of the polarisation vector on passing through the plate and these will suffer Fresnel loss at any Brewster surface subsequently encountered. Thus the filter selects only a narrow range of wavelengths for which there is negligible net rotation of the polarisation plane, and for which reflective losses within the cavity are then negligible, and it achieves this without spatial dispersion and with equal selectivity for all sizes of beam.

The wavelength transmitted with zero net rotation depends firstly on the angle between the incident polarisation vector and the optic axis and secondly on the thickness of the plate. Tuning is achieved by rotating the plate in its own plane, which alters the included angle between the optic axis and the laser axis and hence the effective refractivities of the plate, (for a fuller description of the propagation of light through birefringent materials, see for example [25,26,27]). It will be clear that two plates of different thicknesses, but with identical orientations of optic axis relative to the laser axis, will only transmit the same wavelength without net rotation of its polarisation if the plates' thicknesses are in an integer ratio. By stacking several plates together in the correct orientation a very narrow bandwidth filter is produced.

Bloom [24] analysed many such stacks, not only as a function of thickness ratios but also as a function of the angle between the optic axis and the polarisation plane.

His results showed that the maximum discrimination would be achieved with a stack of three plates in a thickness ratio of 1:4:16 and with the optic axis in the plane of the plates and at 45° to the polarisation plane. The filter itself would also be at Brewster's angle to the beam to provide six more Brewster surface in the laser cavity. Accordingly this design has been adopted here, and by several others [8,11].

1-6-2-3 Fabry-Perot etalons

The bandwidth of the birefringent filter just described depends on the gain of the dye as well as on the geometry of the filter. For a small range of wavelengths around the nominal pass wavelength, the rotation of polarisation will be small enough to give insufficient losses at Brewster surfaces, and these wavelengths will be retained in the output. Clearly, this bandwidth will be larger for the higher gain dyes such as Rh6G than for the coumarins, as we show later, but may be of the order of 0.05nm for a carefully aligned three plate filter. To narrow the linewidth still further it is thus necessary to introduce a further selective element, which should also allow continuous tuning within the passband of the birefringent filter. A suitable device is the Fabry-Perot etalon.

The original application in 1899 involved two optically flat partially reflecting plates held accurately parallel, but whose separation could be varied. Multiple beam reflections between the two plates produced interference

F1 fringes (fringes of equal inclination) in transmission, whose separation depended on the distance between the plates and the wavelength. By scanning the plate separation, and observing the transmission of the pair of plates, a spectrum having an extremely high resolution was obtained from the interferometer.

Modern applications can also use fixed plates, and often the partially reflecting surfaces are multilayer dielectric coatings laid down on the surface of an accurately polished quartz plate. This is termed an etalon, and is commonly used in tunable dye lasers. For a solid etalon of course, only a few wavelengths will undergo constructive interference in transmission, namely those which satisfy the relation

$$N\lambda = 2nt.\cos(\theta)$$

where N is an integer, n is the refractivity, t is the thickness of the etalon and θ is the angle between the beam and the normal to the surface within the material. For small angles of incidence, i, θ can be approximated by $\theta = i/n$. From this expression it is clear that for different values of i, different wavelengths will experience constructive interference in transmission, and that by rotating the etalon about any axis normal to the beam, the pass wavelength can be tuned over a small range.

Hercher [28] has shown that the tuning of an etalon is independent of its thickness and is given in differential form (for small values of i) by

$$d\lambda = \frac{\lambda i^2}{2n^2}$$

1F2 The frequency separation of adjacent transmission peaks is given by [28]

$$\Delta\nu = \frac{c}{2nt}$$

and is termed the free spectral range, FSR, of the etalon.

For a quartz etalon 0.5mm thick, the value of the FSR is about 200GHz, or about 0.2nm in the visible, rather larger than the bandwidth due to the birefringent filter. The bandwidth of a single transmission peak (full width at half maximum, FWHM) is given by [29]

$$FWHM = \frac{c(1-R)}{2\pi nt\sqrt{R}}$$

where R is the reflectance ($0 \leq R \leq 1$). For the same etalon as before with 30% reflectance surfaces the FSR is about 80GHz (0.07nm) and the finesse, which is the ratio between the FSR and the bandwidth, is 2.5. The finesse can also be expressed in terms of the reflectance by

$$F = \frac{\pi\sqrt{R}}{1-R}$$

The finesse can thus be increased and the transmission bandwidth reduced by increasing the reflectance. However, as Hercher has shown [28], for a particular laser there is an optimum reflectance, beyond which the output power is significantly reduced.

1-6-3 Single mode operation

A laser operating with both a birefringent filter and an etalon may well have a linewidth very much smaller than the width of the etalon transmission peak. Ultimately a single longitudinal mode may oscillate, with a linewidth limited by the mechanical stability of the laser and the quality factor (Q-factor) of the resonator.

In order to obtain single mode operation, it is only necessary to introduce losses greater than the gain for all other modes, which will then cease to oscillate. In most dye lasers another effect, that of mode competition, assists this selection and can be the principal factor in achieving single mode operation. Mode competition is a consequence of the nature of stimulated emission. Suppose that one longitudinal mode is momentarily more intense than all others. The photon flux from this mode is therefore the greatest, and any excited molecules within the active medium will have a higher probability of encountering photons from this one mode than for any other. Hence, when stimulated emission occurs, more photons for the given mode will be produced than for any other, enhancing the effect and selecting only the one or two modes for which the gain is highest.

The combination of a birefringent filter and an etalon (sometimes two) then serves to select the centre frequency at which such mode competition occurs and the laser medium itself then selects a single axial mode. Tuning in frequency is then carried out by careful tilting of the etalon. Provided there are no spatial hole-burning

effects (as is so in a ring laser), the tuning range can be quite large, approaching that of the passband of the birefringent filter.

With low gain dyes, such as the coumarins, single mode operation can be easier to achieve than with the high gains of those such as Rhodamine 6G, as the lower gain means that more modes will be operating close to their threshold, and the losses needed to supress them will be smaller. The drawback is that the power in even the single mode is likely to be low. For Rh6G the power can be much higher and so more discriminating frequency selective elements have to be used to assist the suppression of the unwanted modes. Frequently this involves the use of a second, thick, etalon (typically 1cm thick) acting in combination with the thin one [11]. The tuning range is then limited by the bandwidth of the thick etalon. Some workers, (Wagstaff and Dunn) [4], have introduced the use of a thick, air-spaced, etalon which is scanned piezoelectrically. Single mode scans of up to 60GHz in the visible (0.05nm) have been achieved with this alone (ie without tilting the thin etalon).

The linewidth of the laser output is determined ultimately by the quality factor Q and the mechanical stability. The Q-factor may be defined in several ways. In terms of the frequency bandwidth $\Delta\nu$ at frequency ν, we have:

$$\Delta\nu = \nu/Q$$

More generally, in terms of energy, we can write:

$$Q = \frac{\omega U}{dU/dt}$$

where U is the coherent energy stored in the laser resonator and ω is the angular frequency of the oscillation.

To obtain low values of linewidth, we require a large value of Q in the first equation above. From the second, we see that this requires a very small rate of coherent energy loss from the resonator. In the steady state operation of the laser, the net coherent energy loss (coherent energy input due to stimulated emission minus coherent energy output due to mirror transmission, etc) is equal to the rate of spontaneous emission into the laser mode. To achieve high Q values, the laser should be operated well above threshold so that the fractional energy loss is small.

The spontaneous emission, or noise, limit in most lasers usually leads to such small linewidths (high Q values) that other factors, such as the mechanical stability of the laser, dominate. An actively stabilised helium-neon laser may achieve a linewidth of 1-10Hz, providing the frequency itself is held stable (by locking on to the hyperfine absorption features of iodine, for example), but the practical limit for many lasers is much higher than this. Using a single mode ring dye laser, for example, Wagstaff and Dunn [4], have obtained a jitter of 10MHz for their experiments on Mercury.

1-6-4 High power pumping

Pumping a dye with high power pulsed beams from a xenon ion or nitrogen laser, for example, must necessarily excite far more dye molecules than would a beam of only a few watts from a cw argon ion laser. This means that the power within each axial mode is very much greater for pulsed lasers and single mode operation much more difficult to achieve. This can be eased, however, by the use of a very short laser cavity, as for example by Saikan [18], who obtained single mode outputs of the order of 1kW from a nitrogen pumped dye laser. The linewidth was 420MHz and the effective cavity length 10cm. Single mode operation has only occasionally been reported, and only for nitrogen laser pumping. Although several workers (eg Schearer [30]) have obtained narrow linewidths with xenon lasers, they have all used short cavities (about 10cm), several dispersive elements and single mode operation was not discussed.

For a long cavity (1m) xenon pumped dye laser, such as one including an intracavity frequency doubling element, single mode operation is likely to be very difficult to achieve, particularly if a high gain dye is used, and the linewidths determined by the birefringent filter, etalon and the dye gain.

1-6-5 Laser output coupling

The semiclassical model of a laser system yields a differential equation linking the intensity I of a laser

oscillation with the initial gain of the medium α_o, as:

$$\frac{1}{I}\frac{dI}{dz} = \frac{\alpha_o}{1 + I/I_s}$$

where z is the distance travelled by the beam through the gain medium and I_s is the saturation intensity of the medium, being the intensity at which the population inversion falls to half its initial value.

For a single pass of the beam through the gain medium of length l, and assuming that the gain is small, so that dI is much less than I, we obtain:

$$dI_{gain} = \alpha_o . I . l / (1 + I/I_s)$$

The losses in a laser cavity are firstly those due to mirror transmissions (or "useful" losses), β_m, and secondly those due to scattering, self absorption by the medium and diffraction, which may be considered together as a single "parasitic" loss, β_p. Both β_m and β_p are here considered as fractional losses. Thus the loss for a single pass of the beam around the cavity is given by:

$$dI_{loss} = (\beta_m + \beta_p) . I$$

If A is the cross-sectional area of the beam, we obtain an equation for the output power P in the steady state as:

$$P = A\beta_m I_s \left(\frac{\alpha_o}{\beta_m + \beta_p} - 1 \right)$$

which is the normal working relationship between the output power, mirror transmission and parasitic loss. The general form of this equation is shown in Fig 1-6, for different values of parasitic loss. The peak of each curve represents the maximum power which may be extracted

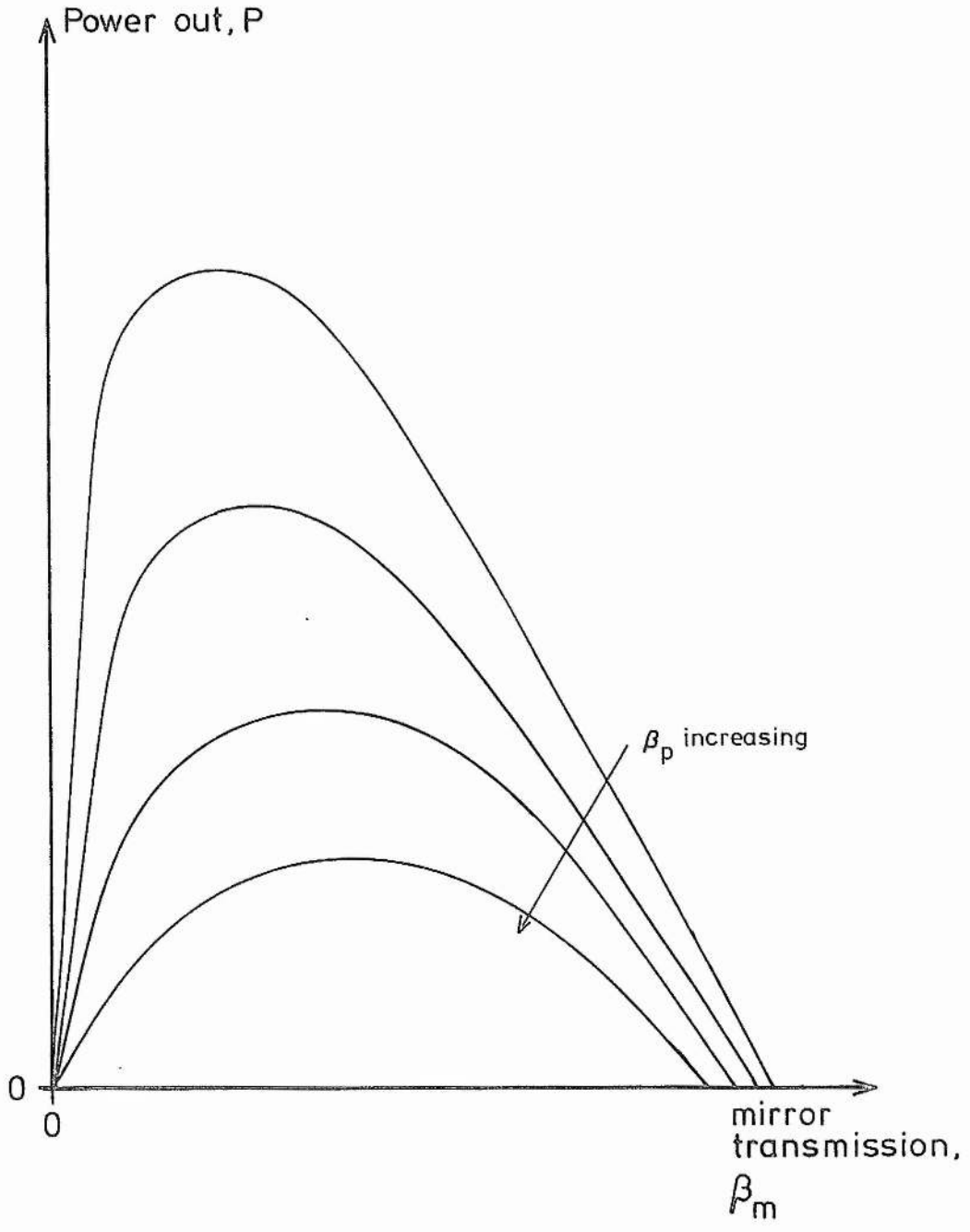

Fig 1-6: The output power, P, of a laser as a function of mirror transmission, β_m for different parasitic losses, β_p.

from the laser and the mirror transmission to achieve this power. The scale of Fig 1-6 is determined principally by the small signal gain α_o and the saturation intensity I_S, both of which depend on the laser transition concerned. In practical terms, obtaining a larger output power requires an increase in the length of the gain medium or a reduction of the parasitic losses, perhaps by different focusing to reduce diffraction effects and better mirror coatings to minimise reflective scattering.

The application of Fig 1-6 to predict the maximum power expected from a Xenon ion laser is discussed in Chapter 4.

REFERENCES CHAPTER 1

1 Hansch TW, Levenson MD, Schawlow AL; Phys Rev Lett 26 946 (1971)

2 Hansch TW, Shakin IS, Schawlow AL; Nature 235 63 (1972)

3 Hansch TW, Lee SA, Wallenstein R, Weiman C; Phys Rev Lett 34 307-9 (1975)

4 Wagstaff CE, Dunn MH; Opt Commum 35 353-8 (1980)

5 Tarasov LV; "Laser Physics", MIR, Moscow, 1983

6 Kogelnik HW, et al; IEEE J Quant Electr QE-8 373-9 (1972)

7 Dunn MH, Ferguson AI; Opt Commun 20 214-9 (1977)

8 Ferguson AI, Dunn MH; Opt Commun 23 177-82 (1977)

9 Huffer W, Scheider R, Brinkmann U; Appl Phys 15 157-61 (1978)

10 Wagstaff CE, Dunn MH, Ferguson AI, Bastow SJ; Opt Commun 25 379-83 (1978)

11 Wagstaff CE, Dunn MH; J Phys D 12 355-68 (1979)

12 Dunn CE, Dunn MH; Optica Acta 28 1413-23 (1981)

13 Ferguson AI, Dunn MH; Opt Commun 23 227-30 (1977)

14 Bastow SJ, Dunn MH; Opt Commun 35 259-63 (1980)

15 Capelle G, Phillips D; Appl Opt 9 2742-5 (1970)

16 Myer JA, Johnson CL, Kierstead E, Sharma RD, Itzkan I Appl Phys Lett 16 3-5 (1970)

17 Hansch TW; Appl Opt 11 895-8 (1972)

18 Saiken S; Appl Phys 17 41-4 (1978)

19 Grove RE, et al; Appl Phys Lett 23 442-3 (1973)

20 Schroeder HW, Welling H, Wellhausen B; Appl Phys 4 343-8 (1973)

21 Marowsky G, Cubeddu R; J Appl Phys 47 5470-1 (1976)

22 Green JM, Hohimer JP, Tittel FK; Opt Commum 7 349-50 (1973)

23 Schroeder HW, et al; Appl Phys 14 377-80 (1977)

24 Bloom A; J Opt Soc Am 64 447-52 (1974)

REFERENCES CHAPTER 1 (cont)

25 Born M, Wolf E; "Principles of optics", Pergamon, London, (1959)

26 Klein MV; "Optics", Wiley, New York, (1970)

27 Francon M, Mallick S; "Polarisation Interferometers" Wiley Interscience, London, (1971)

28 Hercher M; Appl Opt 8 1103-6 (1969)

29 Peterson DG, Yariv A; Appl Opt 5 985-91 (1966)

30 Schearer LD; IEEE J Quant Electr QE-11 935-7 (1975)

31 Shimoda K; "Introduction to Laser Physics" Springer-Verlag, Berlin, (1984)

Chapter 2: Frequency doubling theory and materials

B1

2-1: Frequency doubling

The process of second harmonic generation (SHG), commonly called frequency doubling, involves the excitation of solid crystalline material into a resonance between the crystalline electric field and an applied external field, such as that within a beam of light. As with any forced oscillation, by careful choice of various parameters, a resonance at twice the driving frequency can often be achieved, and for certain materials it is thus possible to generate ultraviolet (UV) light by passing a beam of visible light through the crystal. The details of the theory of these processes and their optimisation is the subject of the first half of this chapter.

2-1-1: Basic principles of SHG

Maxwell's wave equation in the presence of a polarisable medium is given in scalar form by:

$$\mu_0 \ddot{P} + \mu_0 \varepsilon_0 \ddot{E} - \nabla^2 E = 0 \qquad (1)$$

where E is the electric field strength and P is the macroscopic polarisation. For small field strengths we take the polarisation to be proportional to E:

$$P = \varepsilon_0 \chi E \qquad (2).$$

In the presence of high fields (of the order of the interatomic field) this is no longer true and must be replaced by:

$$P = \varepsilon_0 \chi_1 E + \varepsilon_0 \chi_2 E^2 \qquad (3).$$

To solve (1) in the presence of a nonlinear polarisation given by (3), we assume there exists a plane harmonic wave propagating along the axis of the crystal, having the form:

$$E_1 = E_{10} \cos(\omega_1 t - k_1 z) \qquad (4)$$

where the frequency ω_1 and wavenumber k_1 are related (from (1)) via:

$$\mu_o \varepsilon_o \chi_1 \ddot{E}_1 + \mu_o \varepsilon_o \ddot{E}_1 - \nabla^2 E_1 = 0 \qquad (5)$$

by

$$k_1^2 - \mu_o \varepsilon_o (1 + \chi_1) \omega_1^2 = 0 \qquad (6).$$

The E_1 wave induces in the medium a nonlinear polarisation of the form:

$$P_2 = \varepsilon_o \chi_2 E_1^2 \qquad (7).$$

This gives rise to a wave, E_2 , which is a solution of:

$$\mu_o \varepsilon_o \ddot{E}_2 (1 + \chi_1) + \mu_o \varepsilon_o \chi_2 (\ddot{E}_1^2) - \nabla^2 E_2 = 0 \qquad (8).$$

{This has neglected the contribution made to P_2 by E_2 itself, on the not unreasonable assumption that $E_2 << E_1$. The term ignored is $\mu_o \varepsilon_o \chi_2 (\ddot{E}_2^2)$ }.

We must now find E_2 (the generated wave) by attempting a solution of (8) having the form:

$$E_2 = E_{20}(z) \cos(2\omega_1 t - k_2 z + \phi) \qquad (9)$$

where ϕ is a phase factor and k_2 is the wavenumber, both still to be determined. The spatial frequency of E_2 is of course $2\omega_1$, (i.e. double the fundamental frequency). If (9) and (4) are written in complex notation, namely:

$$E_2 = \{E_{20} \exp[i(2\omega_1 t - k_2 z)] + E_{20}^* \exp[-i(2\omega_1 t - k_2 z)]\}/2$$

and

$$E_1 = \{E_{10} \exp[i(\omega_1 t - k_1 z)] + E_{10}^{*} \exp[-i(\omega_1 t - k_1 z)]\}/2$$

and then substituted into (8), we get:

$$\mu_o \varepsilon_o \omega_1^2 \chi_2 E_{10}^2 \exp[i(k_2 - 2k_1)z] = ik_2 \frac{\partial E_{20}}{\partial z} + E_{20}\{k_2^2 - \mu_o \varepsilon_o (1+\chi_1)(2\omega_1)^2\}/2 \qquad (10)$$

where E_{20} is assumed to vary very slowly with distance along the beam (z), so that terms in $\frac{\partial^2 E_{20}}{\partial z^2}$ may be ignored.

The wavenumber (k_2) and frequency ($2\omega_1$) are related by (6):

$$k_2^2 - \mu_o \varepsilon_o (1 + \chi_1)(2\omega_1)^2 = 0 \qquad (6a)$$

so (10) reduces to:

$$\frac{\partial E_{20}}{\partial z} = \frac{-i \mu_o \varepsilon_o \omega_1^2 \chi_2}{k_2} E_{10}^2 \exp[i(k_2 - 2k_1)z] \qquad (11).$$

In order to find the final amplitude E_{20} of the generated second harmonic (SH), equation (11) is integrated over the length of the medium, assuming E_{10} is constant (i.e. that the generation efficiency is low, so that negligible power is drained from the fundamental beam).

This gives:

$$E_{20} = \frac{\mu_o \varepsilon_o \omega_1^2 \chi_2 L}{k_2} E_{10}^2 \left(\frac{1 - \exp(\Delta k L)}{\Delta k L}\right) \qquad (12)$$

where $\Delta k = (k_2 - 2k_1)$ and L is the length of the medium.

The mean SH flux is given by the Poynting vector:

$$S_2 = 0.5 \varepsilon_o c n_2 E_{20} E_{20}^* \qquad (13)$$

where n_2 is the refractivity at the SH wavelength. Thus, we get, after some algebra:

$$S_2 = \frac{2\pi^2 \chi_2^2 L^2}{n_2 n_1^2 \lambda_1^2 c \varepsilon_o} S_1^2 \operatorname{sinc}^2\left(\frac{\Delta k L}{2}\right) \qquad (14)$$

where λ_1 is the free space wavelength of the fundamental wave and n_1 the refractivity at the fundamental wavelength.

2-1-2 Powers expected

The medium just described will behave in this way when the electric field is strong enough to induce a nonlinear polarisation. This will occur when the applied electric field strength is approaching that of the interatomic field, which is given approximately by:

$$E = e/(4\pi \varepsilon_o R^2)$$

where R is of the order of the atomic spacing. Thus E approaches 10^{11} V/m. Referring to the nonlinear equation for the polarisation, (3), we see that nonlinear effects will be significant when $\varepsilon_o \chi_2 E^2$ approaches the same order of size as $\varepsilon_o \chi_1 E$, from which we predict that $\chi_2 E \simeq \chi_1$. As χ_1 is around unity, we expect χ_2 to be of the order of

C1 10^{-11} m/V. In practice it is found to be in the range 10^{-11} to 10^{-12} m/V for most materials.

Using $\chi_2 = 10^{-12}$ m/V and λ_1 = 600nm, we have, from (14), and for the moment disregarding the sinc^2 term:

$$S_2 \simeq 10^{-8} S_1^2 L^2 \qquad (15)$$

or, in terms of powers:

$$P_2 \simeq 10^{-8} P_1^2 L^2 / A \qquad (16)$$

where A is the cross-sectional area of the beam.

Typical powers of fundamental wavelength laser beams would be 10W in a collimated beam of diameter of about 2mm, giving a generated power of 1mW per metre of crystal length. If the beam were focused, however, to a spot of the order of 10 microns in diameter, then the generated power rises to about 100W/m over the length where focusing was maintained.

2-1-3 The need for phasematching

In the above discussion, the $\text{sinc}^2(\Delta kL)$ was neglected. This term specifies the degree of phasematching between the fundamental-induced nonlinear polarisation in the medium (of spatial period $2k_1$), and the generated SH wave (of spatial period k_2). For the case of $k_2 = 2k_1$, all the SH waves radiated from different points in the medium due to the nonlinear polarisation are in phase in forward

C2

propagation, and so the SH power is at a maximum, as $\text{sinc}^2(0) = 1$.

If, however, $k_2 \neq 2k_1$, then the contributions to SH waves from different parts of the medium are not all in phase, so destructive interference results and the SH power is reduced.

From (14) it is seen that there is an optimum length L_c for maximum SH generation, given by:

$$L_c = \frac{\pi}{\Delta k} = \frac{\lambda_1}{4(n_2 - n_1)} \qquad (17).$$

This is known as the coherence length.

Normally, the refractivities n_1 and n_2 are different due to dispersion, so that L_c is of the order of a few wavelengths. In this case the SH power is small. If, however, the refractivities are close to each other or exactly equal, then the coherence length tends to infinity and the SH power becomes large, limited only by absorption and defocusing effects. The process of obtaining $n_1 = n_2$ is that of phasematching, which is discussed in detail later, (Sec 2-1-5).

2-1-4 Nonlinear anisotropic media

Section 2-1-1 developed a discussion of simple SHG in an isotropic medium. In practice, all second order nonlinear media are anisotropic and, because of phasematching techniques, the polarisation of the

C3 generating and SH waves are often different, so we must extend the discussion somewhat.

In an anisotropic medium, the scalar equation (3) for the nonlinear polarisation must be replaced by a description in terms of the components of the electric field and polarisation, namely:

$$P_i = \varepsilon_o d_{ijk} E_j E_k \qquad (18)$$

where d_{ijk} is a three rank tensor describing the nonlinear susceptibilities, and summation over repeated indices is implied. Such a tensor has 27 components, but some are redundant as interchange of j and k leaves the polarisation unchanged, and so (18) becomes:

$$\begin{pmatrix} P_1 \\ P_2 \\ P_3 \end{pmatrix} = \varepsilon_o \begin{pmatrix} d_{11} & d_{12} & d_{13} & d_{14} & d_{15} & d_{16} \\ \cdot & & & & & \\ d_{31} & \cdot & \cdot & \cdot & \cdot & d_{36} \end{pmatrix} \begin{pmatrix} E_1^2 \\ E_2^2 \\ E_3^2 \\ 2E_2E_3 \\ 2E_1E_3 \\ 2E_1E_2 \end{pmatrix}$$

The specification of the 18 elements of the d_{jk} matrix provides a complete description of the nonlinear properties of the anisotropic material.

In addition, many of the elements of d_{jk} are zero, a consequence of crystal symmetry. For the crystal class $\bar{4}2m$ only d_{14}, d_{25} $(=d_{14})$ and d_{36} are non-zero, this being applied in the cases of ADA and Urea, and for the class

mm2, of which LFM is a member, the non-zero elements are d_{15} , d_{24} , d_{31} $(=d_{15})$, d_{32} $(=d_{24})$ and d_{33}. Such dramatic reduction of the significant elements of d_{ijk} greatly simplifies the analysis of SHG. Furthermore, it is almost always possible to reduce the coefficients still further to an effective value d_{eff} , depending on ray propagation directions within the crystal. The form of d_{eff} in a particular case is found from tables such as those in Chapter 3 of [1].

It can be seen, by comparing (7) with (18), that for the case of SHG using a single input beam, the two equations are equivalent, so we can replace χ_2 by d_{eff} in the earlier analysis, in particular in (14) to (16) to give:

$$P_2 = \frac{2\pi^2 d_{eff}^2 L^2 P_1^2}{n_2 n_1^2 \lambda_1^2 c\varepsilon_o A} \operatorname{sinc}^2\left(\frac{\Delta kL}{2}\right) \qquad (20).$$

2-1-5 Phasematching techniques

In general, due to dispersion, Δk $(=k_2 - 2k_1)$ in (12) is not normally zero, and thus also is not $(n_2 - n_1)$ in (17). However, although the condition $\Delta k = 0$ is difficult to achieve in an isotropic medium, it has been shown by Maker et al [2] and Giordmaine [3] that, by a suitable choice of propagation direction and polarisation, it is often possible to obtain $\Delta k = 0$ for anisotropic media. This technique is termed phasematching. In birefringent materials two types are possible, depending on the choice of polarisation.

Phasematching techniques apply equally to the production of harmonic beams from a single fundamental beam and to beam mixing, generating the sum or difference frequencies. Indeed, SHG can be regarded as the result of sum-frequency mixing of two collinear identical beams. Such beams, in whatever context, will have one of two relative polarisations; they will either have parallel polarisations, or can be resolved into components of orthogonal polarisation. The first case, of parallel polarisations for the fundamental beams, is termed a Type I interaction; the orthogonal case is Type II.

Where a single beam is used, as in SHG, Type I or Type II may be selected by a suitable choice of incidence angle and crystal orientaion. In Type I the beam is either an ordinary or an extraordinary ray. In Type II it is a mixture of both, usually in equal amounts. For example, for Type I matching in a negative uniaxial crystal, the fundamental is the ordinary ray and the SH is the extraordinary ray, these being reversed for a positive type crystal. For Type II, the fundamental would be an equal mixture of ordinary and extraordinary rays, with the SH being either an ordinary or an extraordinary ray, depending on circumstances.

For the purpose of this work, phasematching techniques will only be considered for positive uniaxial crystals (e.g. Urea) and negative biaxial crystals (e.g. LFM); analyses for other types may be found in the literature [4,5,6,7,8].

The choice of Type I or Type II depends on the wavelength

D1 range to be covered, the geometry available with a given crystal and the nonlinear coefficients d_{ijk}. Specific examples are discussed later.

2-1-5-1 Uniaxial crystals

For a beam propagating in a uniaxial crystal so that the wave normal of the beam makes an angle θ with the optic axis of the crystal, the extraordinary refractivity along the direction of the beam is given by:

$$\frac{1}{n^2(\theta)} = \frac{\cos^2\theta}{n_o^2} + \frac{\sin^2\theta}{n_e^2} \qquad (21)$$

where n_o and n_e are the ordinary and extraordinary refractivities.

For a positive ($n_e > n_o$) uniaxial crystal (e.g. Urea), the index matching requirement is:

Type I : $$n_{o2} = n_1(\theta) \qquad (22);$$

Type II : $$n_{o2} = [n_1(\theta) + n_{o1}]/2 \qquad (23)$$

where the subscripts refer to the fundamental (1) and SH (2) beams.

By combining equations (21), (22) and (23), we get an expression for the phasematch angle θ_m, that is, the angle of propagation within the crystal with respect to the optic axis for which $\Delta k = 0$, as follows:

Type I :

$$\sin^2\theta_m = \frac{n_{o2}^{-2} - n_{o2}^{-2}}{n_{e1}^{-2} - n_{o1}^{-2}} \qquad (24);$$

Type II :

$$\sin^2\theta_m = \frac{\left[n_{o1} / (2n_{o2} - n_{o1})\right]^2 - 1}{\left(n_{o1} / n_{e1}\right)^2 - 1} \qquad (25).$$

2-1-5-2 Biaxial crystals

For a wave propagating in a biaxial crystal, making angles θ and ϕ with the principal axes Z and X respectively, the refractivity along the direction of propagation is given by:

$$\frac{\sin^2\theta\cos^2\phi}{n^{-2}-n_x^{-2}} + \frac{\sin^2\theta\sin^2\phi}{n^{-2}-n_y^{-2}} + \frac{\cos^2\theta}{n^{-2}-n_z^{-2}} = 0 \qquad (26)$$

where n_x, n_y and n_z are the principal refractivities.

When the wave propagation is confined within one of the principal planes ZX or ZY, in which case $\phi = 0$ or 90° respectively, then (26) is greatly simplified. For example, for propagation in the ZX plane, $\phi = 0$ and (26) reduces to:

$$\frac{1}{n^2} = \frac{\sin^2\theta_m}{n_z^2} + \frac{\cos^2\theta_m}{n_x^2} \qquad (26a).$$

In any situation, the phasematch angle is computed by combining with (26) the appropriate phasematch condition, ((22) or (23) and taking $n_z = n_o$ and n_x or $n_y = n_e$).

For a wave propagating in the ZX plane of a negative biaxial crystal (e.g. LFM) the phasematching angles are given by:

Type I :
$$\sin^2\theta_m = \frac{n_{y1}^{-2} - n_{x2}^{-2}}{n_{z2}^{-2} - n_{x2}^{-2}} \qquad (27);$$

Type II :
$$\sin^2\theta_m = \frac{\left[n_{x1}/(2n_{y2} - n_{y1})\right]^2 - 1}{\left(n_{x1}/n_{z1}\right)^2 - 1} \qquad (28).$$

For waves propagating in the ZY plane, the indices n_x and n_y are interchanged in (27) and (28).

2-1-5-3 Walkoff

The case of $\theta_m = 90°$ is called noncritical phasematching. It is of particular importance because there is then no

difference in direction between the fundamental and SH fluxes, which is normally not the case due to birefringence. As far as the wave normal directions are concerned, the two beams do have the same direction when phasematched, but the direction of the energy flow is that of the ray direction, which is only colinear with the wave normal if the propagation is parallel with or normal to the optic axis.

The general case for a positive crystal is illustrated in Fig 2-1, (for a negative crystal, the angle ρ will carry a positive sign and so appear on the opposite side of the wave normal direction). The direction of the ray can be shown, [8], to be normal to the curve $n(\theta)$, which from (21) is an ellipse. From the geometry of Fig 2-1 we may obtain an expression for the angle ρ of "walkoff" between the fundamental and SH beams, as:

$$\tan(\theta_m - \rho) = \left(\frac{n_o}{n_e}\right)^2 \tan\theta_m \qquad (29).$$

For a negative biaxial crystal such as LFM, the formula for ρ depends on the propagation plane and polarisations. For Type I phasematching with the fundamental beam in the ZX plane at an angle θ_m to the Z axis, and SH in that plane polarised in the Y direction, we have, [10],:

$$\tan(\theta_m + \rho) = \frac{n_{x2}\sqrt{n_{x2}^2 - n_y^2\cos^2\theta_m}}{n_{z2}\, n_y \cos\theta_m} \qquad (30).$$

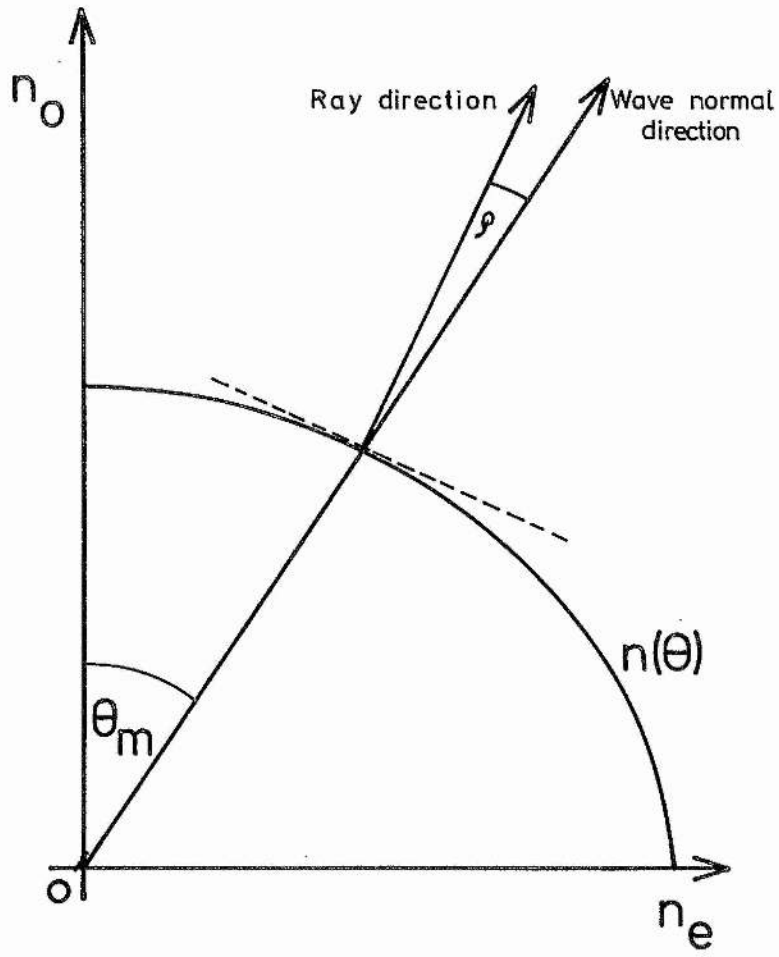

Fig 2-1: The geometry of second harmonic walkoff.

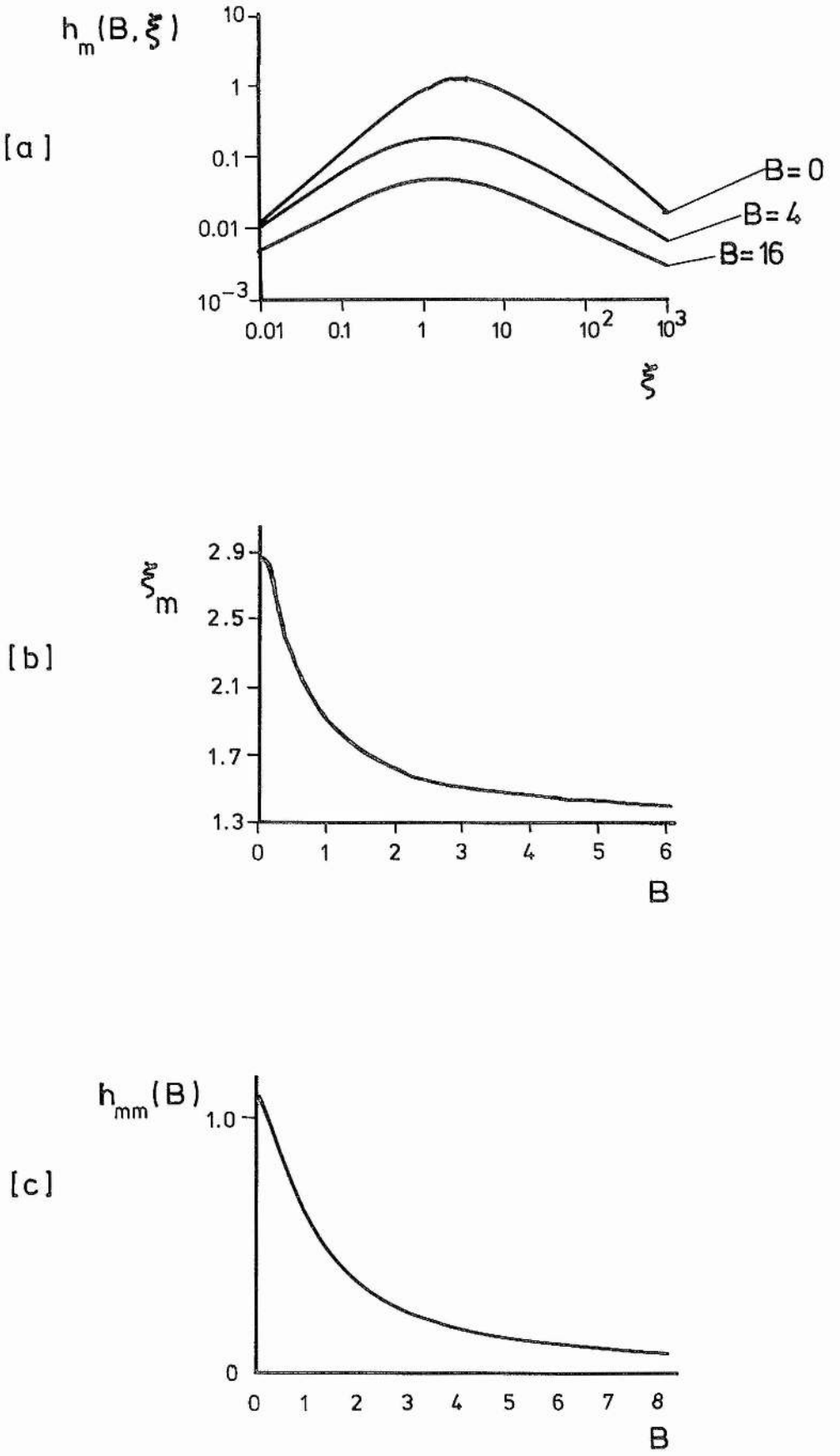

Fig 2-2: Variation of h_{mm}, B and ξ_m,
(from Boyd and Kleinman [15])

The angle ρ is found significant when considering the optimum conversion efficiency and lengths of crystal, as will be shown later (Section 2-1-6).

At the point where $\rho = 0$ the conversion efficiency is at a maximum, and from the above expression it can be seen that this corresponds to $\theta_m = 90^\circ$, that is, noncritical phasematching. Thus if temperature tuning (see later) is possible over an acceptable wavelength range then noncritical phasematching is to be preferred since the maximum UV output would then be obtained.

For LFM, noncritical phasematching is obtained at infrared wavelengths (about 2.47 microns; determined numerically by solving (27) using the refractivity formula in [12]), and so is irrelevant as far as this work is concerned. For Urea, the wavelengths are 597nm (Type II) and 474nm (Type I), [11].

2-1-5-4 Angle and temperature tuning

If phasematching is to be achieved over an extended range of wavelengths, as in the case of a dye laser frequency doubling system, then either the angle θ_m must be varied in accordance with the refractivity variations applied to (24), (25), (27) or (28), or the crystal temperature must be altered, which uses the temperature variation of refractivity to counter dispersion, once the angle θ_m has been chosen approximately.

The first option is called angle tuning, and involves altering the beam propagation direction within the crystal as the laser is tuned in wavelength. There is considerable disadvantage in this method, however, in that as the beam propagation direction within the crystal changes, then so does the focusing and the propagation within the cavity as a whole, and in order to maintain maximum power the laser mirrors must be continually adjusted in their alignment. Furthermore, Fresnel reflection losses at the surface of the crystal can normally only be minimised for one orientation of the beam, and in a narrow wavelength band, for example by the use of antireflection coatings, and any deviation from the optimum orientation will raise the laser threshold and reduce the intracavity power.

The second option is termed temperature tuning. The advantage of this method over angle tuning is that the crystal remains stationary within the laser cavity, and thus focusing and beam orientation, once optimised, remain unaltered. In particular, with a fixed beam direction, losses due to reflection of the crystal faces can be minimised by correct choice of the angle of incidence, Brewster's angle, whose value is unique for a particular material. In this case, for light polarised in the plane of incidence, there is zero reflective loss.

Temperature tuning is often used to extend the wavelength range of UV generation when the phasematching angle is 90°, for example in the case of ADA. It is not necessary to have noncritical phasematching, however, and providing that the change of phasematched wavelength with

temperature is satisfactory, this method is to be preferred over angle tuning for all values of θ_m. An example of this situation is that of ammonium dihydrogen phosphate (ADP), which will temperature tune over the range 589nm (at 20°C) to 627nm (at 100°C) with $\theta_m = 63°$. Further details are given in Chapter 5 of [13].

In all crystals used for laser-driven SHG, the range of wavelengths available for phasematched generation using temperature tuning (at a given crystal orientation) is rather restricted compared with that using angle tuning alone. This is perhaps not surprising, since the variation of refractivity with temperature and dispersion is always small and so any tuning using this effect alone would require a very large temperature variation to be useful compared with other methods. In addition, the range of wavelengths over which temperature tuning can be achieved is always greater than that for angle tuning alone, because even at the wavelength limit for angle tuning, temperature tuning can still be obtained.

The main difficulty involved in temperature tuning is that of maintaining a uniform crystal temperature, both long term in bulk and locally within the region of the beam. At a given orientation and temperature of an ADA crystal, for example, the bandwidth over which the fundamental and SH remain phasematched is about 0.1nm, and within this range a frequency stability may need to be typically 0.002nm scanned over a range of 0.02nm, [14]. Thus, in order that a frequency scan may be achieved over this range without being influenced by phase mismatch within

the crystal, the crystal temperature must be maintained to a bulk accuracy of $\pm 0.05^{\circ}C$. Local heating effects due to absorption of the fundamental beam can also lead to loss of phasematching at high intracavity powers. This has been discussed in further detail by Ferguson and Dunn [14].

The temperature tuning capabilities of the materials considered in this work are now examined.

For LFM there is negligible differential change of refractivities with change of temperature, and so only angle tuning is possible.

For Urea, the temperature tuning dependence has been determined [11] as -0.013nm/K, compared with 0.05nm/K for potassium dihydrogen phosphate (KDP) and 0.37nm/K for ADA [11,14]. Thus Urea is not likely to be a suitable candidate for temperature tuning either, since the crystal would have to be cooled to $-60^{\circ}C$ to phasematch at 1nm below its angular phasematched point at room temperature. The practical lower limit of fundamental wavelength is thus no less than 473nm, (at $-60^{\circ}C$, $\theta_m = 90^{\circ}$, Type I). At lower temperatures the technical difficulties would outweigh the benefits gained over the use of other materials.

ADA offers the best choice of material for temperature tuning. It will phasematch with $\theta_m = 90^{\circ}$ at 585nm and $20^{\circ}C$, and the UV may be tuned over the range 292nm to 302nm by varying the crystal temperature from $15^{\circ}C$ to $85^{\circ}C$ [14] while maintaining noncritical phasematching. As

2F1 discussed later, however, it is not suitable for use in the greeen or blue regions, unlike LFM or Urea.

2-1-6 SHG within laser cavities

Because SHG is quadratically dependent upon fundamental laser power, it is advantageous to insert a nonlinear crystal within a laser cavity where the electric field is high. However, such an inclusion introduces two additional considerations into the laser design. The first involves the focusing of the intracavity beam within the crystal to enhance the SHG still further. Such focusing must be carried out so as to maintain the stability of the laser resonator, as described in Chapter 1, and may also involve additionl effects within the crystal itself, such as thermal lensing. The second consideration is that the additional optical elements within the laser cause additional losses, both from absorption and scattering and also from the conversion of fundamental power to second harmonic. This can have a serious effect on the intracavity power, particularly if the laser is operating near threshold.

2-1-6-1 Focusing effects

A detailed discussion of most aspects of SHG in the presence of focused beams is given by Boyd and Kleinmann [15] and only a brief summary is therefore given here.

The fundamental beam within the crystal is assumed to be a

Gaussian intensity distribution with a beam waist radius of w_o. Two parameters are then used to describe the interaction of the beam with the crystal:

$$\xi = \frac{L}{b} = \frac{L}{w_o^2 k_1} = \frac{L\lambda_1}{2\, n_1 w_o^2} \qquad (31)$$

where ξ is called the focusing parameter, L is the crystal length, and b is the confocal parameter of the beam, equal to $w_o^2 k_1$, where k_1 $(=2\pi n_1/\lambda_1)$ is the wavenumber of the fundamental beam within the crystal, and:

$$B = \frac{1}{2}\rho\sqrt{Lk_1} \qquad (32)$$

where B is termed the double refraction parameter and ρ is the walkoff angle.

Boyd and Kleinmann collected all the optimisable parameters of the SHG interaction within a single function, "h", which they then proceeded to optimise for the case of zero absorption and the beam focused at the centre of the crystal. This process reduced the dependence of h to two variables, B and ξ. The variation of $h_m(B,\xi)$, where the subscript "m" represents optimisation, was computed for various values of B and ξ, and their graphs are shown in Fig 2-2a. It is seen that for any value of B, the curves of $h_m(B,\xi)$ against ξ each have a single maximum, corresponding to an optimum value of ξ, ξ_m.

The value of ξ has its maximum of 2.84 when B = 0, and falls sharply to 1.92 at B = 1, and then reaches a limit of 1.392 when B > 6. Since the crystal length is

proportional to ξ, the optimum length reduces as B rises. This of course is expected, since B rises due mainly to increased walkoff, which means that the length of the crystal over which phasematching can occur is correspondingly reduced. The variation of ξ_m over the range of B = 0 to B = 6 is shown in Fig 2-2b, from Boyd and Kleinmann. This curve is defined by the maxima of Fig 2-2a.

The value of h_m at the peaks of the curves in Fig 2-2a is now considered. This then involves the double optimisation of both ξ and the absorption and position already considered. The variation of $h_m(B, \xi_m)$, here termed $h_{mm}(B)$ is given in Fig 2-2c.

Given the above assumptions of the Boyd and Kleinmann analysis regarding the optimisation, the earlier expression for the SH power, Eq.(20) eventually reduces to:

$$P_2 = \frac{\omega_1^2 d_{eff}^2 L e^{-\alpha L} P_1^2}{\varepsilon_o n_1 n_2 \lambda_1 c^3} h_m(B, \xi_m) \qquad (33)$$

where the possibility of a small absorption has been considered outwith the $h_{mm}(B)$ term by the expression $e^{-\alpha L}$, where α is the absorption coefficient, discussed more fully in a later section.

To illustrated the effect of walkoff and defocusing on the $h_m(B, \xi)$ term, we consider the case of a 1° walkoff in a 1.5cm crystal having a refractivity of 1.5 at 488nm. In such a case, B = 5 approximately, and even with optimum

2F4

focusing, $h_{mm}(B) = 0.13$ (from Fig 2-2c), and thus the SH power is only 13% of its maximum value in the absence of walkoff. The walkoff angle is of course determined by the dispersion and wavelength chosen, but a value of 1° is not untypical for many materials where critical phasematching is present. Alteration of the focus in such a case only serves to reduce the SH power still further, as $h_{mm}(B)$ has assumed optimum focusing in the first place.

2-1-6-2 Walkoff

When critical phasematching is used, the SH and fundamental beams do not overlap over the full length of the crystal, due to walkoff. Thus the length over which SHG takes place is not the full length of the crystal, but the aperture length, l_a, defined as the length of the crystal over which the two beams overlap. This is given in terms of the beam waist w_o and the walkoff angle ρ by:

$$l_a = \sqrt{\pi}.w_o/\rho \qquad (34)$$

Where there is significant walkoff, it is not correct to use the length of the crystal L, in the expression for SH power (20), but to use a more complex expression which depends on the relative sizes of L, l_a and l_f, the effective length of focus in the crystal. A detailed analysis requires the use of numerical integration, discussed fully in [15] and [16]. However, where there is considerable walkoff, and $l_a << L$, it is appropriate to

replace L^2 by Ll_a in (20), (at least approximately), that is, to regard SHG to take place only within the aperture length. As L rises, however, the value of the double refraction parameter B also rises, and thus does the optimum beam waist which increases l_a providing that optimum focusing is maintained.

By combining (31) with (34), we obtain:

$$l_a = \frac{1}{\rho}\sqrt{\frac{L\lambda_1}{2n_1\xi}} \qquad (35)$$

which illustrates the point thus: as L rises, so does B, in proportion to $\sqrt{L}$. This also increases the optimum value of ξ, but once B is larger than about 2, ξ_m varies very little. Thus in the presence of significant walkoff, ξ can be regarded as more or less constant in the above expression, and an increase in crystal length results in a rather smaller increase in SH power, which is then influenced by further absorption.

Hence, in these circumstances, it is the aperture length, l_a, which is the limiting factor in SHG, and not the size of the crystal itself.

For a 1.5cm crystal with a refractivity of 1.5 at 488nm, a walkoff of 1° yields an aperture length of about 2mm, and for the case of LFM, where at this wavlength the walkoff is about 8°, it is about 0.3mm. Clearly, therefore, in the absence of noncritical phasematching, or a close approximation to it, the choice of crystal length is determined by the optical requirements of the laser as a whole, for example in terms of the dimensions of the

Z-fold, rather than by any SHG considerations, unless the two aspects yield comparable optimum sizes for the crystal. A discussion of the optimum crystal size in the case of zero walkoff is presented very comprehensively in [17].

2-1-6-3 Thermal effects

If the material of a nonlinear crystal absorbs even slightly at the fundamental wavelength then a nonuniform temperature profile is set up in the crystal across the width of the beam. Since refractivity is normally temperature dependent, this causes a loss of optimum phasematching as the power of the fundamental rises. This has been analysed in detail by Okada and Ieiri [18] and others, who define a characteristic power P_T, above which thermal effects become significant, namely:

$$P_T = \frac{\lambda_1 k_T}{\alpha_1 L \beta_T} \qquad (36)$$

where k_T is the thermal conductivity, α_1 the absorption per unit length of the fundamental and β_T concerns the change of refractivity with temperature, given by:

$$\beta_T = \frac{dn_2}{dT} - \frac{dn_1}{dT} \qquad (37)$$

Typical values for a nonlinear material such as ADP yield a value of P_T of the order of a few watts CW, a value confirmed experimentally for ADA by Ferguson and Dunn

[14]. For pulsed (or chopped CW) lasers, with a duty cycle well below 1:50, pulse powers of a few hundred watts may be accommodated without thermal degradation of the SH [19].

For all the lasers described here, powers of less than 2W CW or of a few hundred watts in very short pulses are used, and no thermal effects have been observed at the crystals.

2-1-6-4 Crystal absorption

The contribution made by crystal absorption to both the threshold and maximum SH output has been analysed by Zernike and Midwinter [1] and by Ferguson and Dunn [17], in particular for the case of a homogeneously broadened active medium, such as in a dye laser, both with and without thermal effects within the crystal.

For the case of a four level laser, such as a dye laser, operating with an intracavity frequency doubling crystal, whose absorption is α_1 per unit length at the fundamental wavelength, an optimum length of crystal can be deduced for the special case of noncritical phasematching, no thermal effects within the crystal and optimum focusing, as:

$$L_{opt} = \frac{\beta \gamma}{(\eta + \alpha_1 \beta)} \qquad (38)$$

where we have:

$$\eta = \frac{\omega_1^2 d_{eff}^2 h_m(B,\xi)}{\varepsilon_o n_1 n_2 c^3 \lambda_1}$$

γ = the loss in the cavity due to mirrors and other elements, including Fresnel losses from the crystal and cell but not absorption or conversion to SH,

and

$$\beta = \frac{\tau \sigma_e}{\pi w_o^2 h \nu_e}$$

where τ = upper laser level lifetime

σ_e = molecular cross-section for emission

ν_e = lasing frequency

w_o = beam waist radius

h = Planck's constant

Here, we have: $h_m(B,\xi) = h_{mm}(0) = 1.068$.

For this ideal case, graphs of L_{opt} have been prepared in [17] as a function of various parameters such as crystal absorption, and, where thermal effects are also included, the pumping power, which does not affect L_{opt} in the absence of thermal phase mismatch.

The above expression for L_{opt} can be used to determine the maximum generated SH power for a crystal of that length, namely:

$$P_2 = \frac{1}{\beta}\left[\sqrt{\delta + \alpha_1\left(\frac{1}{\eta} - L_{opt}\right)} - \sqrt{\frac{\gamma(\eta + \alpha_1\beta)}{\eta}}\right]^2 \qquad (39)$$

where here we have:

$$\delta = \frac{\tau N_o \sigma_p P_p \sigma_e t}{\pi w_o^2 h \nu_p}$$

and N_o = ground state population,

σ_p = absorption cross-seciotn

P_p = pumping power

t = thickness of the dye jet

ν_p = pumping frequency

Where absorption is zero, ($\alpha_1 = 0$), then (39) reduces to:

$$P_2 = \frac{1}{\beta}(\sqrt{\delta} - \sqrt{\gamma})^2 \qquad (40)$$

This discussion applies only for the case of noncritical phasematching and the theory has been thoroughly tested experimentally [1,13]. However, for the case of materials such as LFM or Urea, which, at the wavelengths of interest in this work require critical phasematching, a rather more complex set of factors must be considered.

Firstly, since there is significant walkoff in the critical phasematching case, the value of the double refraction parameter B is large and thus even with optimum focusing, $h_{mm}(B)$ is less than one tenth of its value in the noncritical case. This then affects the value of η, ostensibly to decrease it and thus to increase the value of L_{opt}. However, an increase of B leads to a decrease of ξ, though for $B > 5$ the value of ξ is more or less constant. This means that the focusing is stronger, with w_o smaller, though only by a factor of 2 from the maximum optimum value. Hence, with larger B, β rises by up to a

factor of 4 at the same time as η falls by up to a factor of 10. Even with absorption present (up to a few %), this causes the optimum length

$$L_{opt} = \frac{\beta\gamma}{(\eta + \alpha_1\beta)} \qquad (38)$$

to rise by up to 40 times for walkoff of even a few degrees. Clearly this is unrealistic, and the theory must be modified heavily to remove the assumption that the SHG takes place over the full length of the crystal. As shown earlier, it is more correct to consider the generation to take place only over the aperture length l_a, which is of the order of millimetres for the cases of LFM and Urea as used here.

The crux of this aspect of the discussion, then, is that the effect of crystal absorption on SH power is negligible if there is significant walkoff due to critical phasematching, since it is the walkoff which affects the generation far more than any other feature of the laser. Thus for intracavity SHG around 486nm with LFM and Urea, crystal absorption will be ignored.

2-2 Second Harmonic Materials

Many materials have been studied in the context of SHG, and have been extensively reported in respect of their refractivities, and the nonvanishing elements of their nonlinear tensor, [4, Table 18.2 and references therein].

Almost all the materials have been examined at the longer

wavelength visible or infrared spectrum, usually at the fundamental or second harmonic wavelength of a Nd:YAG laser. However, only a few have proved suitable for SHG from the blue or blue-green spectrum, due firstly to their low conversion efficiencies at these wavelengths and secondly to their UV absorption bands, which often lie above the second harmonic wavelength. In addition, many materials are unable to achieve phasematching to SH at short enough wavelengths.

Two materials which appear to be particularly suitable in the region of 480nm, however, are lithium formate monohydrate (LFM), $LiCOOH.H_2O$, and Urea $CO(NH_2)_2$. At longer wavelengths the most popular materials are ammonium dihydrogen arsenate (ADA), which will be discussed in detail later along with LFM and Urea, ammonium or potassium dihydrogen phosphate (ADP, KDP), lithium iodate ($LiIO_3$) and potassium pentaborate (KB5).

Most of these materials cover the range of SH down to 250nm by angle or temperature tuning, but further into the UV the SH performance deteriorates somewhat. The short wavelength limit for KDP at room temperature is 259nm. For ADP this limit is about 262nm, and the material can only operate at shorter wavelengths by cooling, to a limit of 244nm at $-125^{\circ}C$ [20]. In such a crystal of ADP, critical phasematching is present. ADA, however, can use noncritical phasematching at similar wavelengths, when the SH power is more than an order of magnitude greater [19]. KB5 will phasematch to as low as 217nm [21] but its nonlinear coefficient is very small, and an order of magnitude less then for many other materials, such as ADA.

The nonlinear coefficient of a material is not the only consideration, however. Absorption of the generated SH can in some cases make an apparently useful material yield very little output, and physical properties and conditions such as temperature and purity of the crystal may also be important. For example, we compare ADP and LFM. The overall conversion efficiency is three to five times greater for ADP than for LFM [20,22] and so ADP would seem a better choice of material. However, in order to obtain phasematched SHG at below 262nm, an ADP crystal must be refrigerated, a process which is not necessary for LFM. Even under refrigeration, ADP will only generate SH to 244nm, whereas LFM will operate as low as 237.5nm [20], and so although at shorter wavelengths self absorption of the SH becomes a significant factor, practical considerations dictate that LFM should be used below 262nm.

Also relevent is second harmonic walkoff. This is the effect that the ray directions of the fundamental and SH are not the same unless the generation is taking place in a plane normal to the optic axis of the crystal. The special case of noncritical phasematching is also that of zero walkoff, and as a result the generation of SH is considerably improved compared with the general case, as already illustrated. Thus another feature to be considered in the choice of nonlinear material is whether or not noncritical phasematching is possible in the spectral range concerned. If it is, then tuning of the laser must be carried out by varying the crystal temperature. If the temperature tuning effects are small, as for example in the case of Urea, then the

H3

material may only be useful for SHG close to the noncritical phasematch point. As an example, we consider ADA and ADP. For a wavelength of 590nm, ADP will phasematch with a wave propagating at 64° to the optic axis, and making an angle of 45° with both the X and Y axes, [22]. The walkoff is then 25mrad [19]. For ADA at the same wavelength, phasematched propagation at 90° to the optic axis is possible at a temperature of 33°C [14], making ADA much more favourable as a nonlinear material in this spectral range. However, if the application of the generated UV involves a tuning range greater than about 0.1nm then the temperature of an ADA crystal must be altered to maintain the phasematching. ADP, on the other hand, has a tuning range ten times larger than ADA at a given temperature and crystal orientation, (discussed further in [14]), making it more suitable when large scans of wavelength are required, despite the lower powers available for a given crystal size.

Urea and LFM both offer advantages over the more common nonlinear materials in the wavelength ranges 237nm to 262nm for LFM and 237nm upwards for Urea.

LFM has an absorption of greater than 50% for wavelengths below 237nm [6], and so we take this as an effective cutoff, even though outputs have been reported as low as 225nm [20]. Room temperature angle tuned phasematching is possible up to 262nm, where ADP, which is then more efficient, has its 90° phasematching point. Eventually, moving into the near infrared, LFM becomes more efficient than ADP [22].

Urea is about 90% transmitting from the visible down to about 200nm [11] and is thus not only suitable for SHG but also for wave mixing experiments, such as described in [11], which yield outputs as low as 228.8nm with good efficiency.

As a consequence of its different structure from LFM, Urea does have two 90° phasematch points in the visible spectrum, at about 474nm and 597nm, depending on the type of phasematching used. However, unlike ADA and ADP, Urea is only feebly sensitive to temperature tuning, (about 1/30 of that of ADA [11,14]), and for SHG to below 237nm, a wave mixing scheme must be used. Halbout et al [11] have compared ADP and Urea for equivalent phasematching schemes, and have shown that, except close to the 90° point of ADP, Urea is more efficient, by a factor of up to about five times for identical sized crystals and at wavelengths above 600nm. From 600nm to 524nm, Urea is on average twice as efficient as ADP.

Thus we can see that investigation of LFM and Urea at fundamental wavelengths below 524nm is likely to yield useful results. Chapter 3 will deal in detail with LFM and Chapter 6 will present the findings concerning Urea.

2-2-1 LFM

Extensive measurements have been made of the refractivities of LFM along all three principal axes, and have been reported by Singh et al [6] and by Naito and Inaba [12]. The latter covers a much larger range of

wavelengths than Singh, and should be considered rather more reliable, for reasons discussed shortly. Singh has reported measurements of the nonlinear optical susceptibility and nonlinear tensor coefficient d_{24} (= d_{32}) as compared with α-quartz, giving a value of d_{24} = 1.27pm/V using single crystals, though application of the material in a frequency doubled laser was not obtained. Subsequently, Dunning et al [20] obtained pulsed UV from LFM crystals, using a pulsed dye laser to pump a sealed cell dye laser, whose output was then passed to the LFM crystal.

The phasematching data used by Dunning was taken from Singh's paper, which produced a dispersion formula of the form:

$$n^2 = 1 + S_o \lambda^2/(\lambda^2 - \lambda_o^2) \qquad (41)$$

where for the three axes the values of S_o and λ_o are as follows:

	S_o	λ_o (in microns)
X	0.8415	0.0953
Y	1.14106	0.1183
Z	1.2454	0.12496

This formula was based upon experimental data in the range 460nm to 1060nm, covering only 9 values of wavelength.

The calculation of phasematch angle for any type of matching in the region of 480nm requires the values of refractivity at around 240nm, and we feel that it is not satisfactory to extrapolate the range of (41) by this

degree, particularly as dispersion normally increases at shorter wavelengths. As will be shown in Chapter 3, there is experimental evidence that this belief is justified.

The work of Naito and Inaba, however, uses experimental data over the entire range 350nm to 1500nm, to produce a dispersion equation of the form:

$$n^2 = A + B\lambda^2/(\lambda^2 - \lambda_o^2) - C\lambda^2 \qquad (42)$$

where the values of A, B, C and λ_o are:

	A	B	C	λ_o(in microns)
X	1.4376	0.4045	0.0005	0.1301
Y	1.6586	0.5006	0.0127	0.1530
Z	1.6714	0.5928	0.0153	0.1592

In this case, extrapolation to a wavelength of 240nm or less must be far more reliable than on the basis of the data of Singh, and we have prepared graphs of the phasematch angle θ_m for Type I matching, measured with respect to the Z axis, using both (41) and (42) for refractivities and (27) for the value of θ_m.

Tables of values of θ_m and the refractivities from 200nm to 800nm, <u>based on (42) only</u>, are given in the Appendix 1. The graphs of phasematch angle against wavelength using the two different sets of refractivities are shown in Fig 2-3, where the comparison is for a beam propagating in the ZX plane and polarised along the Y axis. It is seen that for shorter wavelengths the two sets of results are in considerable disagreement, and results using a crystal of

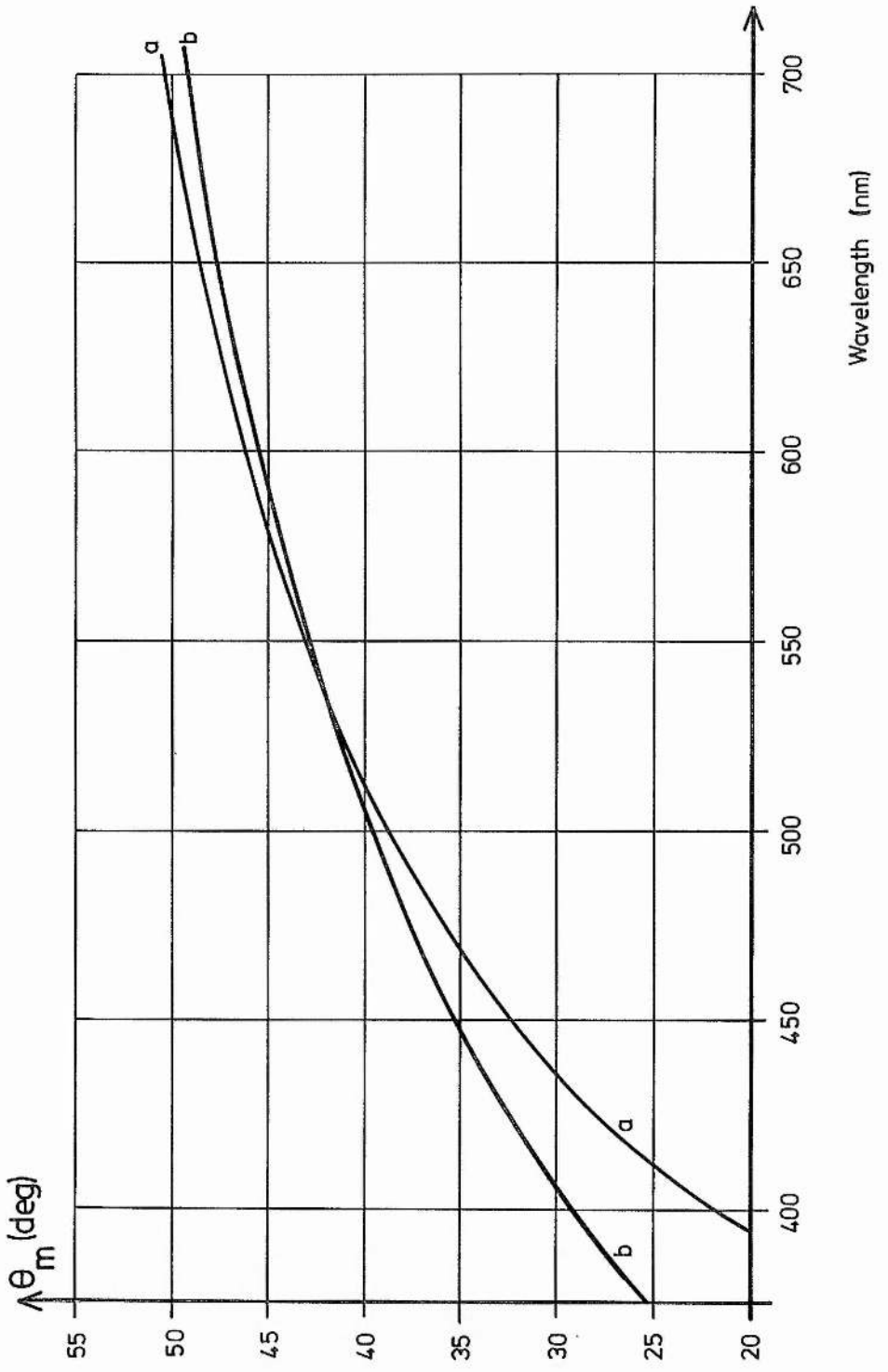

Fig 2-3: Graphs of phasematching angle, θ_m, for the two dispersion formulae; (a) Naito and Inaba [12], (b) Singh et al [6]

known orientation tend to support the results of Naito and Inaba rather than those of Singh (see Section 3-2-4).

The choice of Type I or Type II phasematching for LFM is made as follows. Using (42) to provide values of refractivity for use in (28), we find that for a beam propagating in the ZX plane, Type II is not possible for fundamental wavelengths below about 950nm, and for the ZY plane, the lower limit is about 410nm while the upper is 448nm. For Type I, the use of (27) applied to the ZY plane shows that for the entire range of wavelengths above 400nm, the value of $\sin^2(\theta_m)$ is negative and so the matching scheme is impossible. However, as shown in Fig 2-3 for Type I in the ZX plane, θ_m is real for all wavelengths above 400nm, although below about 470nm the SH is significantly absorbed by the crystal.

Thus the choice lies between Type I in the ZX plane and, for the range 410nm to 448nm only, Type II in the ZY plane. For these cases, the SH polarisations are given from (19) by:

$$\text{Type I} \quad : \quad P_{z2} = \varepsilon_o d_{32} E_y^2$$

$$\text{Type II} \quad : \quad P_{x2} = 2\varepsilon_o d_{15} E_x E_z$$

Measurements by Singh et al [6] have shown that d_{32} is much greater than d_{15}, and so even if we let $E_x = E_y = E_z$, which is often the case, the Type I scheme gives a very much greater SH polarisation where any choice exists, and above 448nm, Type I must be used anyway.

Thus the phasematching scheme for LFM around 480nm is that of Type I with the fundamental polarised as an ordinary wave E_y in the ZX plane, with the generated SH as an extraordinary wave E_z (Fig 2-4).

2-2-2 Urea

Bauerle et al [23] have made determinations of the refractivities, absorption and nonlinear coefficients of Urea, based on earlier work by Kurtz and Perry [24] and have also obtained phasematched SHG in single crystals. More recently, Halbout et al [11] and Cassidy et al [9] have used Urea as a SHG and mixing material, using a pulsed dye laser and and a CW argon ion laser operating on discrete lines between 488nm and 528nm. None of the experiments reported has used Urea as an intracavity frequency doubling element.

The variation of refractivity for Urea is given by the following expressions, determined from data in [11]:

$$n_o^2 = 2.1678 + 0.0139/(\lambda^2 - 0.0207)$$

$$n_e^2 = 2.4917 + 0.0141/(\lambda^2 - 0.0240) \qquad (43)$$

(λ in microns)

The phasematch angle is then determined from (24) or (25) as required. The shortest wavelength at which Type II is possible is 599.9nm and so this type will not be considered further here. For Type I, the limit is 474nm, and the material is 90% transmitting to well below the SH. Thus for generation of tunable UV down to as low as 240nm,

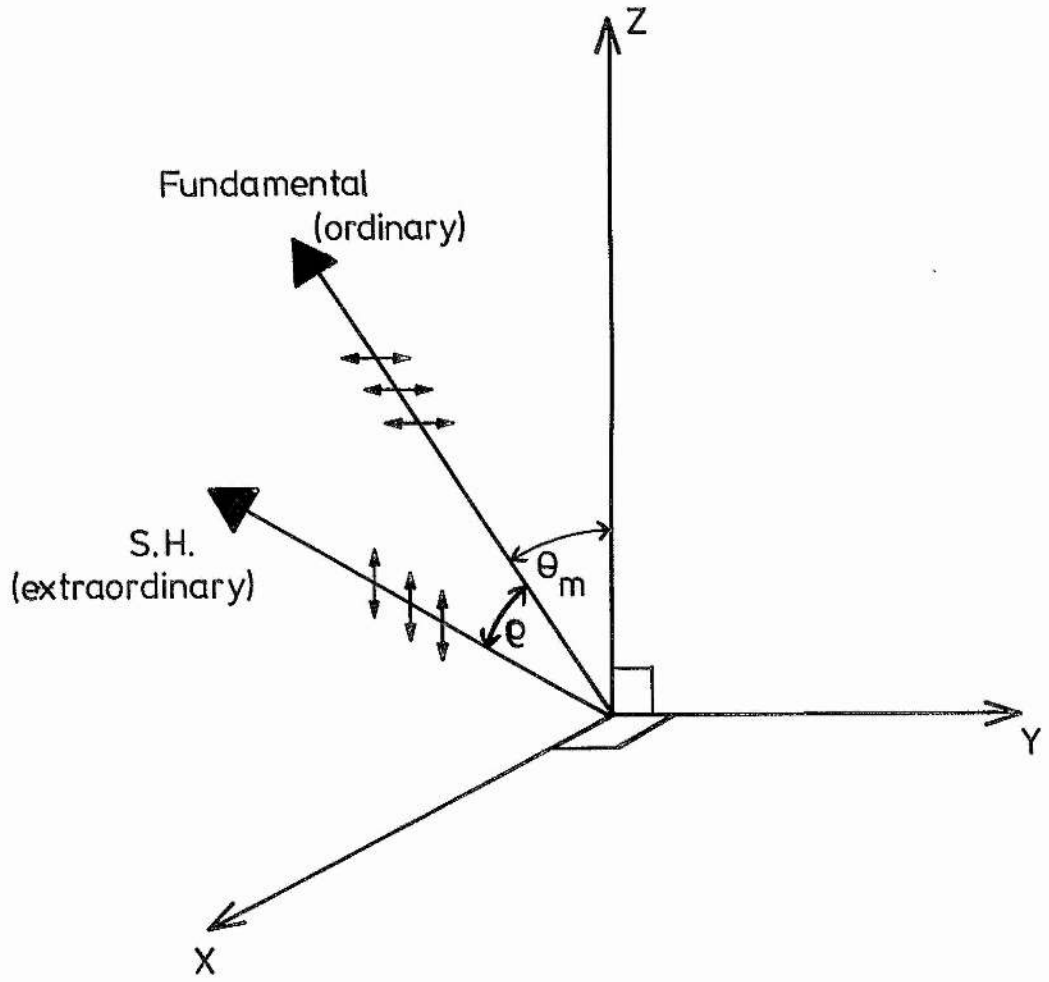

Fig 2-4: Ray propagation in LFM

(allowing for the falloff in efficiency, 237nm is the lower limit), Urea is particularly suitable. The material is also highly resistant to optical damage [25] which is an important feature if intracavity frequency doubling is to be attempted (the damage threshold exceeds 4kW into a 10 micron spot at 355nm).

The analysis of the phasematching possibilities for Urea is simpler than for LFM as the crystal is uniaxial. The SH power is given, from (33) in the case of zero absorption, by:

$$P_2 = \frac{\omega_1^2 L\, h_m(B,\xi)}{\varepsilon_o n_1 n_2 \lambda_1 c^3}\, d_{eff}^2\, P_1^2 \qquad (44).$$

Being a positive type crystal, the effective nonlinear coefficient, d_{eff} , depends on $\sin(2\theta_m)$ rather than on $\sin(\theta_m)$ and is given by:

$$d_{eff} = d_{14} \sin(2\theta_m)\cos(2\phi)$$

where ϕ is the angle the plane containing both the ray and the optic axis makes with the X axis. Thus to maximise P_2 , we require $\phi = 0$ or $90°$, i.e. the beam must propagate in the ZX or ZY planes.

The value of θ_m is of course determined by the wavelength required, but, unlike the case of a negative uniaxial material, the SH power decreases as θ_m approaches $90°$, due to the $\sin^2(2\theta_m)$ term in the expression for P_2 . Furthermore, as θ_m varies from $90°$ towards $45°$ the walkoff of the SH increases, so acting to reduce the generation efficiency.

P_2 can be written as:

$$P_2 \propto \frac{h_m(B,\xi)\ \sin^2(2\theta_m)}{n_1\, n_2\, \lambda_1^3} \qquad (45)$$

We term the right hand side of (45) the power parameter, and it may be evaluated as a function of wavelength to examine the competing effects of walkoff and the $\sin^2(2\theta_m)$ term.

A computer programme to do this was written, which took as input a value of wavelength. The refractivities, phasematching angle and double refraction parameter were then evaluated using (43), (24) and (32) respectively, and printed. The value of $h_{mm}(B)$ could then be found by use of Fig 2-2c and supplied to the computer. This step was necessary as there is no <u>simple</u> analytical relation between B and $h_{mm}(B)$. In using $h_{mm}(B)$, we also assume that optimum focusing is maintained at the crystal. The value of the power parameter was then determined by the programme, and the process continued for all wavelengths over which phasematching is possible.

The resulting graph is shown in Fig 2-5 and shows clearly that below 490nm the $\sin^2(2\theta_m)$ predominates ($\sin^2(2\theta_m)$ = 0.35 at 490nm) and reduces the UV generation very sharply, while the change is very much smaller over the range 500nm to 600nm, namely about 8%.

For the range 300nm to 800nm the refractivities, phasematching angles and walkoff angles (for Type I in the

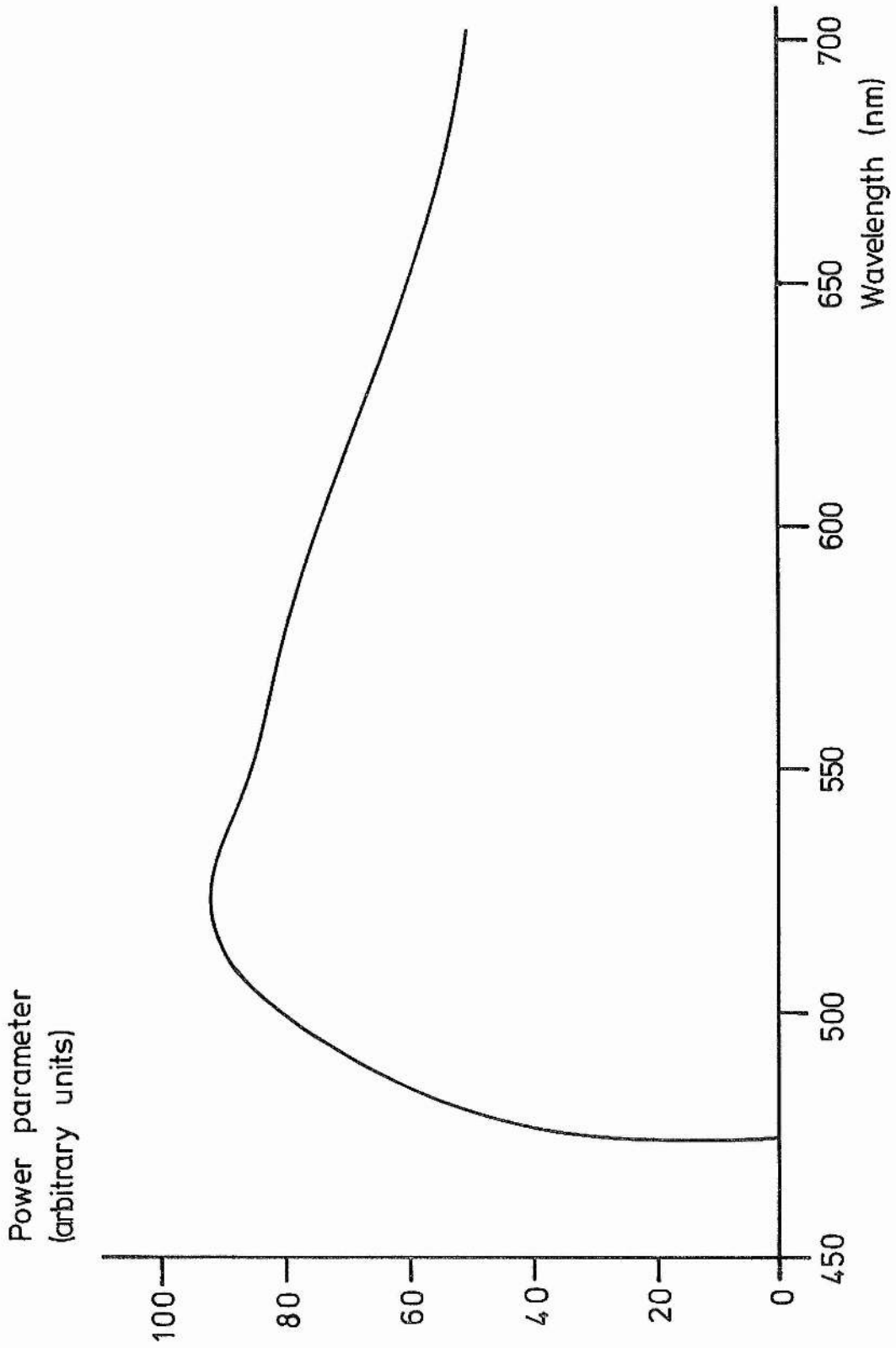

Fig 2-5: "Power parameter"(see Eq.44) for Urea

ZX plane) are given in Appendix 2. The graph of θ_m as a function of wavelength is shown in Fig 2-6. As Urea is a positive type crystal, the fundamental wave propagates as an extraordinary wave in the ZX plane and the SH as an ordinary wave E_y (Fig 2-7).

2-3-3 ADA

ADA is a negative uniaxial crystal, commonly used in frequency doubling Rhodamine 6G (Rh6G) dye lasers, being very efficient, readily temperature tunable, and having its noncritical phasematch point at 585nm (at 20°C). Many tens of milliwatts of tunable UV have been produced over the range 285nm to 315nm by several workers [14,17,26,27,28 and others], often in a single mode with linewidths less than 0.002nm. However, almost no data seems to have been published on the detailed optical properties of ADA, such as refractivity and dispersion. A selection of single wavelength measurements has been made [29,30,31], but we do not consider three measurements of the ordinary refractivity and two of the extraordinary are sufficient to generate a dispersion formula for use in determining phasematch angles as already described.

The first reported use of ADA as a doubling material was in 1976 by Frohlich et al [27] who used it within a Rh6G dye laser. It would seem that their design of crystal was then accepted by subsequent workers without further investigation, though how the original choice of ADA and its orientation was made is not clear. More recently (1980), Marshall et al [28] have produced improved values

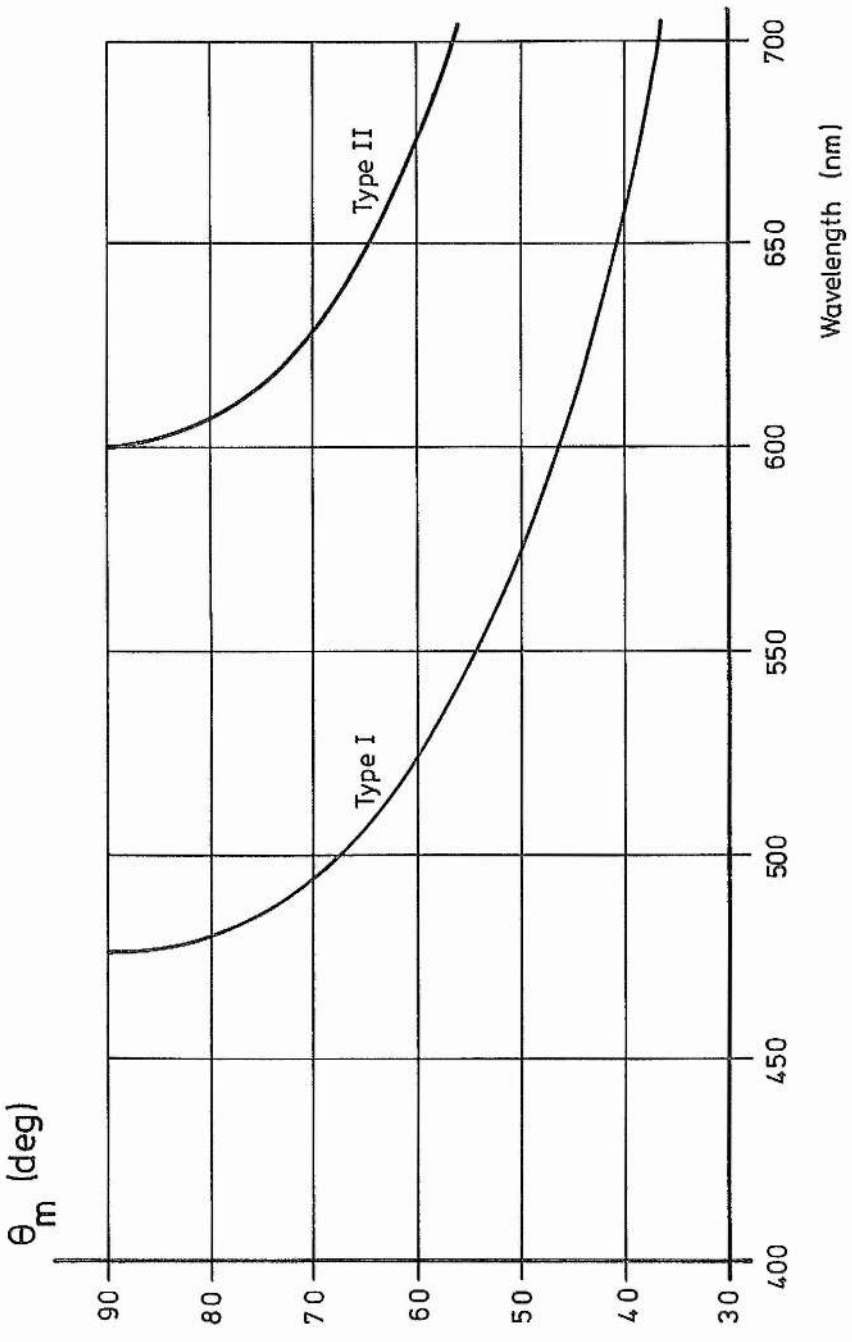

Fig 2-6: Phasematching angles for Urea

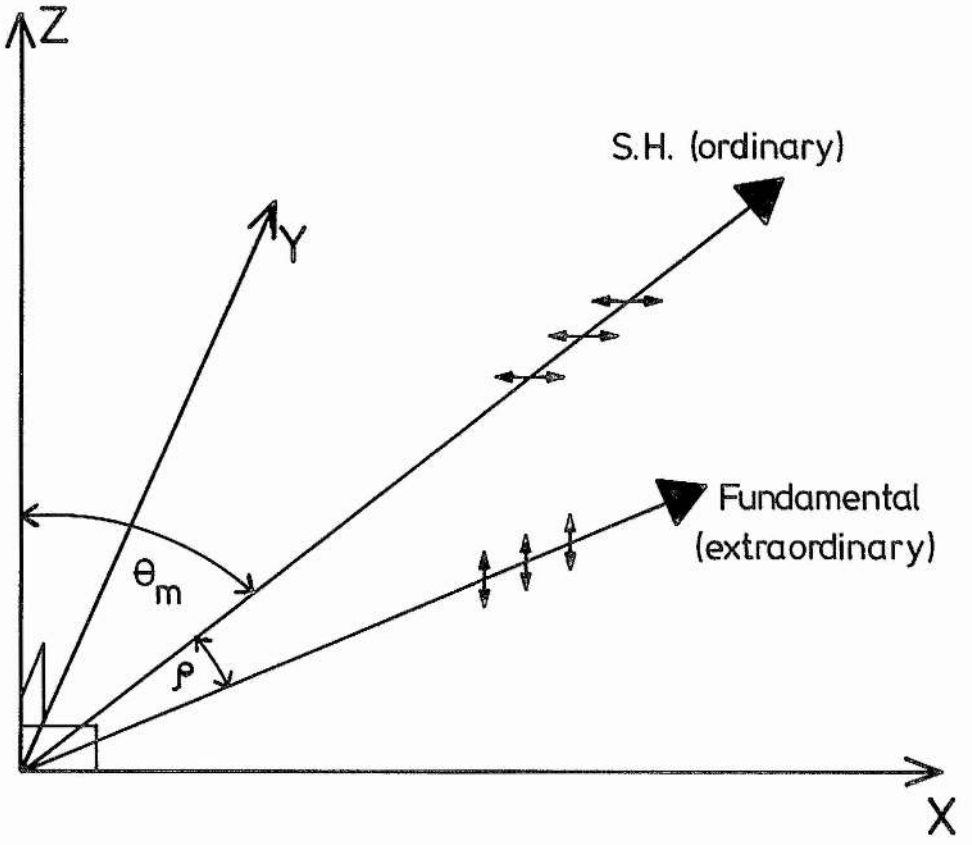

Fig 2-7: Ray propagation in Urea

of the Sellmeier constants, which fit closely their experimental observations. These yield a dispersion formula of the form:

$$n^2 = 1 + C\lambda^2/(\lambda^2-\lambda_o^2) \qquad (\lambda \text{ in microns})$$

where the values of the constants are:

	C	λ_o (microns)
ordinary ray	1.42969	0.113755
extraordinary ray	1.27100	0.111264

The phasematch angle is then found from:

$$\sin^2\theta_m = \frac{(n_{o2}^2 - n_{o1}^2)\, n_{e2}^2}{(n_{o2}^2 - n_{e1}^2)\, n_{o1}^2}$$

Since ADA has its 90° phasematch point within the tuning range of the Rh6G dye, the normal arrangement is to have the fundamental beam propagating as an equal mixture of X and Y components, and thus at 45° to both axes, with the electric vector polarised normal to the Z axis, being an ordinary ray (Fig 2-8). The SH is then the extraordinary ray, polarised parallel to the Z axis.

The crystal geometry is discussed more fully in Chapter 5, which deals with a pulsed Rh6G dye laser using ADA as the doubling material.

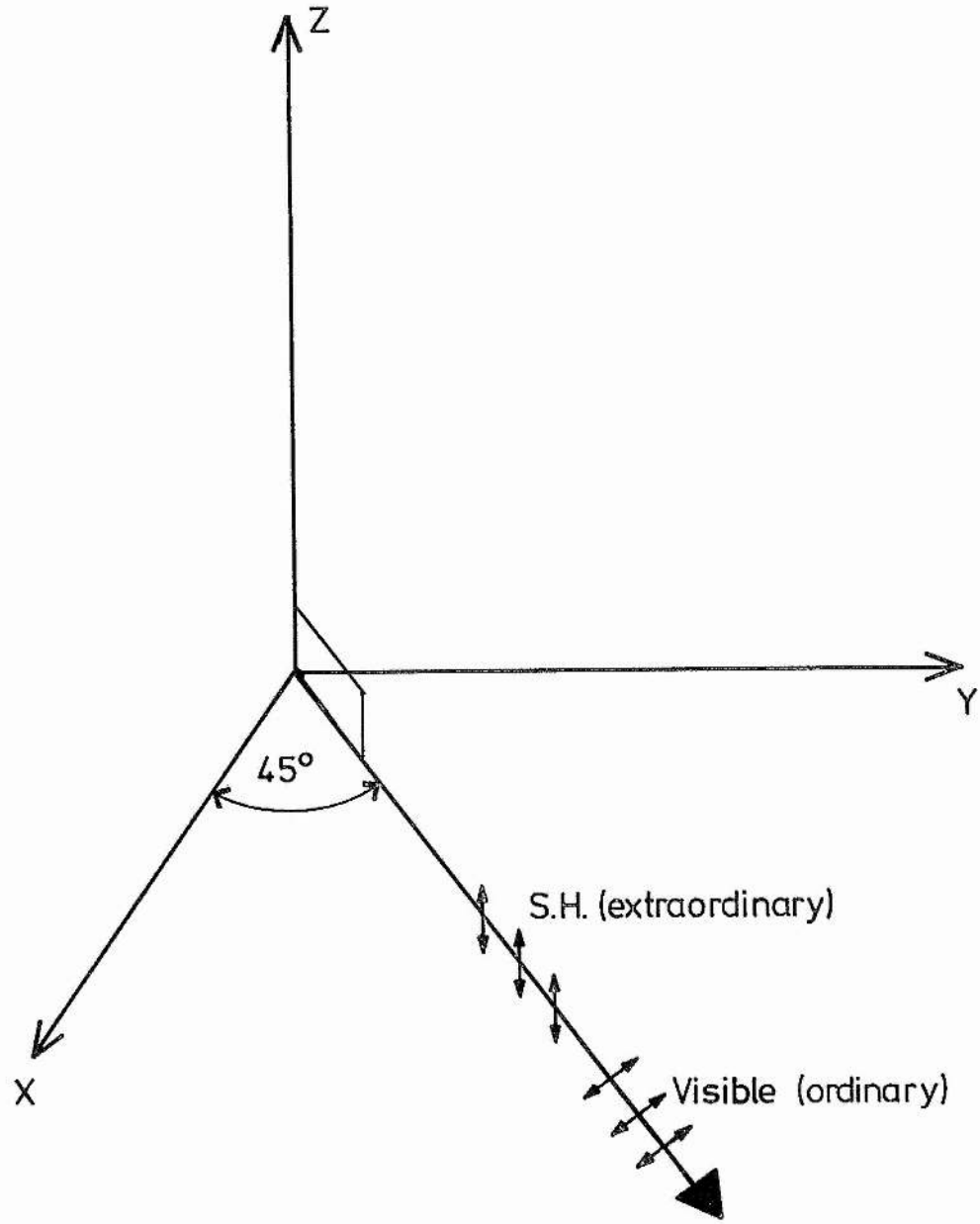

Fig 2-8: Ray propagation in ADA

EF1

REFERENCES CHAPTER 2

1 Zernike F, Midwinter JE; "Applied nonlinear optics" Wiley, New York, (1973)

2 Maker PD, Terhune RW, Nisenoff M, Savage CM; Phys Rev Lett 8 21-2 (1962)

3 Giordmaine JA; Phys Rev Lett 8 19-20 (1962)

4 Singh S; "Nonlinear optical materials" in "Handbook of lasers" 489-525

5 Singh S, Draegert DA, Geusic JE; Phys Rev D 2 (1970)

6 Singh S, Bonner WA, Potopowicz JR, Van Uitert LG; Appl Phys Lett 17 292-4 (1970)

7 Born M, Wolf E; "Principles of optics" Pergamon London (1959) Section 14.3.3

8 Hoben MV; J Appl Phys 38 4365-72 (1967)

9 Reference [7], page 673-4

10 Dewey HJ; IEEE J Quant Electr QE-12 303-6 (1976) {The formula for walkoff angle as quoted in this paper refers to KB5 and to a different set of axes to that used for LFM, but the relevent formula may be obtained by a cyclic rotation of X, Y and Z}

11 Halbout J-M, Blit S, Donaldson W, Tang CL; IEEE J Quant Electr QE-15 1176-9 (1979)

12 Naito H, Inaba H; Optoelectronics 5 256-9 (1973)

13 Ferguson AI; PhD thesis, University of St Andrews (1977)

14 Ferguson AI, Dunn MH; Opt Commun 23 177-182 (1977)

15 Boyd GD, Kleinman DA; J Appl Phys 39 3597-3639 (1968)

16 Boyd GD, Askin JM, Dziedzic JM, Kleinman DA; Phys Rev 137 A1305-20 (1965)

17 Ferguson AI, Dunn MH; IEEE J Quant Electr QE-13 751-6 (1977)

18 Odaka M, Ieiri S; IEEE J Quant Electr QE-7 469 (1971)

19 Ferguson AI, Dunn MH, Maitland A; Opt Commun 19 10-13 (1976)

20 Dunning FB, Tittel FK, Stebbings RF; Opt Commun 7 181-3 (1973)

REFERENCES CHAPTER 2 (cont)

21 Dewey CF, Cook WR, Hodgson RT, Wynne JJ;
Appl Phys Lett 26 714-6 (1979)

22 Gabel C, Hercher M; IEEE J Quant Electr QE-8 850-1
(1972)

23 Bauerle D, Betzler K, Hesse H, Kapplian S, Loose P;
Phys Stat Sol(a) 42 K119-121 (1977)

24 Kurtz SK, Perry TT; J Appl Phys 39 3798 (1968)

25 Cassidy C, Halbout J-M, Donaldson W, Tang CL;
Opt Commun 29 243-6 (1979)

26 Wagstaff CE, Dunn MH; J Phys D 12 355-68 (1979)

27 Frohlich D, Stein L, Schroeder HW, Welling H;
Appl Phys 11 97 (1976)

28 Marshall CM, Stickel RE, Dunning FB, Tittel FK;
Appl Opt 19 1980-83 (1980)

29 Orszag M; Opt & Quant Electr 8 295 (1976)

30 Winchell AN; "Microscopic characteristics of
artificial minerals" Wiley New York (1931)

31 Beasley JD; Appl Opt 10 1934-6 (1971)

Appendix 1

Refractivities and phasematching angles for LFM

lambda nm	Nx	Ny	Nz	theta deg
200	1.46246	1.69263	1.81349	0.00
202	1.45904	1.68296	1.79873	0.00
204	1.45581	1.67401	1.78520	0.00
206	1.45274	1.66570	1.77274	0.00
208	1.44984	1.65797	1.76124	0.00
210	1.44708	1.65076	1.75060	0.00
212	1.44445	1.64402	1.74071	0.00
214	1.44195	1.63770	1.73151	0.00
216	1.43957	1.63178	1.72293	0.00
218	1.43730	1.62620	1.71490	0.00
220	1.43513	1.62096	1.70737	0.00
222	1.43306	1.61600	1.70031	0.00
224	1.43108	1.61132	1.69366	0.00
226	1.42918	1.60689	1.68740	0.00
228	1.42736	1.60270	1.68149	0.00
230	1.42562	1.59871	1.67590	0.00
232	1.42395	1.59493	1.67061	0.00
234	1.42234	1.59133	1.66559	0.00
236	1.42080	1.58790	1.66083	0.00
238	1.41931	1.58464	1.65631	0.00
240	1.41789	1.58152	1.65200	0.00
242	1.41651	1.57854	1.64790	0.00
244	1.41519	1.57570	1.64399	0.00
246	1.41391	1.57297	1.64026	0.00
248	1.41268	1.57036	1.63669	0.00
250	1.41149	1.56786	1.63328	0.00
252	1.41034	1.56546	1.63002	0.00
254	1.40923	1.56316	1.62689	0.00
256	1.40816	1.56094	1.62389	0.00
258	1.40712	1.55881	1.62101	0.00
260	1.40612	1.55677	1.61825	0.00
262	1.40515	1.55479	1.61559	24.01
264	1.40421	1.55290	1.61304	21.29
266	1.40330	1.55107	1.61058	18.46
268	1.40242	1.54930	1.60821	15.43
270	1.40156	1.54760	1.60593	12.04
272	1.40073	1.54595	1.60373	7.76
274	1.39993	1.54436	1.60161	0.00
276	1.39915	1.54283	1.59956	0.00
278	1.39839	1.54134	1.59759	0.00
280	1.39765	1.53990	1.59568	0.00
282	1.39694	1.53851	1.59383	0.00
284	1.39624	1.53717	1.59204	0.00
286	1.39557	1.53586	1.59031	0.00
288	1.39491	1.53459	1.58864	0.00
290	1.39427	1.53337	1.58702	0.00
292	1.39364	1.53218	1.58545	0.00
294	1.39304	1.53102	1.58392	0.00
296	1.39245	1.52990	1.58244	0.00
298	1.39187	1.52881	1.58101	0.00

Appendix 1

Refractivities and phasematching angles for LFM

lambda nm	Nx	Ny	Nz	theta deg
300	1.39131	1.52775	1.57962	0.00
302	1.39077	1.52673	1.57827	0.00
304	1.39023	1.52573	1.57696	0.00
306	1.38971	1.52475	1.57568	0.00
308	1.38921	1.52381	1.57444	0.00
310	1.38871	1.52289	1.57324	0.00
312	1.38823	1.52199	1.57206	0.00
314	1.38776	1.52112	1.57092	0.00
316	1.38730	1.52027	1.56981	0.00
318	1.38685	1.51944	1.56873	0.00
320	1.38642	1.51864	1.56768	0.00
322	1.38599	1.51785	1.56665	0.00
324	1.38557	1.51708	1.56565	0.00
326	1.38516	1.51633	1.56468	0.00
328	1.38476	1.51560	1.56373	0.00
330	1.38437	1.51489	1.56280	0.00
332	1.38399	1.51419	1.56190	0.00
334	1.38362	1.51351	1.56101	0.00
336	1.38325	1.51285	1.56015	0.00
338	1.38289	1.51220	1.55931	0.00
340	1.38254	1.51157	1.55849	0.00
342	1.38220	1.51095	1.55769	0.00
344	1.38187	1.51035	1.55691	0.00
346	1.38154	1.50975	1.55614	0.00
348	1.38122	1.50918	1.55539	0.00
350	1.38090	1.50861	1.55466	0.00
352	1.38059	1.50806	1.55394	0.00
354	1.38029	1.50751	1.55324	0.00
356	1.37999	1.50698	1.55256	0.00
358	1.37970	1.50647	1.55189	0.00
360	1.37942	1.50596	1.55123	0.00
362	1.37914	1.50546	1.55059	0.00
364	1.37887	1.50497	1.54996	0.75
366	1.37860	1.50449	1.54935	5.10
368	1.37834	1.50403	1.54875	7.17
370	1.37808	1.50357	1.54816	8.78
372	1.37782	1.50312	1.54758	10.13
374	1.37758	1.50268	1.54701	11.32
376	1.37733	1.50225	1.54645	12.41
378	1.37709	1.50182	1.54591	13.40
380	1.37686	1.50141	1.54538	14.32
382	1.37663	1.50100	1.54485	15.19
384	1.37640	1.50060	1.54434	16.00
386	1.37618	1.50021	1.54383	16.78
388	1.37596	1.49982	1.54334	17.52
390	1.37574	1.49944	1.54286	18.23
392	1.37553	1.49907	1.54238	18.90
394	1.37533	1.49871	1.54191	19.55
396	1.37512	1.49835	1.54145	20.18
398	1.37492	1.49800	1.54100	20.79

Appendix 1

Refractivities and phasematching angles for LFM

lambda nm	Nx	Ny	Nz	theta deg
400	1.37473	1.49765	1.54056	21.37
402	1.37453	1.49731	1.54013	21.94
404	1.37434	1.49698	1.53970	22.49
406	1.37416	1.49665	1.53928	23.02
408	1.37397	1.49633	1.53887	23.54
410	1.37379	1.49601	1.53846	24.04
412	1.37361	1.49570	1.53807	24.53
414	1.37344	1.49540	1.53768	25.01
416	1.37327	1.49510	1.53729	25.47
418	1.37310	1.49480	1.53691	25.93
420	1.37293	1.49451	1.53654	26.37
422	1.37277	1.49422	1.53618	26.80
424	1.37261	1.49394	1.53582	27.22
426	1.37245	1.49366	1.53546	27.63
428	1.37229	1.49339	1.53512	28.03
430	1.37214	1.49312	1.53478	28.43
432	1.37199	1.49286	1.53444	28.81
434	1.37184	1.49260	1.53411	29.19
436	1.37169	1.49234	1.53378	29.56
438	1.37155	1.49209	1.53346	29.92
440	1.37141	1.49184	1.53314	30.27
442	1.37127	1.49160	1.53283	30.62
444	1.37113	1.49136	1.53253	30.96
446	1.37099	1.49112	1.53223	31.29
448	1.37086	1.49089	1.53193	31.62
450	1.37073	1.49066	1.53164	31.94
452	1.37060	1.49043	1.53135	32.26
454	1.37047	1.49021	1.53106	32.56
456	1.37034	1.48999	1.53078	32.87
458	1.37022	1.48977	1.53051	33.17
460	1.37010	1.48956	1.53024	33.46
462	1.36998	1.48935	1.52997	33.74
464	1.36986	1.48914	1.52971	34.03
466	1.36974	1.48893	1.52945	34.30
468	1.36962	1.48873	1.52919	34.58
470	1.36951	1.48853	1.52894	34.84
472	1.36940	1.48834	1.52869	35.11
474	1.36929	1.48814	1.52844	35.37
476	1.36918	1.48795	1.52820	35.62
478	1.36907	1.48776	1.52796	35.87
480	1.36896	1.48758	1.52773	36.12
482	1.36886	1.48739	1.52749	36.36
484	1.36875	1.48721	1.52726	36.60
486	1.36865	1.48703	1.52704	36.83
488	1.36855	1.48686	1.52681	37.07
490	1.36845	1.48668	1.52659	37.29
492	1.36835	1.48651	1.52638	37.52
494	1.36826	1.48634	1.52616	37.74
496	1.36816	1.48618	1.52595	37.96
498	1.36807	1.48601	1.52574	38.17

Appendix 1

Refractivities and phasematching angles for LFM

lambda nm	Nx	Ny	Nz	theta deg
500	1.36797	1.48585	1.52553	38.38
502	1.36788	1.48569	1.52533	38.59
504	1.36779	1.48553	1.52513	38.79
506	1.36770	1.48537	1.52493	38.99
508	1.36761	1.48521	1.52473	39.19
510	1.36753	1.48506	1.52454	39.39
512	1.36744	1.48491	1.52435	39.58
514	1.36735	1.48476	1.52416	39.77
516	1.36727	1.48461	1.52397	39.96
518	1.36719	1.48447	1.52379	40.14
520	1.36710	1.48432	1.52361	40.33
522	1.36702	1.48418	1.52343	40.51
524	1.36694	1.48404	1.52325	40.68
526	1.36687	1.48390	1.52307	40.86
528	1.36679	1.48376	1.52290	41.03
530	1.36671	1.48362	1.52273	41.20
532	1.36663	1.48349	1.52256	41.37
534	1.36656	1.48336	1.52239	41.53
536	1.36648	1.48323	1.52222	41.70
538	1.36641	1.48310	1.52206	41.86
540	1.36634	1.48297	1.52190	42.02
542	1.36627	1.48284	1.52174	42.17
544	1.36620	1.48271	1.52158	42.33
546	1.36613	1.48259	1.52142	42.48
548	1.36606	1.48247	1.52127	42.63
550	1.36599	1.48234	1.52111	42.78
552	1.36592	1.48222	1.52096	42.93
554	1.36585	1.48211	1.52081	43.07
556	1.36579	1.48199	1.52066	43.22
558	1.36572	1.48187	1.52051	43.36
560	1.36566	1.48176	1.52037	43.50
562	1.36559	1.48164	1.52023	43.64
564	1.36553	1.48153	1.52008	43.77
566	1.36547	1.48142	1.51994	43.91
568	1.36541	1.48131	1.51980	44.04
570	1.36535	1.48120	1.51967	44.17
572	1.36529	1.48109	1.51953	44.30
574	1.36523	1.48098	1.51939	44.43
576	1.36517	1.48087	1.51926	44.55
578	1.36511	1.48077	1.51913	44.68
580	1.36505	1.48066	1.51900	44.80
582	1.36499	1.48056	1.51887	44.93
584	1.36494	1.48046	1.51874	45.05
586	1.36488	1.48036	1.51861	45.17
588	1.36483	1.48026	1.51849	45.28
590	1.36477	1.48016	1.51836	45.40
592	1.36472	1.48006	1.51824	45.52
594	1.36466	1.47996	1.51812	45.63
596	1.36461	1.47987	1.51800	45.74
598	1.36456	1.47977	1.51788	45.85

Appendix 1

Refractivities and phasematching angles for LFM

lambda nm	Nx	Ny	Nz	theta deg
600	1.36451	1.47968	1.51776	45.96
602	1.36445	1.47958	1.51764	46.07
604	1.36440	1.47949	1.51752	46.18
606	1.36435	1.47940	1.51741	46.29
608	1.36430	1.47931	1.51729	46.39
610	1.36425	1.47922	1.51718	46.49
612	1.36421	1.47913	1.51707	46.60
614	1.36416	1.47904	1.51696	46.70
616	1.36411	1.47895	1.51685	46.80
618	1.36406	1.47886	1.51674	46.90
620	1.36402	1.47878	1.51663	47.00
622	1.36397	1.47869	1.51652	47.09
624	1.36392	1.47861	1.51642	47.19
626	1.36388	1.47852	1.51631	47.28
628	1.36383	1.47844	1.51621	47.38
630	1.36379	1.47836	1.51610	47.47
632	1.36374	1.47827	1.51600	47.56
634	1.36370	1.47819	1.51590	47.65
636	1.36366	1.47811	1.51580	47.74
638	1.36362	1.47803	1.51570	47.83
640	1.36357	1.47795	1.51560	47.92
642	1.36353	1.47787	1.51550	48.01
644	1.36349	1.47780	1.51540	48.10
646	1.36345	1.47772	1.51530	48.18
648	1.36341	1.47764	1.51521	48.27
650	1.36337	1.47756	1.51511	48.35
652	1.36333	1.47749	1.51502	48.43
654	1.36329	1.47741	1.51492	48.51
656	1.36325	1.47734	1.51483	48.59
658	1.36321	1.47727	1.51474	48.68
660	1.36317	1.47719	1.51465	48.75
662	1.36313	1.47712	1.51456	48.83
664	1.36310	1.47705	1.51447	48.91
666	1.36306	1.47698	1.51438	48.99
668	1.36302	1.47691	1.51429	49.06
670	1.36298	1.47683	1.51420	49.14
672	1.36295	1.47676	1.51411	49.21
674	1.36291	1.47670	1.51403	49.29
676	1.36288	1.47663	1.51394	49.36
678	1.36284	1.47656	1.51386	49.43
680	1.36281	1.47649	1.51377	49.51
682	1.36277	1.47642	1.51369	49.58
684	1.36274	1.47636	1.51360	49.65
686	1.36270	1.47629	1.51352	49.72
688	1.36267	1.47622	1.51344	49.79
690	1.36263	1.47616	1.51336	49.85
692	1.36260	1.47609	1.51328	49.92
694	1.36257	1.47603	1.51319	49.99
696	1.36254	1.47596	1.51311	50.05
698	1.36250	1.47590	1.51304	50.12

Appendix 1

Refractivities and phasematching angles for LFM

lambda nm	Nx	Ny	Nz	theta deg
700	1.36247	1.47584	1.51296	50.18
702	1.36244	1.47577	1.51288	50.25
704	1.36241	1.47571	1.51280	50.31
706	1.36238	1.47565	1.51272	50.38
708	1.36235	1.47559	1.51265	50.44
710	1.36231	1.47553	1.51257	50.50
712	1.36228	1.47546	1.51249	50.56
714	1.36225	1.47540	1.51242	50.62
716	1.36222	1.47534	1.51234	50.68
718	1.36219	1.47528	1.51227	50.74
720	1.36217	1.47523	1.51220	50.80
722	1.36214	1.47517	1.51212	50.86
724	1.36211	1.47511	1.51205	50.92
726	1.36208	1.47505	1.51198	50.98
728	1.36205	1.47499	1.51191	51.03
730	1.36202	1.47493	1.51184	51.09
732	1.36199	1.47488	1.51177	51.14
734	1.36197	1.47482	1.51169	51.20
736	1.36194	1.47476	1.51162	51.25
738	1.36191	1.47471	1.51156	51.31
740	1.36188	1.47465	1.51149	51.36
742	1.36186	1.47460	1.51142	51.42
744	1.36183	1.47454	1.51135	51.47
746	1.36180	1.47449	1.51128	51.52
748	1.36178	1.47443	1.51121	51.57
750	1.36175	1.47438	1.51115	51.62
752	1.36173	1.47433	1.51108	51.67
754	1.36170	1.47427	1.51101	51.72
756	1.36168	1.47422	1.51095	51.77
758	1.36165	1.47417	1.51088	51.82
760	1.36162	1.47411	1.51082	51.87
762	1.36160	1.47406	1.51075	51.92
764	1.36158	1.47401	1.51069	51.97
766	1.36155	1.47396	1.51062	52.02
768	1.36153	1.47391	1.51056	52.06
770	1.36150	1.47385	1.51050	52.11
772	1.36148	1.47380	1.51043	52.16
774	1.36146	1.47375	1.51037	52.20
776	1.36143	1.47370	1.51031	52.25
778	1.36141	1.47365	1.51025	52.29
780	1.36139	1.47360	1.51019	52.34
782	1.36136	1.47355	1.51012	52.38
784	1.36134	1.47350	1.51006	52.43
786	1.36132	1.47345	1.51000	52.47
788	1.36130	1.47341	1.50994	52.51
790	1.36127	1.47336	1.50988	52.56
792	1.36125	1.47331	1.50982	52.60
794	1.36123	1.47326	1.50976	52.64
796	1.36121	1.47321	1.50970	52.68
798	1.36119	1.47317	1.50965	52.72
800	1.36116	1.47312	1.50959	52.77

Appendix 2

Type I phasematching in Urea

Lambda nm	n(o)	n(e)	theta deg	rho deg
300	1.53895	3.14484	0.00	0.0
305	1.53623	2.75780	0.00	0.0
310	1.53367	2.51957	0.00	0.0
315	1.53128	2.35646	0.00	0.0
320	1.52903	2.23708	0.00	0.0
325	1.52692	2.14563	0.00	0.0
330	1.52493	2.07318	0.00	0.0
335	1.52305	2.01429	0.00	0.0
340	1.52127	1.96543	0.00	0.0
345	1.51959	1.92423	0.00	0.0
350	1.51801	1.88900	0.00	0.0
355	1.51650	1.85852	0.00	0.0
360	1.51507	1.83189	0.00	0.0
365	1.51371	1.80843	0.00	0.0
370	1.51242	1.78760	0.00	0.0
375	1.51119	1.76899	0.00	0.0
380	1.51002	1.75225	0.00	0.0
385	1.50891	1.73713	0.00	0.0
390	1.50784	1.72340	0.00	0.0
395	1.50682	1.71088	0.00	0.0
400	1.50585	1.69941	0.00	0.0
405	1.50492	1.68888	0.00	0.0
410	1.50403	1.67917	0.00	0.0
415	1.50317	1.67019	0.00	0.0
420	1.50236	1.66187	0.00	0.0
425	1.50157	1.65413	0.00	0.0
430	1.50082	1.64693	0.00	0.0
435	1.50009	1.64019	0.00	0.0
440	1.49940	1.63389	0.00	0.0
445	1.49873	1.62798	0.00	0.0
450	1.49808	1.62243	0.00	0.0
455	1.49746	1.61721	0.00	0.0
460	1.49687	1.61229	0.00	0.0
465	1.49629	1.60764	0.00	0.0
470	1.49574	1.60325	0.00	0.0
475	1.49520	1.59909	83.66	-0.9
480	1.49469	1.59515	78.20	-1.7
485	1.49419	1.59140	74.66	-2.1
490	1.49370	1.58785	71.86	-2.4
495	1.49324	1.58447	69.50	-2.7
500	1.49279	1.58125	67.45	-2.9
505	1.49235	1.57817	65.61	-3.1
510	1.49193	1.57524	63.94	-3.2
515	1.49152	1.57244	62.42	-3.3
520	1.49113	1.56977	61.01	-3.4
525	1.49075	1.56721	59.69	-3.5
530	1.49038	1.56476	58.46	-3.6
535	1.49002	1.56241	57.31	-3.7
540	1.48967	1.56015	56.22	-3.7
545	1.48933	1.55799	55.19	-3.8
550	1.48900	1.55592	54.21	-3.8

Appendix 2

Type I phasematching in Urea

Lambda nm	n(o)	n(e)	theta deg	rho deg
555	1.48868	1.55392	53.28	-3.8
560	1.48837	1.55200	52.39	-3.8
565	1.48807	1.55015	51.54	-3.9
570	1.48778	1.54837	50.72	-3.9
575	1.48750	1.54666	49.94	-3.9
580	1.48722	1.54501	49.19	-3.9
585	1.48695	1.54341	48.47	-3.9
590	1.48669	1.54187	47.78	-3.9
595	1.48644	1.54039	47.11	-3.9
600	1.48619	1.53895	46.46	-3.9
605	1.48595	1.53757	45.84	-3.9
610	1.48572	1.53623	45.24	-3.9
615	1.48549	1.53493	44.65	-3.9
620	1.48527	1.53367	44.09	-3.9
625	1.48505	1.53246	43.54	-3.9
630	1.48484	1.53128	43.01	-3.9
635	1.48463	1.53014	42.49	-3.9
640	1.48443	1.52903	41.99	-3.9
645	1.48424	1.52796	41.50	-3.9
650	1.48405	1.52692	41.03	-3.9
655	1.48386	1.52591	40.57	-3.8
660	1.48368	1.52493	40.12	-3.8
665	1.48350	1.52397	39.68	-3.8
670	1.48333	1.52305	39.25	-3.8
675	1.48316	1.52215	38.84	-3.8
680	1.48299	1.52127	38.43	-3.8
685	1.48283	1.52042	38.04	-3.8
690	1.48267	1.51959	37.65	-3.7
695	1.48252	1.51879	37.27	-3.7
700	1.48237	1.51801	36.90	-3.7
705	1.48222	1.51724	36.54	-3.7
710	1.48208	1.51650	36.19	-3.7
715	1.48194	1.51578	35.85	-3.7
720	1.48180	1.51507	35.51	-3.6
725	1.48166	1.51438	35.18	-3.6
730	1.48153	1.51371	34.86	-3.6
735	1.48140	1.51306	34.54	-3.6
740	1.48128	1.51242	34.23	-3.6
745	1.48115	1.51180	33.93	-3.6
750	1.48103	1.51119	33.63	-3.5
755	1.48091	1.51060	33.34	-3.5
760	1.48080	1.51002	33.05	-3.5
765	1.48068	1.50946	32.77	-3.5
770	1.48057	1.50891	32.49	-3.5
775	1.48046	1.50837	32.22	-3.5
780	1.48036	1.50784	31.96	-3.4
785	1.48025	1.50733	31.70	-3.4
790	1.48015	1.50682	31.44	-3.4
795	1.48005	1.50633	31.19	-3.4
800	1.47995	1.50585	30.95	-3.4

3A1

CHAPTER 3: Intracavity frequency doubling using Lithium Formate Monohydrate in a Coumarin 102 laser.

3-1 Dye laser design

The details of the general design of dye lasers as used in this work are given in Chapter 1, and only the points relevent to the specific system of frequency doubling in Lithium Formate Monohydrate (LFM) will be discussed here.

3-1-1 Coumarin 102 dye

The dye used for the laser was Coumarin 102 (C102), also known as Coumarin 480. The dye is available commercially, (Kodak No. 11928), and is in the form of fine yellowish white crystals. Information sheets from Coherent Inc (CRL) recommended that the dye be made up as follows: 0.5g of crystals are dissolved in 100ml of Benzyl alcohol at room temperature, and this is then added to 1200ml of Ethylene glycol while the dye laser is running, to obtain 80% absorption of the pumping radiation. In practice we found that 1200ml was rather too much, and only about 800ml to 1000ml was needed. This gives a solution with a molarity in the range 1.5×10^{-3} M (1200ml) to 2.17×10^{-3} M (800ml).

3-1-1-1 Absorption and fluorescence

C102 absorbs strongly in the violet and ultraviolet and fluoresces over the range 410nm to 580nm approximately. The absorption and fluorescence curves are shown in Fig 3-1, derived from Drexhage [1]. Measurements of the stimulated emmission gain of C102 as a function of wavelength have been carried out by Dienes [2] and the curve is shown in Fig 3-2, though it must be noted that

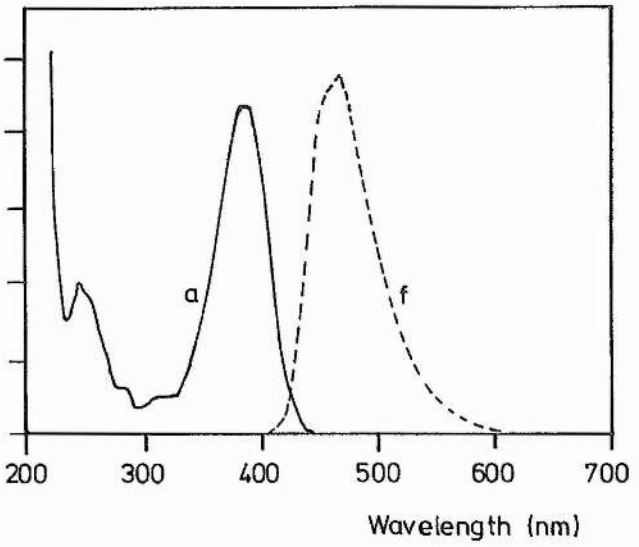

Fig 3-1: Absorption and fluorescence spectra for Coumarin 102 (from Drexhage [1])

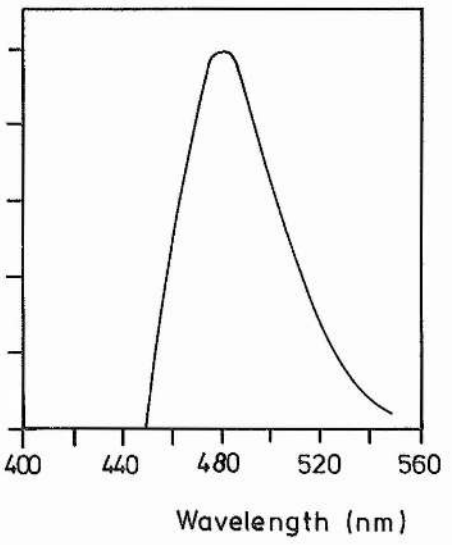

Fig 3-2: Stimulated emission gain curve for Coumarin 102 (from Dienes [2])

2 this curve was obtained from a 1.5×10^{-3} M ethanol solution.

3-1-1-2 Degradation

The useful lifetime of the coumarin dyes is short and is measured in terms of watt-hours (Whr) of pumping excitation. The standard reference dye for dye lasers working in the visible region is Rhodamine 6G (Rh6G), whose lifetime is over 1000Whr [3]. By comparison, C102 has a lifetime of less than 100Whr with violet pumping and less than 50Whr with UV pumping [3]. In practice, these seem to be optimistic figures.

Many dyes suffer loss of molecules able to yield to stimulated emission, by the photobleaching of the dye solution by the pumping radiation acting on excited state singlet or ground state triplet molecules. However, in the case of certain coumarin dyes, this may not be the most significant effect in the gradual degradation of their lasing qualities. Winters et al [4] have shown conclusively that in the case of Coumarin 1 (C1) a carboxylic derivative of the dye is produced irreversibly. The absorption bands of this acid cover the lasing bands of the original dye, and it is this absorption, rather than a significant reduction in dye concentration due to photobleaching, that causes the loss of laser action. They also showed that concentrations of the acid of as little as 5% of that of the original dye would have a significant effect on the laser threshold. They have measured a rate of acid production of 10^{-3} molecules per absorbed photon, and from a 1.5×10^{-3} M solution, the relative concentration of acid would be produced after

6.9Whr of pumping at 400nm and 100% absorption of the pumping radiation.

We have used C102 rather than C1, but suggest that a similar oxidation takes place on the No 4 carbon atom, yielding a derivative which absorbs strongly at the lasing wavelengths of C102, the derivative being here termed C102b. The proposed structure and production routes for all these processes are shown in Fig 3-3. Winters undertook chromatography of the acid derivative of C1 and found its mobility to be extremely low, and that filtration of the contaminated solution through activated alumina could assist with the removal of the acid. We have found that a similar process seems to operate with C102 (Section 3-2-5).

3-1-2 Pump laser

The pump laser used was a CRL CR3000K Krypton ion laser, operating on the three violet lines at 415.4nm, 413.1nm and 406.7nm. A power of 3W was normally used. The absorption of C102 at these wavelengths is not very high, but is the best available, as no other ion laser has an output closer to the dye absorption peak at 390nm, though the use of different solvents has been found to shift the absorption and fluorescence bands to be more favourable to krypton ion pumping [1]. As it is, most of the power is contained in the two shorter wavelength violet lines, and the overall efficiency of an optimised dye laser using violet pumping can be as high as 17% (compared with 25% for Rh6G with green pumping and 12% for C102 with UV

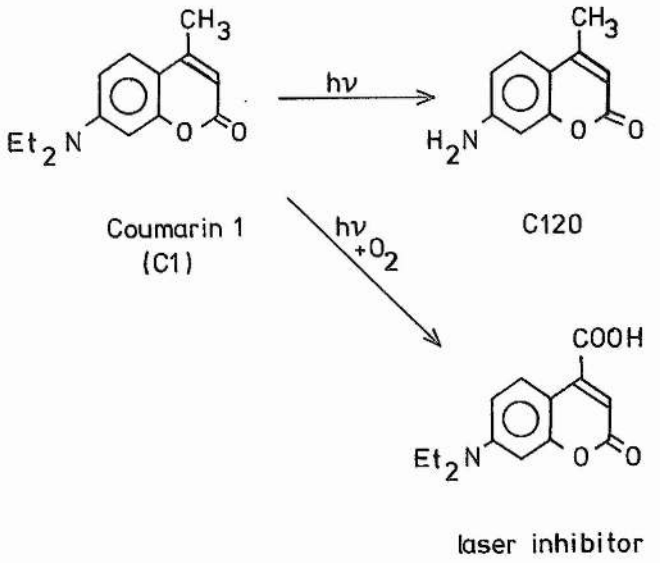

(a): Degradation of Coumarin 1
(from Winters et al [4])

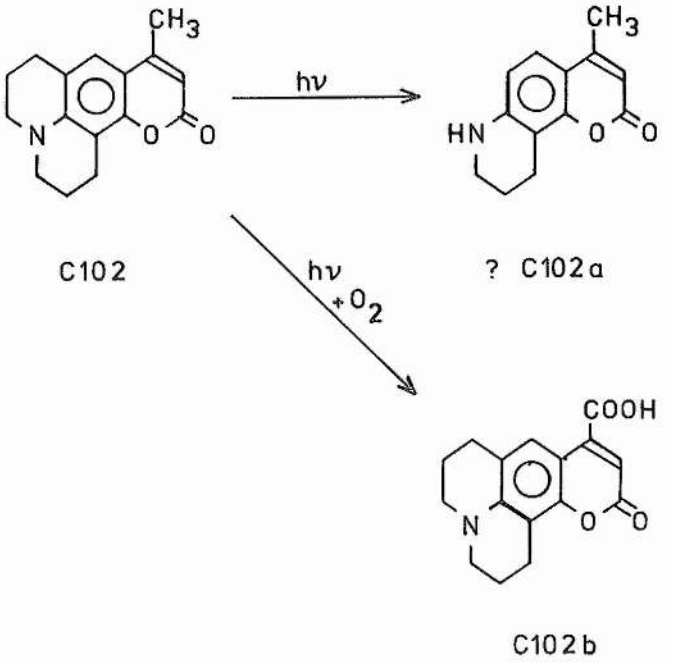

(b): Our proposal for similar effects
with Coumarin 102

Fig 3-3: Photodegradation of Coumarin dyes

pumping), [3]. Our laser, with no frequency doubling elements within the cavity has obtained 11% efficiency.

3-1-3 Mechanical details

The dye laser structure follows closely that of well proven systems operated by Ferguson and others [5,6,7]. Photographs of the dye laser assembly are given in Plates 3-1 and 3-2. The various optical conponents are carried on adjustable mountings clamped to a 5cm diameter invar rod. The mirrors in particular are on triple screw mountings, one screw acting as a pivot and the other two allowing angular adjustment about perpendicular axes. Translation through short lengths, such as when adjusting focusing, is achieved by turning all three screws equally. The mirrors are clamped into small recesses in the mounts, and are not apertured in any way in the vertical plane.

Because the mirrors may all be translated along the axis of the laser cavity as required, it is not necessary to make the crystal mounting itself adjustable to any great extent. For ease of handling, and to allow intracavity frequency doubling to be compared directly with extracavity doubling, by removing the entire crystal assembly, the crystal and the two mirrors forming the Z-fold are mounted on a 6mm metal plate which is then bolted to the invar bar. A general view of this assembly is shown in Plate 3-3.

Tuning of the laser is achieved by a 1-, 2-, or 3-plate birefringent filter, which is mounted at Brewster's angle

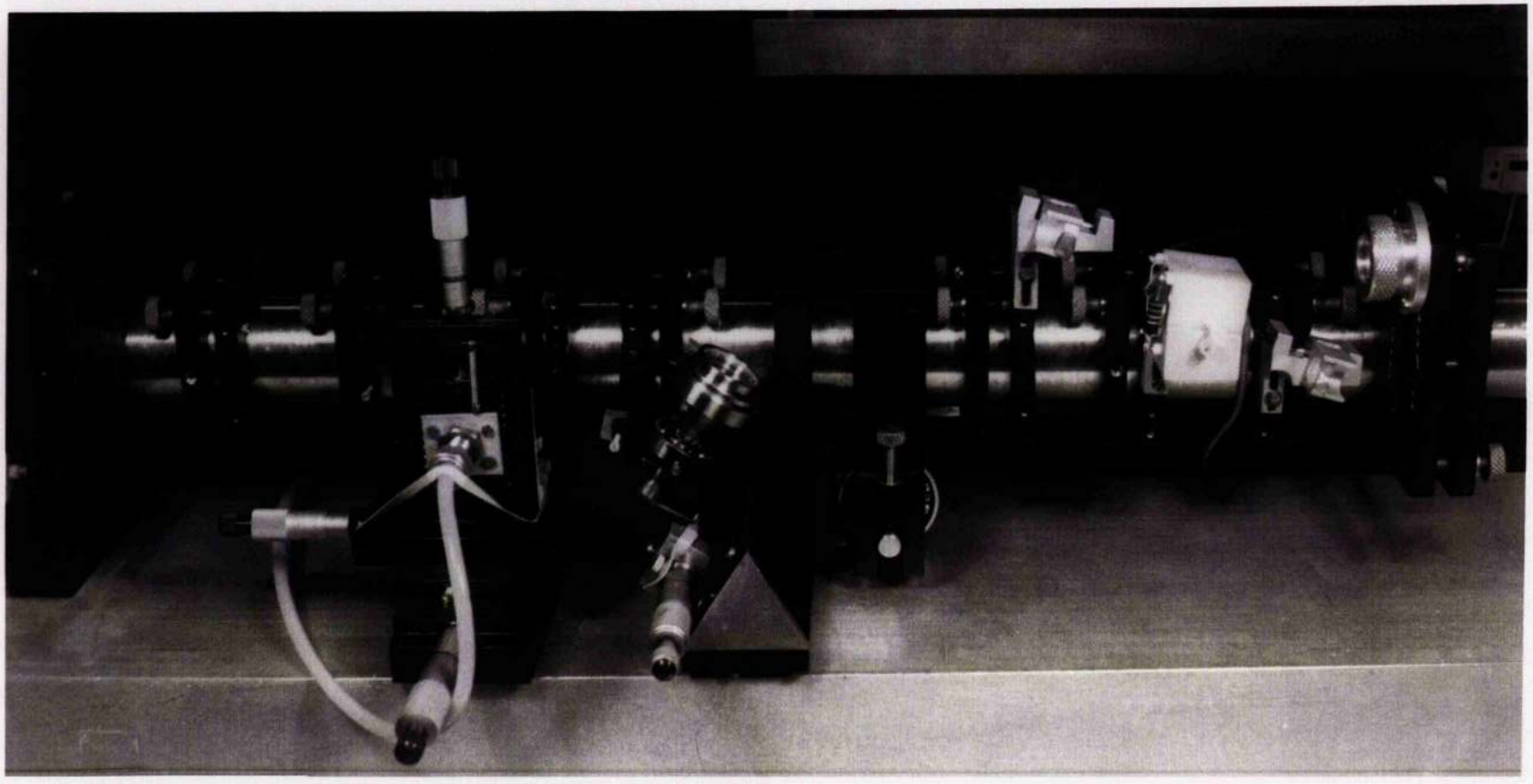

Plate 3-1

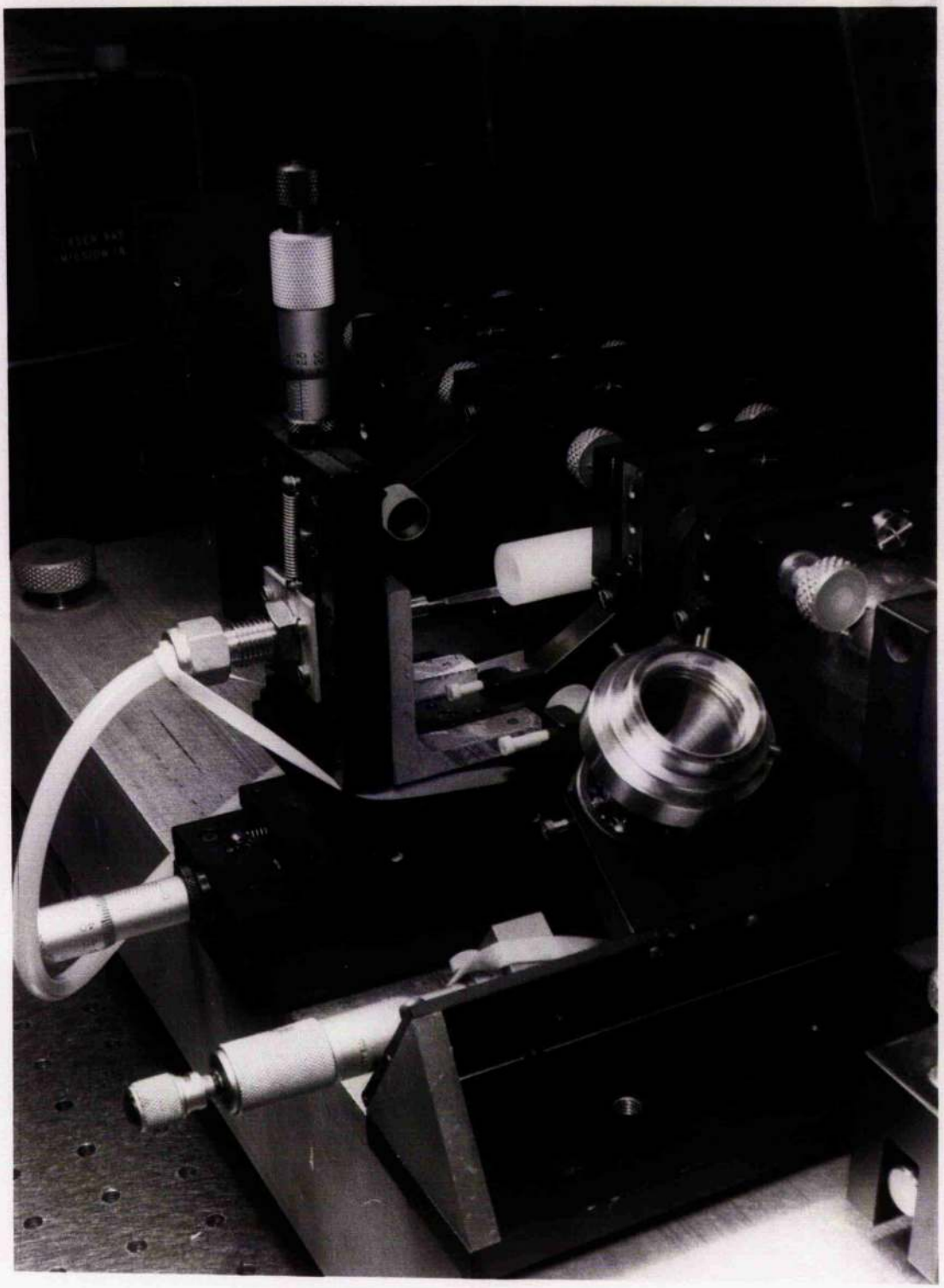

Plate 3-2

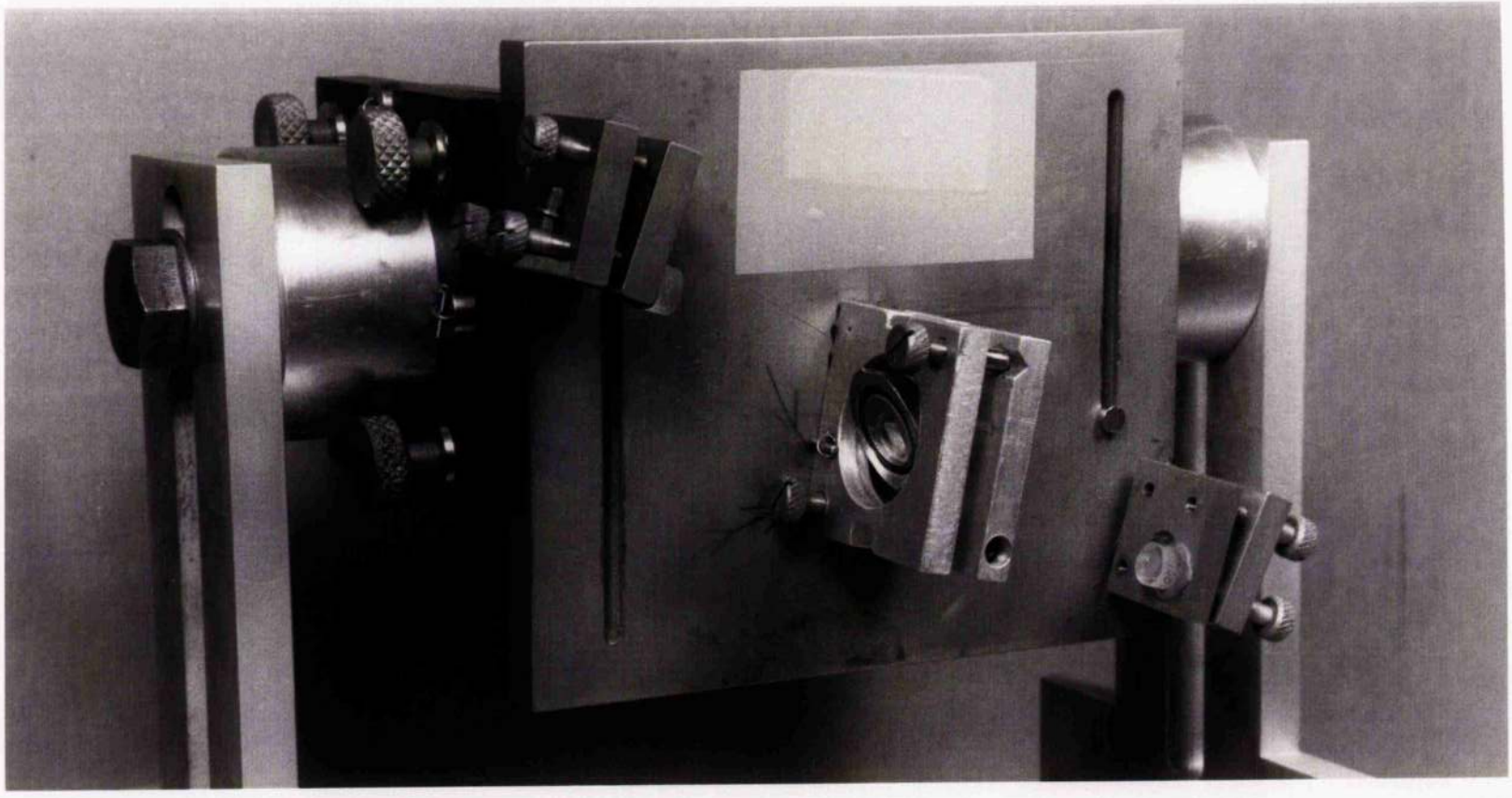

Plate 3-3

to the laser axis, and rotates about an axis normal to its own plane. The quartz plates are held in stainless steel rings and rotation is by a micrometer screw thrusting on a sidearm to the axle. A view of the assembly is given in Plate 3-4.

3-1-4 Optical details

A diagram of the optical layout of the dye laser when used with LFM for frequency doubling is shown in Fig 3-4.

3-1-4-1 Mirrors

For operation with LFM, the dye laser has used readily available commercial mirrors. Those for the Z-fold around the crystal (R_3 and R_4) and above the jet (R_2) are all Spectra Physics Inc No G3813-007, of 10cm radius of curvature, and that below the jet is also from Spectra Physics, G3845-003, of 5cm radius of curvature. All of these mirrors are for argon ion lasers operating in the blue-green, principally on the 488nm line, and have very high reflectivities (>99.6%) in this region. The plane mirror R_5 would, in an ideal laser, be highly transparent to UV and highly reflective to the visible, and also R_4 would be highly reflecting at both wavelengths, in order to maximise the intracavity visible power and to couple out as much UV as possible. The coating on such a mirror has to be tailored to the wavelengths required and is expensive if a small quantity of mirrors is to be made.

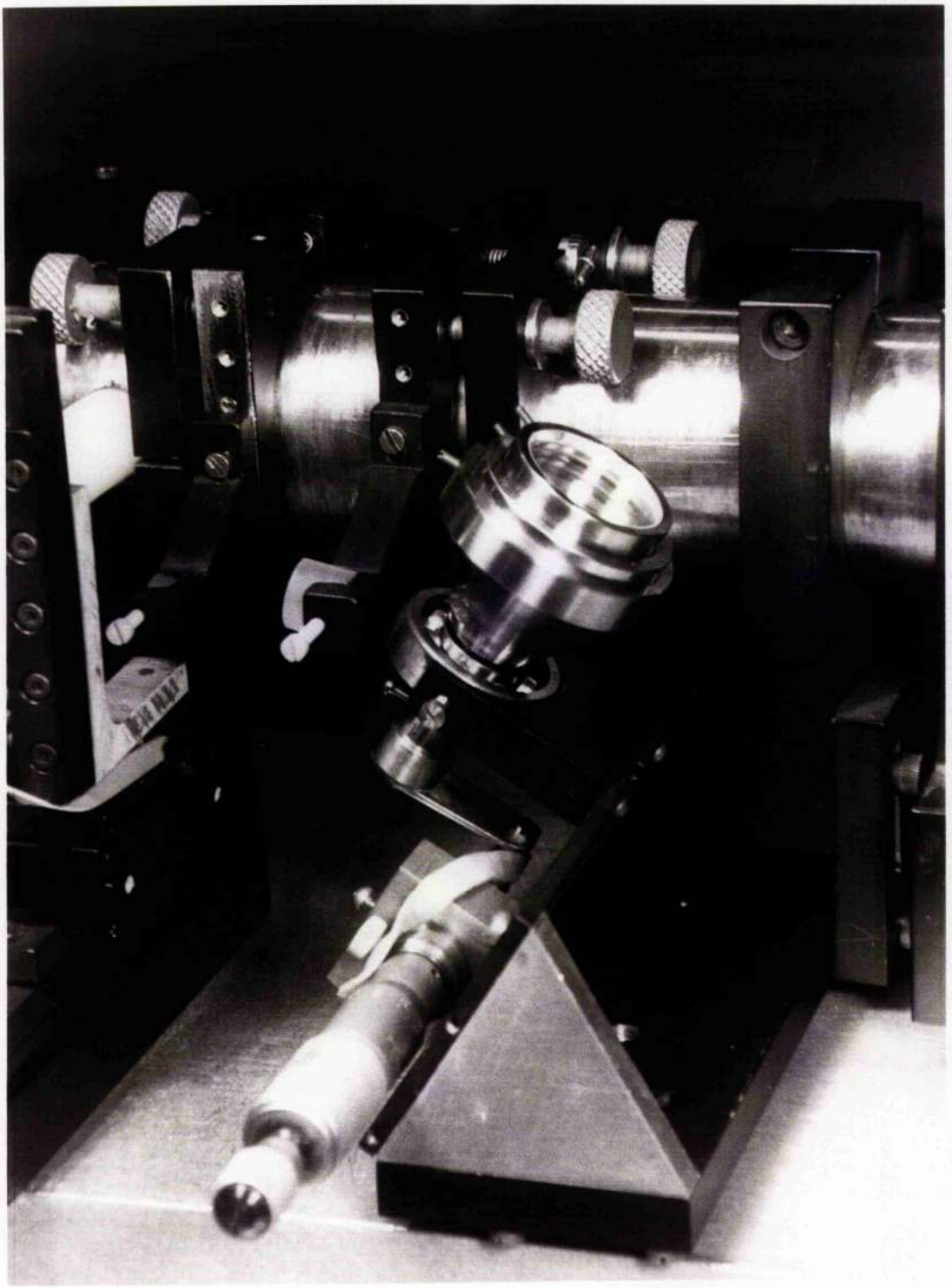

Plate 3-4

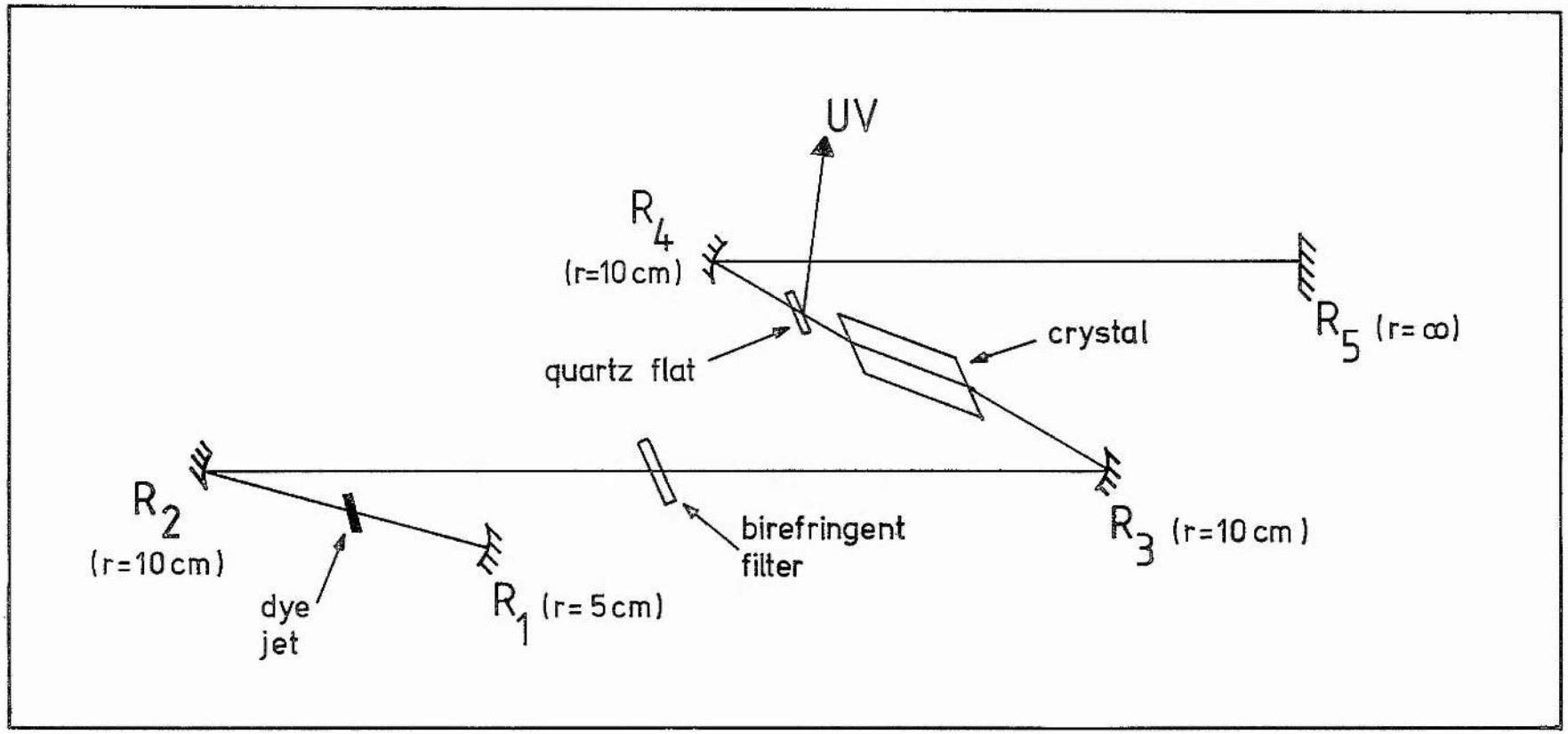

Fig 3-4: Dye laser schematic

No suitable mirror was available commercially, and so a compromise was reached whereby R_4 was highly reflecting in the visible and the UV was coupled out by reflection off a quartz plate (Section 3-1-4-3). The mirror used for R_5 was from CRL, No 903-004-00, flat, and reflecting >99.7% from 450.0nm to 514.5nm. The krypton ion pumping beam was focused into the dye jet by a 7.5cm radius of curvature Spectra Physics mirror.

3-1-4-2 Tuning elements

Tuning the laser, that is, actively controlling the frequency at which it operates, is achieved by two methods. The principal tuning is by means of a birefringent filter, as already described in Chapter 1. In this laser, a three-plate filter was used, with plates of thicknesses 0.41mm, 1.61mm and 6.39mm, with the optic axis of the quartz lying in the plane of the plates and the beam propagating at 45° to this axis for maximum discrimination. When the three plates are adjusted to optimum, a linewidth of less than 0.035nm in the visible is obtained. A three-plate filter usually introduces rather more loss into the cavity than can be accomodated by the the low gain of coumarin dyes, at least when all other losses, such as those at the crystal and cell are considered as well. Unless fresh dye was used, we found the three-plate filter often prevented the laser from operating, and eventually only a single plate, the thinnest, was used. This was found to give much the same linewidth as that using three plates, indicating that because of the high threshold for laser action (due to the

low gain and comparatively high losses), the discrimination of the single plate was perfectly adequate. We did note, however that at the extremes of the tuning range, the laser would oscillate at two wavelengths if only one plate was in the cavity.

3-1-4-3 UV coupling out

As already explained, the optimum UV output would be obtained through R_5, having R_4 highly reflective to UV and R_5 highly transparent. As suitable mirrors were not available for this method, the UV was coupled out by means of a quartz plate between the crystal cell and R_4 and set at Brewster's angle to the beam, offering minimum Fresnel loss to the visible component. The UV is polarised with its electric vector normal to that of the visible, and hence a fraction is reflected at each air-quartz or quartz-air interface.

The Fresnel relation for reflection coefficient, r, for a wave with electric vector parallel to the plane of the interface is given by:

$$r = \frac{n_i \cos\theta_i - n_t \cos\theta_t}{n_i \cos\theta_i + n_t \cos\theta_t} \qquad (1)$$

where n and θ are the refractivity and angle between the ray and the surface normal in the incident (i) and transmission (t) regions. Brewster's angle is also given by:

$$\frac{n_t}{n_i} = \tan\theta_B \qquad (2).$$

3C3

For air, n_i = 1.00 and for quartz, n_t = 1.54 (blue) and 1.57 (UV). Hence Brewster's angle θ_B (= θ_i in this case) equals 57°.0 and θ_i = 90° - θ_t equals 33°.0 . Thus from (1), the reflection coefficient has the value r = -0.415. The fraction of energy reflected equals the square of the fractional amplitude reflected and is termed the reflectance, R. Thus in this case, R = 17.2%, and this is the fraction of UV reflected at the first (air-quartz) interface. At the second surface, the numerical values of θ_i and θ_t and of n_i and n_t are reversed in (1), but the value of R is the same as for the air-quartz interface. Since there is then only 82.8% of the original incident energy then present, only 14.2% of the original is then reflected at the second interface. Further reflections (Fig 3-5) then reduce still further the total UV energy reflected off the quartz plate to a total of about 29% of that leaving the crystal cell, not allowing for any absorption losses there may be within the quartz and assuming that no etalon effects exist due to the plate's flatness. This figure is about half that which could reasonably be expected with good quality coatings on R_4 and R_5 (perhaps 80% reflectance at R_4 and 75% transmittance at R_5, giving a net output of 60%).

An additional loss not yet mentioned is that of reflective losses at the quartz windows of the crystal cell. These are also at Brewster's angle to the visible beam and also cause 29% reflective losses to the UV, which is unavoidable if index matching fluids in contact with the crystal are to be avoided. Thus at best, with good mirrors only 43% of the generated UV is available, and with quartz plate coupling-out only 21% is obtained.

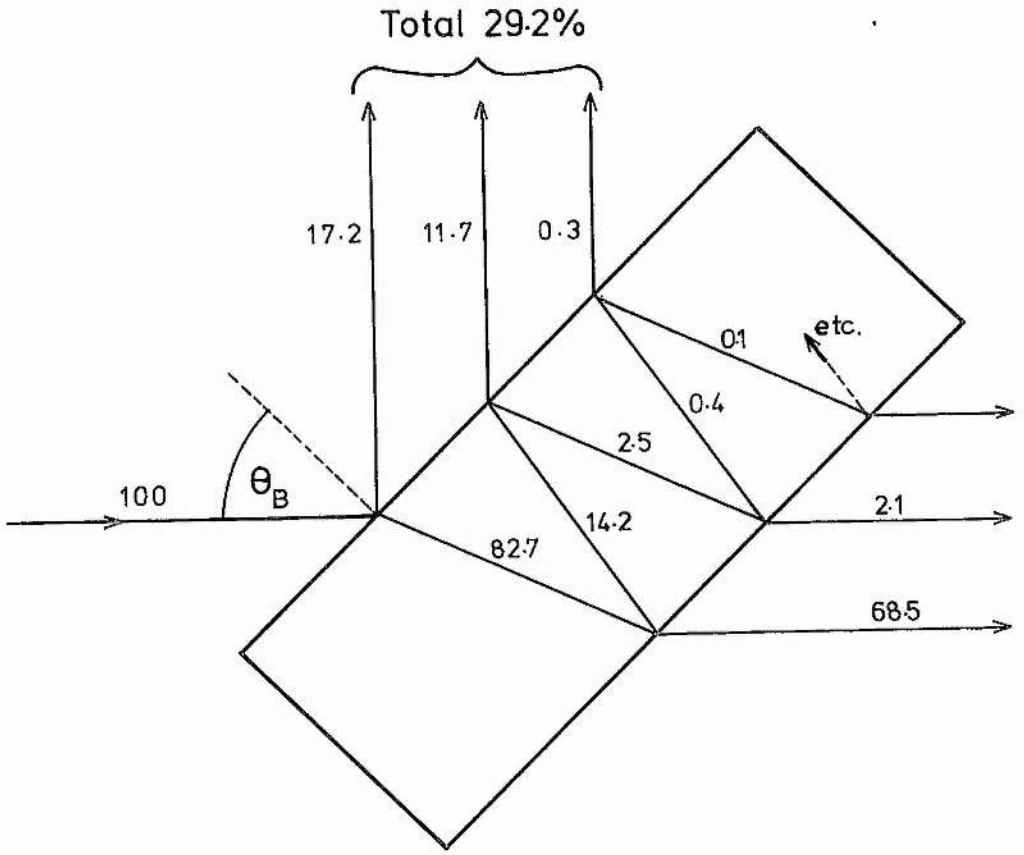

Fig 3-5: Reflection of the UV off a quartz plate at the Brewster angle.
Figures represent the percentages of incident beam energy

These figures would generally apply to all lasers of this design, subject to small variations with mirror quality and wavelength, and are not unique to the coumarin laser.

3-1-5 LFM Crystal details

3-1-5-1 Crystal design

The analysis of the optimum beam orientation in the crystal has already been discussed in Chapter 2. The result was that the visible beam should propagate in the ZX plane, being polarised in the Y direction, with the UV polarised parallel to the Z axis, (Fig 2-3).

In order to obtain minimum insertion loss to the cavity when the crystal is in place, the entrance and exit faces are at Brewster's angle to the visible beam, and this must be considered when the crystal is cut. Crystals for use in this type of application are usually square in cross-section, with the beam propagating parallel to one pair of sides and preferably along the axis of symmetry.

For phasematching at 486nm, the angle between the beam and the Z axis must be about 37°, (Chapter 2, Appendix 1) and thus the crystal design is uniquely determined with the exception of the senses of the Brewster-angled surfaces, and is shown in Fig 3-6 and 3-7. In order to obtain phasematching at other wavelengths, the crystal has to be rotated about its Y axis (to alter θ_m), clockwise as seen from above for longer wavelengths, with θ_m increasing. The crystal actually used was cut by Quantum Technology

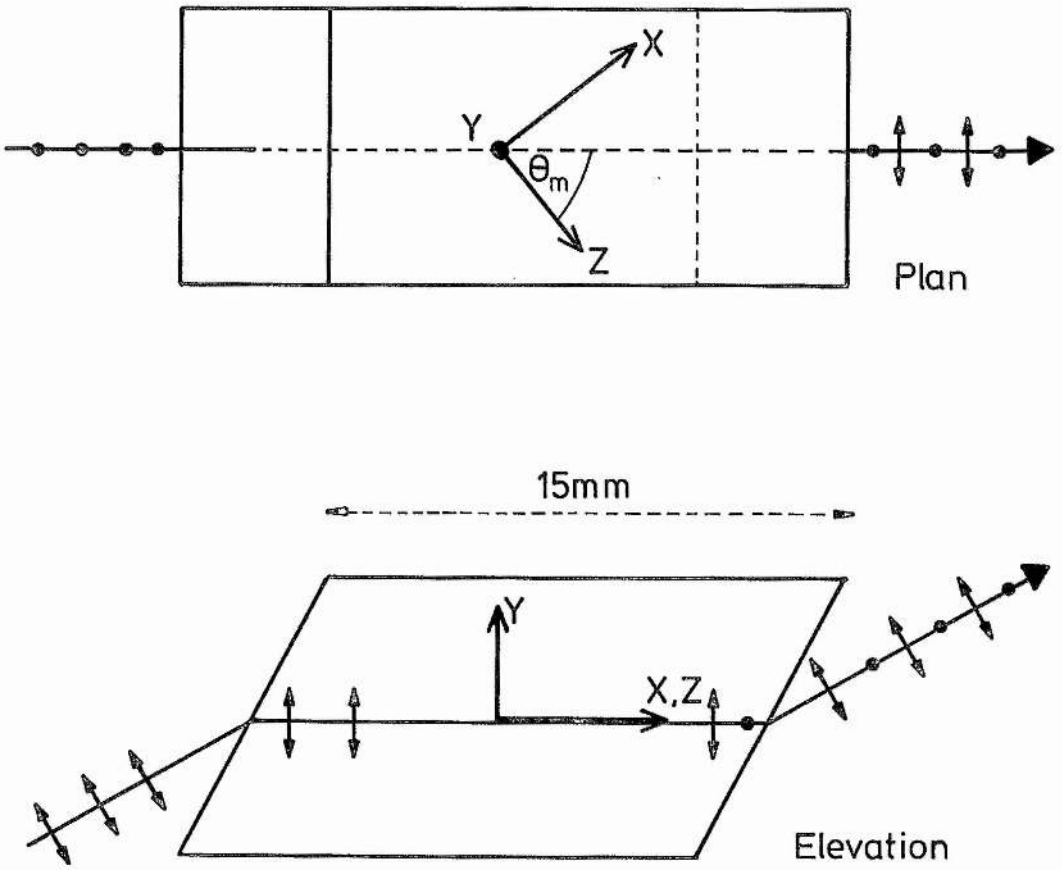

Fig 3-6: LFM crystal design, showing visible and UV polarisations

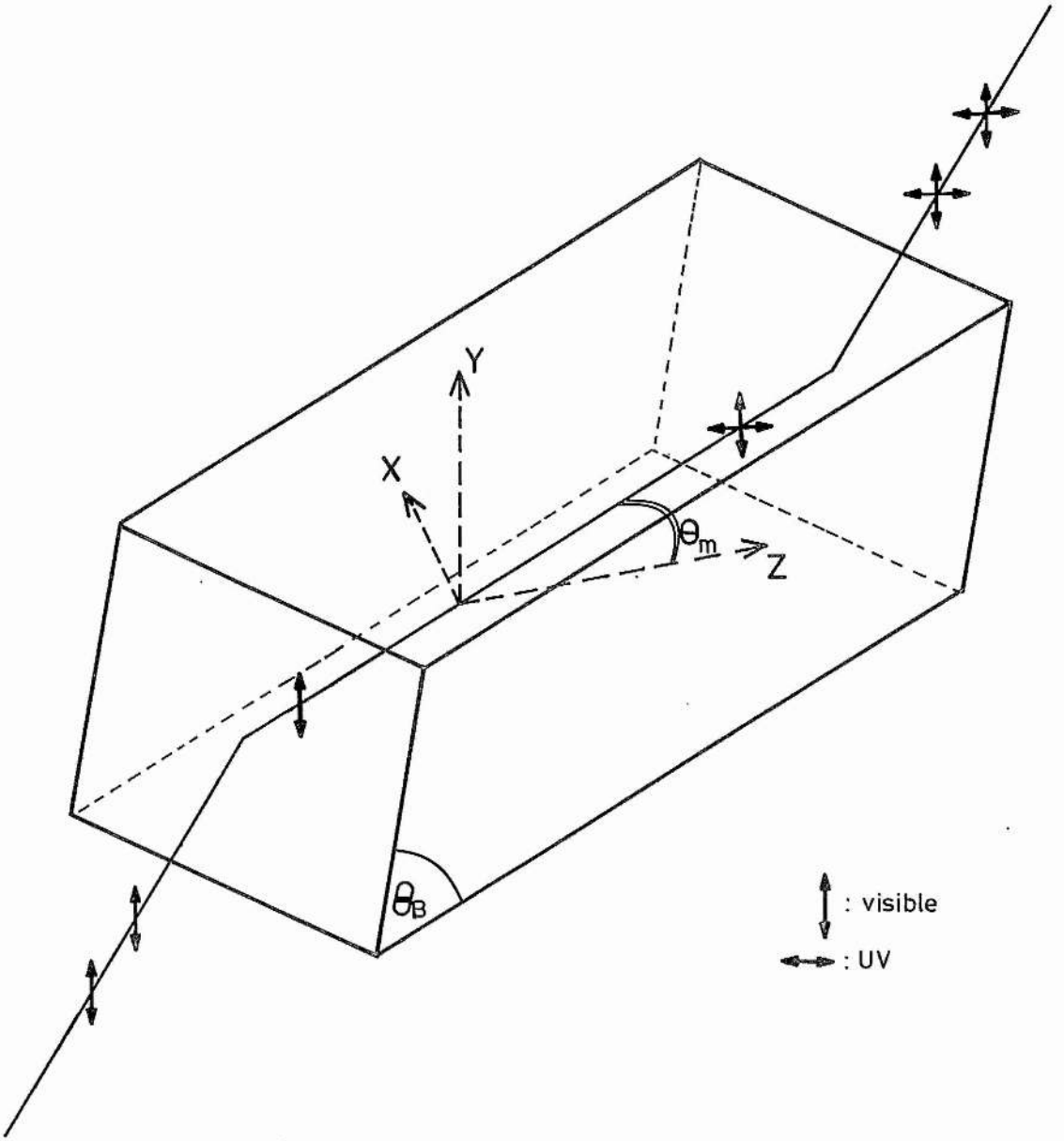

Fig 3-7: Optical arrangement of the LFM crystal, showing polarisations.
S.H. walkoff is ignored

Inc., and is 5mm square in section and 15mm long. As shown in Chapter 2, this is very much longer than optimum, but was chosen to match the well tested existing design of dye laser, in which the geometry and analysis of the Z-fold depends significantly on crystal length. The Brewster-angled surfaces at the ends of the crystal were polished flat to an accuracy of $\lambda/4$.

3-1-5-2 Cell design and mounting

LFM is not susceptible to temperature tuning, so a crystal oven is not required. However, the crystal is likely to dehydrate in a dry atmosphere, and thus should be kept in a sealed cell to maintain humidity and to minimise the risk of the Brewster surfaces deteriorating by such dehydration. To this end, the LFM crystal is held in a stainless steel tube, 12.5mm diameter, with quartz windows polished to $\lambda/10$ flatness which are held in place by rubber O-rings. A small quantity of powdered LFM is also included in an attempt to maintain optimum vapour pressure. Hopefully, if any dehydration does occur, it will take place rapidly from the large surface area of powder before the optical surfaces are significantly affected. Singh et al [8] quote an optimum humidity of over 40% to prevent surface degradation. A drawing of the crystal cell is shown in Fig 3-8.

The angle tuning of LFM requires the crystal to be rotated about the crystalline Y axis which in this case is normal to the base of the crystal (Fig 3-6). The rotation is

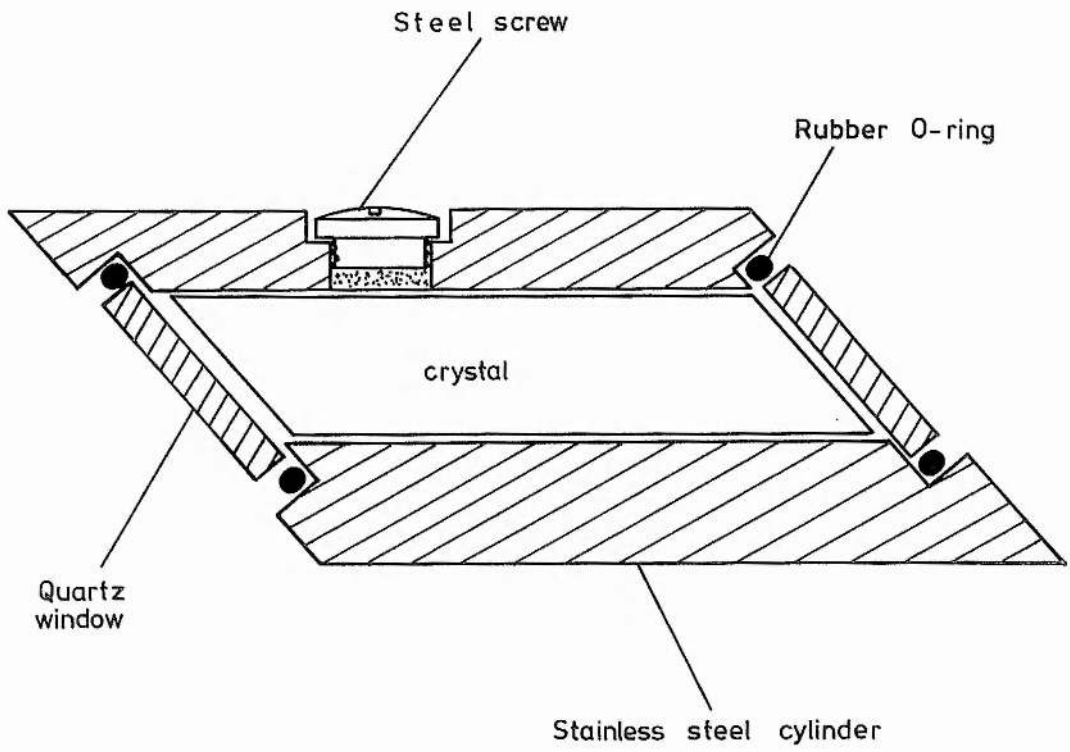

Fig 3-8: Cross-section of the LFM crystal cell. Powdered LFM is held by a gauze under the screw

achieved by supporting the cell inside a three point suspension assembly, similar to but much smaller than those used to control the laser mirrors. The cell mount, however, has only two screws, the third being replaced by a ballbearing, since very small translations of the cell are not needed. The rotation of the cell is achieved by turning the screw that is on the same horizontal level as the ball bearing. The plates of the mounting are not vertical, but at a suitable angle to the cavity so that the incident beam strikes the cell windows at Brewster's angle and the angle of the Z-fold is also maintained. A photograph of the assembly is shown in Plate 3-5.

3-2 Experimental results

3-2-1 Tuning and power curves

Tuning profiles of power against wavelength have been plotted for various versions of the laser, all using C102 dye as described earlier. Fig 3-9 shows the profile for a three-mirror cavity (i.e. without the Z-fold), tuned with a two-plate birefringent filter. This is given to indicate the broad lasing properties of C102. Power readings were obtained with a CRL power meter.

Fig 3-10 shows the tuning curve for the frequency doubled laser, normalised to the same scale as Fig 3-9, the intracavity peak power being 1.25W in the visible and 70μW at the crystal in the UV. Intracavity power was determined using a Hamamatsu S780-8BQ photodiode, which

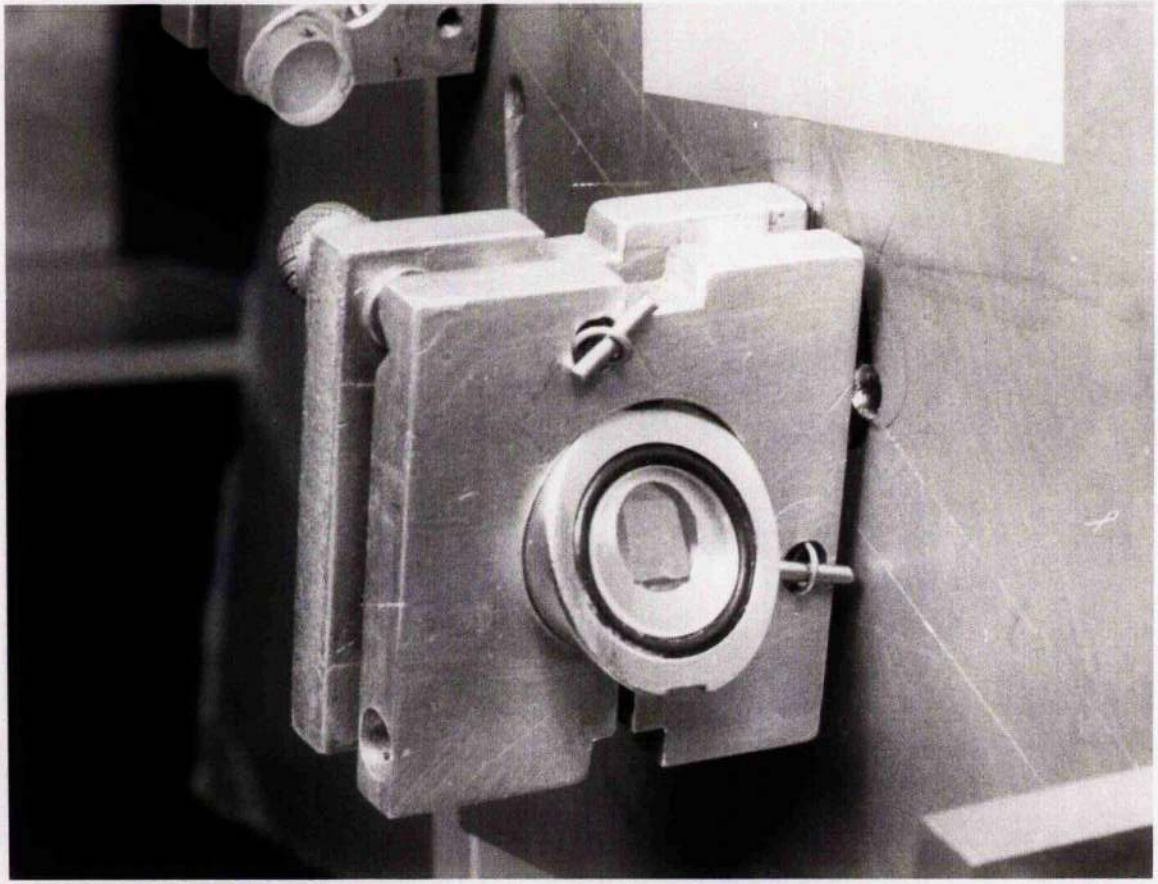

Plate 3-5

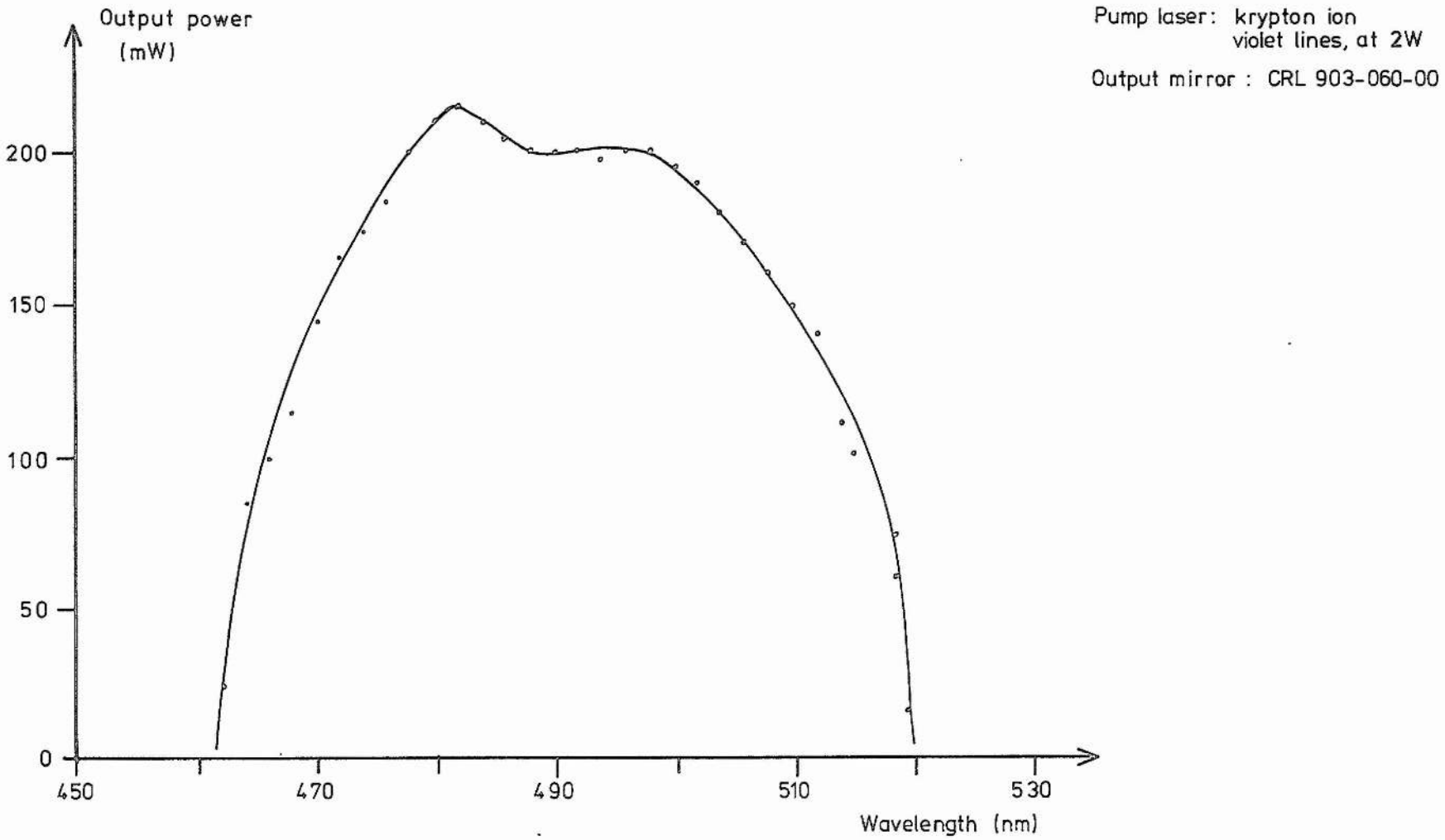

Fig 3-9: Tuning curve of C102

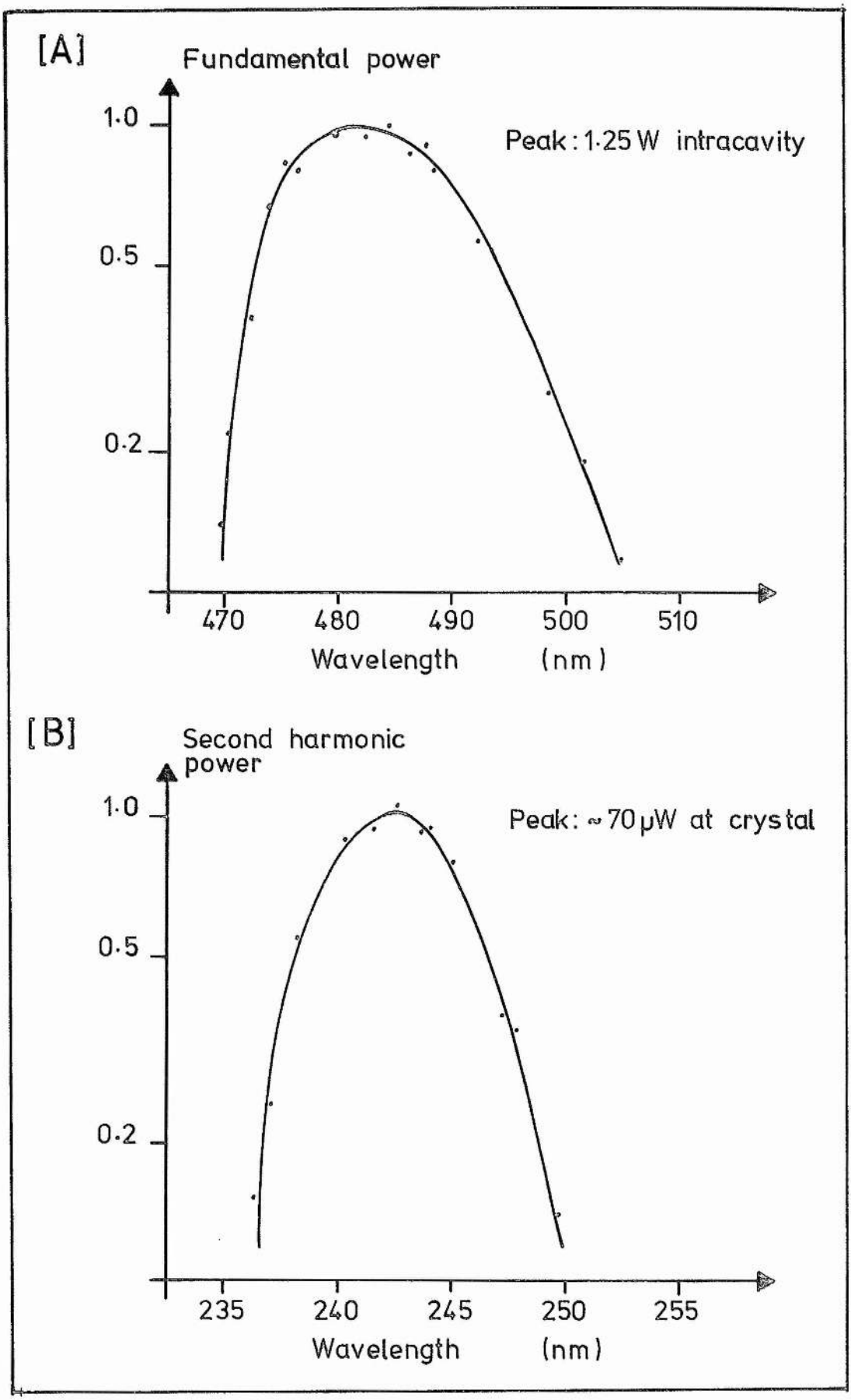

Fig 3-10: Visible and UV tuning curves for the C 102 laser

had been calibrated against wavelength in combination with the coumarin output mirror, using a beam of measured power from an argon ion laser incident on to the mirror and observing the signal from the photodiode due to the transmitted beam. The UV power was measured after reflection off the quartz plate by a calibrated Hamamatsu R166UH photomultiplier, fitted with calibrated visible blocking filters, and the intracrystal power then deduced.

3-2-2 Linewidth

Linewidths in the visible and UV have been measured using a Rank Monospex 1000 scanning spectrometer. With a single plate filter in the cavity, linewidths of 0.043nm in the visible and 0.020nm in the UV were obtained.

3-2-3 UV generation

3-2-3-1 Powers

The generation efficiency of LFM is low compared with more common materials such as ADA, and so only low UV powers have been obtained. A maximum generated power of 70μW at 244nm was obtained, corresponding to a conversion efficiency of 5.6×10^{-5}, with a linewidth of 0.020nm.

The theory of SHG predicts a quadratic dependence between the fundamental and SH powers, providing that thermal mismatching effects do not occur. This has been tested for LFM for intracavity powers up to 1W, as shown in Fig 3-11. To compare our experimental observations with

the theoretical predictions, we have also plotted on Fig 3-11 the expected graphs for the two cases of focusing to beam waist radii of 20μm and 15μm, using Equation (33) and Fig 2-2a of Chapter 2. The exact size of the beam waist in the crystal is not known, but is expected to be close to 20μm for this cavity [Chapter 1, reference 10]. This is confirmed by examination of Fig 3-11.

3-2-3-2 Angle tuning

The variation of phasematch angle with wavelength has been examined and is illustrated in Fig 3-12. The dependence is only determined relative to an arbitrary zero at 474nm. The results are in poor agreement with those of Dunning et al [10] for reasons to be discussed later. The angle referred to in Fig 3-12 is that of the beam inside the crystal, relative to the crystalline axes, and changes with wavelength at a rate of 8.1nm/degree, compared with a rate of 12.5nm/degree measured from the graph in Dunning.

In the case of a temperature tuned material such as ADA the optical alignment of the cavity is unchanged during tuning. However, the LFM crystal must be rotated by several degrees to maintain phasematching over the range 474nm to 496nm, and this always involves realignment of the cavity. It is then not always possible to obtain lasing with the beam going through the centre of the crystal, and thus the phasematching condition is not as easy to achieve as might be supposed. Also, whereas for a fixed crystal, slight faults on the crystal surfaces, or dust particles, can normally be avoided in the alignment,

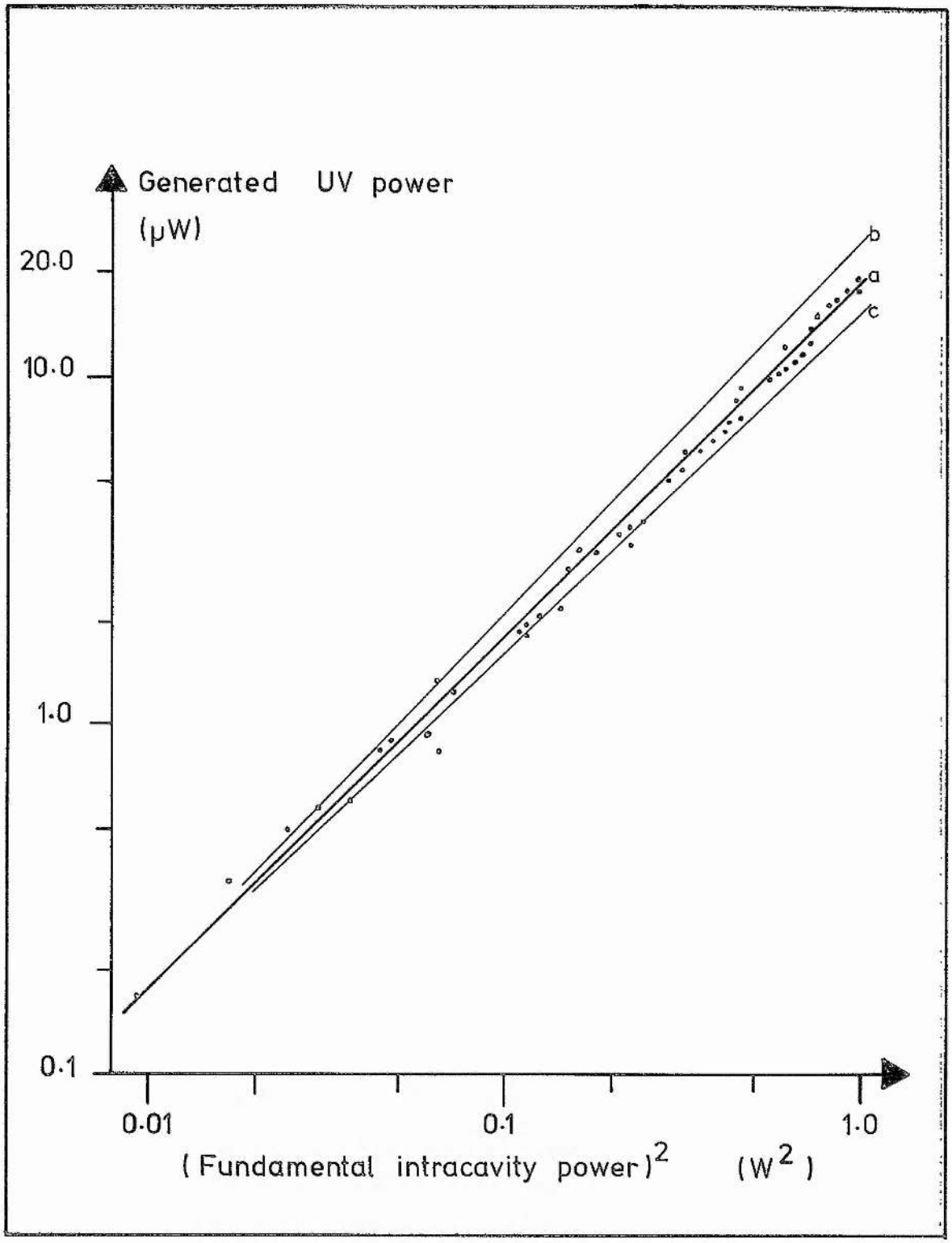

Fig 3-11: Quadratic relation between visible and UV powers

a) experimental
b) theoretical, focusing to w_0 = 20μm
c) ditto, w_0 = 15 μm

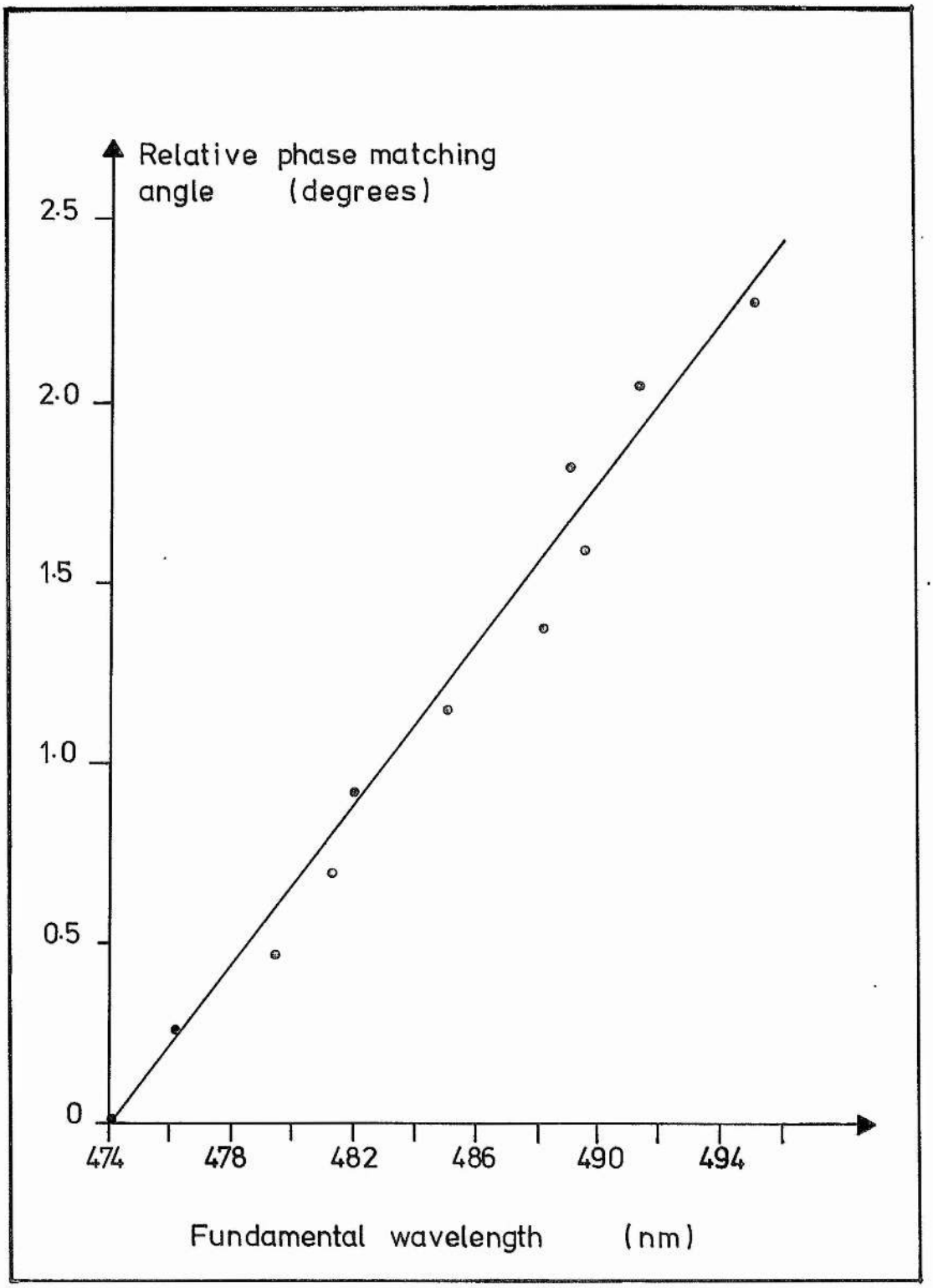

Fig 3-12: Variation of phasematching angle for our crystal

this is not always possible when the crystal has to be rotated, and the laser power available at different wavelengths has been seriously affected by such defects.

Thus the power curves of Fig 3-10 are not necessarily continuous profiles, but refer to the best powers reliably obtained at the different wavelengths, a factor also to be considered in discussing the apparent discrepancy between the power values in Fig 3-10 and 3-11.

3-2-4 Apparent error in crystal design

As already discussed in Section 2-2-1, two independent sets of refractivity data have been published for LFM, those of Naito and Inaba [11] covering a much larger wavelength range than those of Singh [8] and discrepancies occur between their predictions of the phasematching angle at 486nm.

Our crystal design was based on the graph of phasematch angle against wavelength given in Dunning et al [10] which itself was based on the work of Singh (though it must be emphasised that the paper by Naito and Inaba was published at about the same time as that of Dunning). From this graph, which was based entirely on theory and had not been experimentally verified, we determined a phasematch angle of 38° to $38^{\circ}.5$ for a wavelength of 486nm, and the LFM crystal was duly cut so that this angle would be attained by a beam propagating parallel to the sides of the crystal.

:D4

However, our experimental observations at around 486nm disagree with these figures and their variation with wavelength. In particular, the experimental analysis of change of phasematch angle with wavelength (Fig 3-12) shows a rate of change of 8.1 $\pm$ 0.5 nm/degree. Numerical analysis based on the paper by Singh shows a rate of 12.5nm/degree, which of course is also shown by the graph in Dunning. The results of Naito and Inaba, however, when used to produce a similar graph, predict a rate of 7.2 $\pm$ 0.2 nm/degree at 486nm, in much closer agreement with our experimental observations. It must be emphasised that neither Singh nor Dunning attempted to verify their phasematching predicitions experimentally, and we believe that our work to be the first occasion on which the theoretical predictions have been tested and the results reported.

Even were there an error of up to a degree or so in the crystal cut (which has not been tested by X-ray analysis), our results would still tend to support the results from Naito and Inaba over those of Dunning. A further test, that of determining the phasematching wavelength for an on-axis beam is not at all easy to make, due to the difficulty in guaranteeing the crystal to be in correct alignment in the cavity. Optically this can only be achieved accurately by observing , at a suitable distance from the laser, the slight Fresnel reflections off the Brewster surfaces of the crystal, but these reflections are intercepted by the crystal cell and cannot be used. The accuracy needed for a good test of phasematching wavelength is one better than 0.25 degrees in the crystal alignment. We cannot be certain that the optical

surfaces of the cell itself are parallel to those of the crystal to anything approaching this accuracy, and so precise optical determination of the on-axis phasematching wavelength is also not possible using reflections from the cell windows. Even using X-ray analysis, only the crystalline axes positions in relation to the crystal sides can be determined, and the position of the crystal within the cavity is still subject to error.

3-2-5 Dye purification

We have already described the effects of photochemical oxidation of Coumarin 1 (C1) as analysed by Winters et al [4], in Section 3-1-1-2. In summary, the original dye can be oxidised to a carboxylic acid which absorbs strongly at the lasing wavelength of the original dye, leading rapidly to the loss of laser action.

We have found that after only about 10 watt hours of excitation by violet krypton ion laser radiation, Coumarin 102 (C102) solution takes on a much darker brownish yellow colour, compared with the pale off-yellow tint of fresh solution, suggesting that some additional blue absorbing material is present after that time.

As shown in Fig 3-3, the structures of C1 and C102 are very similar, particularly with regard to the methyl group at the 4-position. We therefore suggest that a very similar oxidation process is occuring in C102 to that which has been shown to take place in C1.

E1 Winters suggested three methods of overcoming the problem of the acid derivative:

(1) the replacement of dissolved oxygen in the dye solution with a non-oxidising triplet state quencher,

(2) replacement of the methyl group with a less reactive group such as CF_3,

(3) removal of the photochemically produced laser inhibitor by suitable filtering.

Of these options, a combination of (1) and (3) seems the most appropriate and certainly the easiest. Winters established that (1) may be achieved by placing the laser in a nitrogen atmosphere, although the presence of even small amounts of oxygen tended to nullify the effect. Clearly we were not likely to achieve this oxygen free atmosphere using an open stream dye laser, even with a nitrogen-filled box over the apparatus, since apertures were essential for adjustments and for the beam entrance and exit. Furthermore, the dye cannot return to the reservoir without some turbulence leading to bubbling, or by being spread over a large surface area to reduce the flow speed and minimise turbulence. Both these options encourage the dissolution of any oxygen present, in both cases by increasing the surface area of the dye solution. We have thus not attempted to reduce the oxygen content of our dye solution.

The third option, that of filtering, is the easiest method of increasing the dye lifetime. Winters found that the acid derivative of C1 had very low mobility on an alumina chromatography slide, and if our supposition of there being a similar derivative of C102 is correct, the use of

an alumina filtration column would remove a large fraction of any acid produced from ClO2 solution.

We have produced a suitable filter, which comprises a 3cm diameter pyrex tube, 50cm long, with a fibreglass plug at each end and filled with activated alumina. The lower end tapers to fit into a rubber bung which leads to a 1 litre sidearm conical flask, and the upper end carries a 1 litre reservoir. Filtration is carried out by filling the upper flask with degraded dye solution and producing a soft vacuum in the lower flask. This serves no purpose other than to speed the flow of dye through the column, which would otherwise take over a day to filter through, due to the high viscocity and surface tension of the ehylene glycol and the fine particular nature of the alumina. With a single pumping of the lower flask, followed by sealing off, the column takes about 6 hours to filter.

The filtered dye solution is only slightly paler than before filtration, but the effect on the laser performance is considerable. The filtered solution has a much lower pumping threshold than the degraded solution, (of the order of 1 Watt after filtration compare with up to 2.5 Watts before), and lasts over twice as long as fresh solution before the threshold again rises to 2.5W. The reduction of the pumping threshold is almost certainly due to the removal of absorbing chemicals by the filtration. The latter effect could be due to one of two causes. Either the original dye crystals are slightly contaminated with traces of the absorbing acid created by long exposure to daylight, or, possibly, the dye solution contains a

proportion of other lasing materials generated during the three-step oxidation already proposed or along a parallel route, as in [4].

Winters observed five products from the photo-oxidation processes in C1, two of which are known to lase in the blue and one of these is a commercially available dye, Coumarin 120, which has a higher gain than either C1 or C102 and has a fluorescence peak at a much shorter wavelength [2]. We propose that the improvement in performance of <u>filtered</u> C102 solution following the degradation could be due to the production of a structure similar to C120, here designated C102a (see Fig 3-3), thus yielding a mixture which is rather more efficient than pure C102 solution. Although we have not attempted to run dye that has been degraded and filtered more than twice, there has been a slight improvement in threshold and power on each occasion, and it may be that the dye would continue to improve as a steadily increasing proportion of a more efficient dye is produced.

The increase of laser lifetime of filtered solution would also be explained by the production of C102a. Its fluorescence maximum would be expected near 440nm and the gain could drop by a factor of four at 480nm, which is the peak of the C102 gain. The acid derivative of C1, however, has its absorption maximum at 470nm and any similar absorbing derivative of C102 (i.e. C102<u>b</u>) would be expected to absorb close to this wavelength as well, and thus well clear of the C102a fluorescence. Hence C102a, if generated, could continue to lase even though the emission from C102 was being absorbed, providing of course

that the laser were properly tuned to the shorter wavelength. This is supported by our observations that degraded and filtered C102 solution has a slightly blue-shifted tuning range (by about 1nm), compared with fresh solution.

3-3 Comparison with extracavity frequency doubling

In order to assess the usefulness of LFM as a frequency doubling material, it is necessary to compare its performance in the two cases of intracavity and extracavity doubling.

The intracavity results have already been discussed. Extracavity doubling is achieved by setting up a standard (linear) dye laser cavity, with tuning element, and passing the output beam through the LFM crystal, focusing it at the same time (Fig 3-13), and monitoring the resultant UV. The main disadvantage of this method is that astigmatism is introduced into the beam by focusing it through the crystal surfaces at an angle. Also, the emerging beam is diverging, and must be refocused on to the photomultiplier tube, giving uncertain UV losses at the second lens.

In order to make a reliable comparison between the two cases, therefore, the beam geometry must be as far as possible the same at the crystal and detectors, and this is best achieved by the arrangement shown in Fig 3-14. In Fig 3-14a we show the cavity already described, with the two detectors in position, the photodiode monitoring

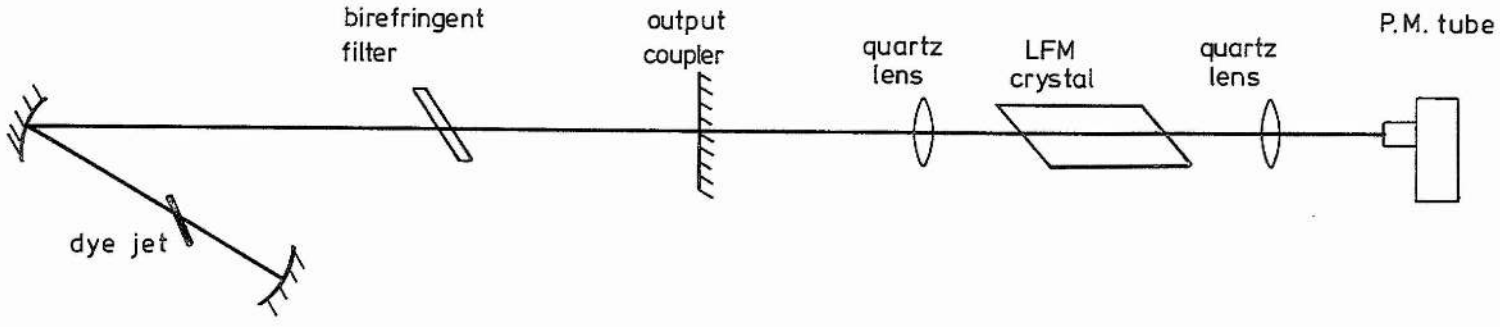

Fig 3-13: Extracavity frequency doubling schematic

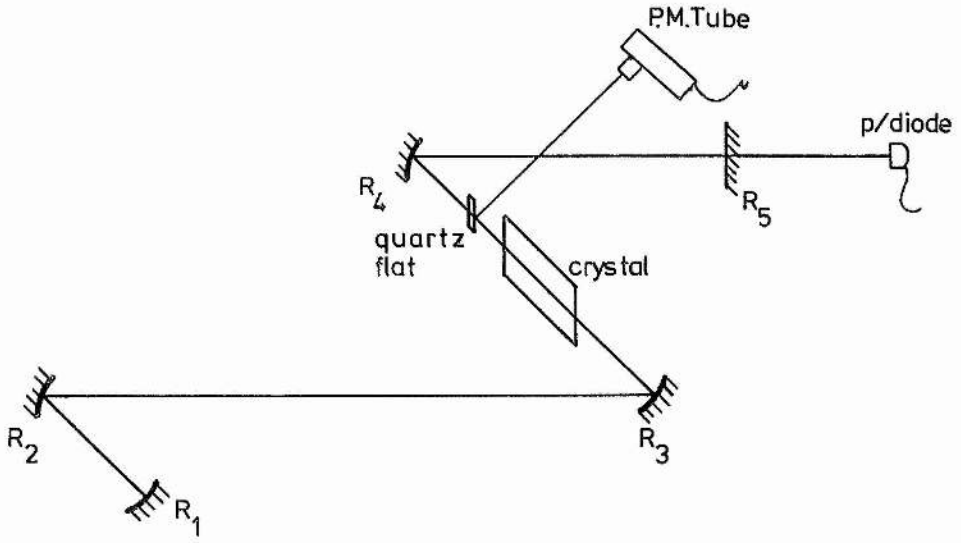

(a) normal cavity

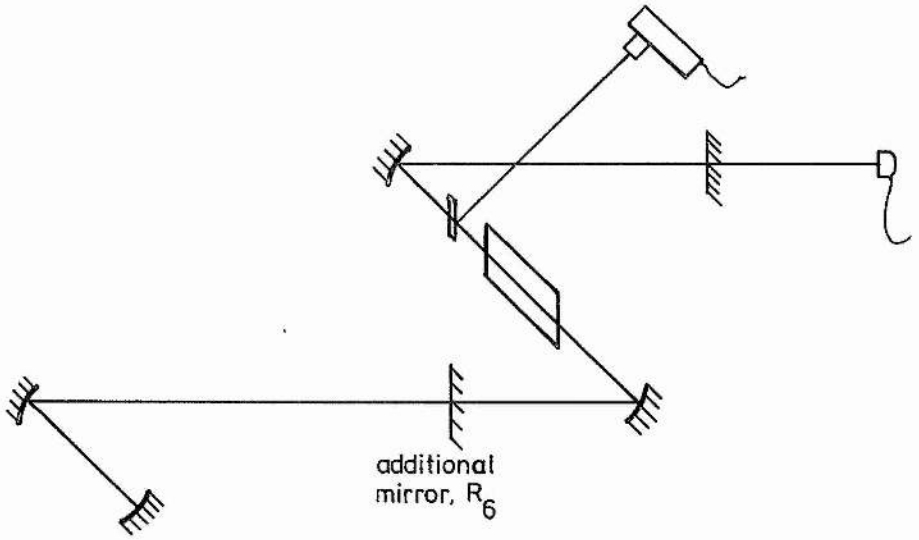

(b) modified for extracavity frequency doubling

Fig 3-14: Cavity conversion

F1

the visible power incident on to R_5 and the photomultiplier monitoring the generated UV reflected off the quartz plate. The crystal is placed extracavity by inserting a suitable coumarin 102 output coupler (CRL 903-060-00), which in this case has a radius of curvature of 15m and reflects 1.3% over the range 468nm to 482nm. Although this is not the full lasing range of the dye, it is satisfactory for this purpose and was used in obtaining the original power curves of Fig 3-9, with which comparison can be made. The mirror, designated R_6, is placed between the birefringent filter and R , and forms a tunable cavity R_1-R_2-R_6, whose output beam then passes to the crystal (Fig 3-14b).

Providing that only R_6 is moved in adjusting this shorter cavity for maximum power, the beam will pass through the crystal in exactly the same orientation as when the crystal was inside the cavity R_1 to R_5. Furthermore, since the photodiode monitors the power incident on to R_5, a direct power comparison may be made between the two arrangements.

Placing the second output coupler R_6 as close as possible to R_3, within the mechanical constraints of the Z-fold, also ensures that the divergence of the beam incident on to R_3 is approximately the same as when the crystal is intracavity. This is necessary because otherwise the size of the focused spot inside the crystal will be significantly different and the UV generation will not be optimised. The region between R_2 and R_3 in Fig 3-14a is one where the intracavity beam should be approximately parallel [13]; likewise between R_4 and R_5. Thus the

F2

insertion of a virtually plane mirror R_6 should have negligible effect on the shape of the beam reaching R_3 in the second arrangement.

However, we have found that when R_6 is in place, the cavity R_1-R_2-R_6 is rather badly optimised with regard to the position of R_2, and that unless R_2 is moved, the cavity is almost unstable and certainly does not produced very much power. Thus mirror R_2 was moved slightly away from the jet causing the beam on to R_6 (and thus also on to R_3) to converge more. This means that the size of the focused spot in the crystal is now much smaller than before. As shown earlier (Chapter 2, Sec 2-1-6-1) the SH power depends not only on the fundamental power but <u>also</u> on the area of the focused spot in the crystal. We would therefore expect in this case that the generated SH power will be very much less than before, even allowing for the different pumping power, unless the beam is refocused to its original spot size by replacing R_2 with a mirror of longer focal length. This would then involve altering the whole geometry of the Z-fold arrangement, introducing further difficulties into the comparison. As then expected, the UV powers observed in the arrangement of Fig 3-14a are more than an order of magnitude less than might be expected in the optimum case. This comparison between intracavity and extracavity frequency doubling is thus inconclusive.

<u>3-4 Optimised intracavity frequency doubling</u>

The best output obtainable from a C102 standing wave

F3 laser, containing a birefringent filter but no frequency doubling elements, is typically 400mW broad band when using a 3W pump laser. The output coupler would normally transmit around 5% so there would be a circulating power of about 8W in the cavity.

In our frequency doubled laser, the intracavity power is about 1.25W, again with a 3W pump. This much lower power is due to the rather low gain of C102 combined with the extra losses due to the extra mirrors, the crystal and the crystal cell. However, even these intracavity powers are over three times higher than those available extracavity, and thus offer more than an order of magnitude improvement in the UV powers generated.

In order to obtain higher intracavity powers, the various sources of loss must be considered. Firstly, the mirror coatings, while designed for normal incidence beams at their quoted wavelengths, are not tailored to maximum reflectance when incident angles of 15° or more are involved, as in the case of the mirrors focusing into the crystal, R_3 and R_4. Secondly, with any crystal which cannot be temperature tuned to obtain phasematching, the crystal must be tilted off-axis for UV generation at all but a narrow band of wavelengths. Such tilting introduces further losses and severely reduces the intracavity power. Thus ideally, a crystal should only be used over a narrow wavelength range and further crystals obtained for use outside this range. Thirdly, the use of an additional pair of Brewster windows on the crystal cell introduces further losses, though these are small, since unless the refractivities of the crystal and

cell windows are the same, Brewster's angle is not the same for both and a compromise must be reached. The only reasonable solution to this problem is to use an index matching fluid between the crystal and quartz. This is naturally only possible if the fluid does not attack the surface of the crystal, and, of course, it must be UV transparent. These conditions are difficult to achieve simultaneously, since most matching fluids that are safe for use on water-based crystals also degrade in transparency under UV irradiation.

Finally, and most significantly, is the bulk optical properties of the LFM itself. We have observed considerable scattering within the crystal and at the surfaces, and consider that this aspect of the laser is the most important one in which improvements must be made.

If the losses described can be reduced significantly, then it is reasonable to expect intracavity powers of 3W to 6W with a single tuning element and a 3W pump. If these figures are achieved, then UV powers of between 400μW and 1.6mW can be generated, and even with the 30% output coupling used here, the smaller of these figures represents an improvement by a factor of 50 in the best powers that can be obtained by extracavity doubling.

3-5 Single frequency operation as a ring laser.

For high resolution spectroscopic applications, single frequency operation in the UV is essential. Considerable work has been carried out on this aspect of laser

development [5,6,12] and the trend has been towards the use of travelling-wave rather than standing-wave systems.

The advantages of the travelling-wave systems are that single frequency operation is generally easier to obtain and control, and the circulating powers can be much higher, as spatial hole burning effects are eliminated. The disadvantage is that because of additional mirrors and other optical elements, the threshold pump power is much higher.

We have set the laser into a travelling-wave configuration as shown in Fig 3-15. The only changes that are required in the conversion from a standing-wave laser are that R_1 must be moved to approximately its own focal length away from the dye jet and then tilted upwards at R_7 which must be at about the same height above the laser base as R_5, and that R_5 must reflect the beam from the crystal region not back at R_4 but slightly below it to R_7. Ideally, as shown by Wagstaff et al [13] and applied to the ring laser by Wagstaff and Dunn [6], the geometry of the Z-fold is unchanged in the conversion, and the angles between the beams in the jet region should be slightly modified. In practice these changes are small enough to be ignored without serious loss of laser power, and we have not attempted any such changes to the jet region.

R_7 is a plane mirror, and in our case it it identical to R_5, and thus the photodiode which monitors the intracavity power can intercept either of the faint beams transmitted by these mirrors. In practice, the beam alignment in the cavity prevented the beam being seen beyond R_5, and so the

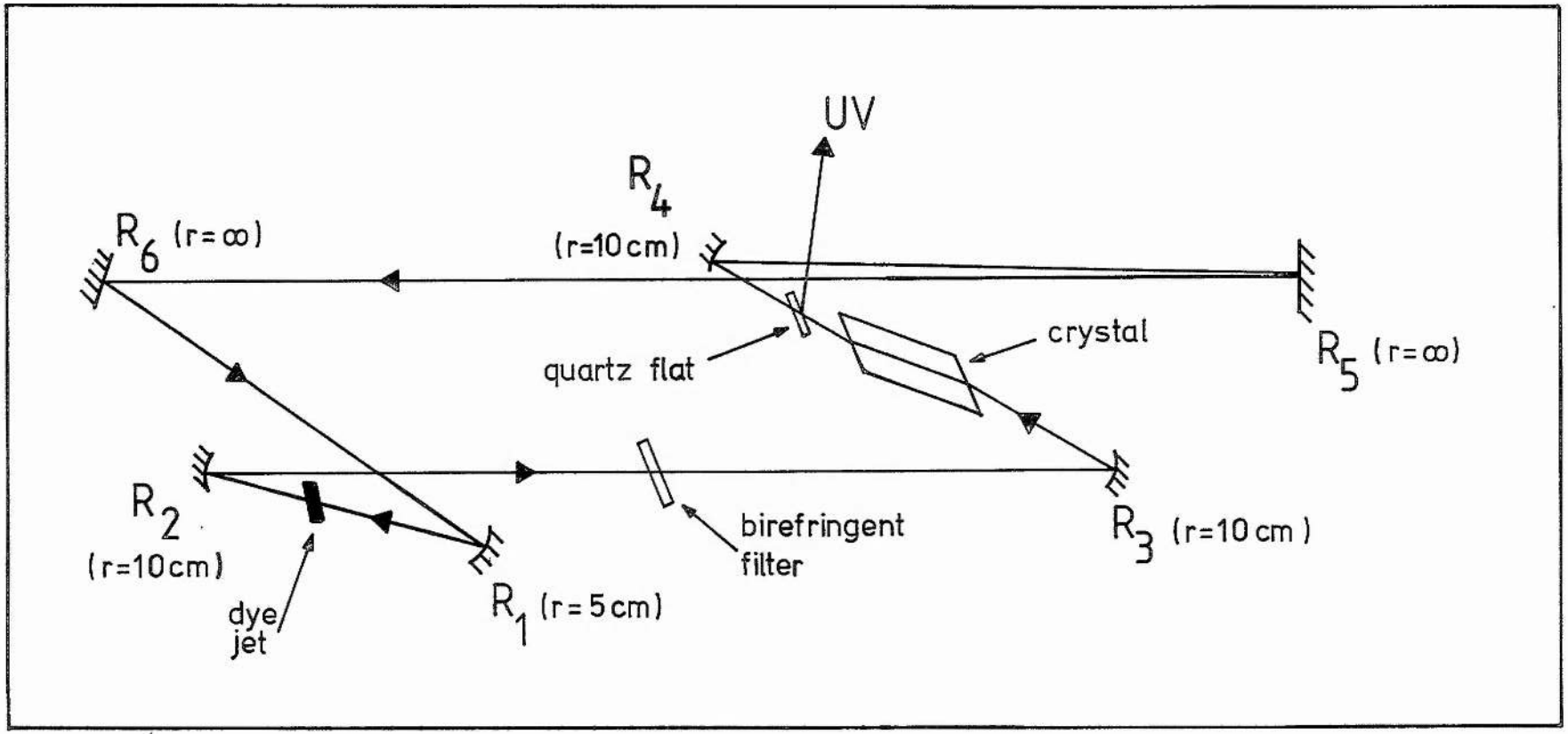

Fig 3-15: Frequency doubled ring laser schematic

photodiode was moved to the other end of the laser.

The threshold of this system was about 1.8W (compared with between 0.8W and 1W when set as a standing-wave cavity). As expected, intracavity power has been as high as 2.5W at 483nm and 2.0W at 488nm, but due to the higher threshold and increased losses, the tuning range is only 468nm to 505nm. This compares with 462nm to 515nm for a standing-wave system without the doubling element, or slightly smaller than that when the LFM crystal is included. In this latter case, the range is more dependent on dye purity.

With a 1mm uncoated etalon included in the ring cavity, the laser operates in a single longitudinal mode. In this condition the laser is bistable and switches direction of wave travel randomly during operation. This of course means that the UV repeatedly changes its direction of leaving the crystal, and to maintain single directional operation, a suitable optical diode such as a Faraday isolator [14] must be included in the cavity. This then introduces considerable further losses and raises the threshold excessively. We have attempted to use such a device in this laser, but with no success in obtaining lasing in the first place. We suggest that although travelling-wave lasers are suited for use with high gain dyes such as Rh6G, they are not so with the coumarin dyes.

Another method of obtaining single directional operation, such as the use of an external mirror [6], could be used, provided the transmission of R_5 or R_7 was sufficient to

allow enough radiation back into the cavity in the preferred direction without causing too much loss of intracavity power, and would be more suited to coumarin lasers. This aspect of the design has not been pursued.

:F1

REFERENCES CHAPTER 3

1 Drexhage KH; "Structure and properties of laser dyes" in "Topics in applied physics", 1-Dye lasers, ed. Schafer FP, Springer-Verlag, Berlin, 1977

2 Dienes A; Appl Phys 7 135-9 (1975)

3 Dye data sheets, as supplied by Coherent Inc.

4 Winters BH, Mandleberg HI, Mohr WB; Appl Phys Lett 25 723-5 (1974)

5 Ferguson AI, Dunn MH; Opt Commun 23 177-82 (1977)

6 Wagstaff CE, Dunn MH; J Phys D 12 355-68 (1979)

7 Ferguson AI; PhD thesis, University of St Andrews (1977)

8 Singh S, Bonner WA, Potopowicz JR, Van Uitert LG; Appl Phys Lett 17 292-4 (1970)

9 Gabel C, Hercher M; IEEE J Quant Electr 8 850-1 (1972)

10 Dunning FB, Tittel FK, Stebbings RF; Opt Commum 7 181-3 (1973)

11 Naito H, Inaba H; Optoelectronics 5 265-9 (1973)

12 Wagstaff CE, Dunn MH; Opt Commun 35 353-8 (1980)

13 Wagstaff CE, Dunn MH, Ferguson AI, Bastow SJ; Opt Commun 25 397-83 (1978)

14 Dunn CE; PhD thesis, University of St Andrews (1982)

A1

CHAPTER 4: The xenon ion laser and its development for use as a dye laser pump source.

4-1 The need for the xenon laser

A common use for powerful lasers is in the pumping of tunable dye lasers, whose output may be used in a variety of spectroscopic applications or for the generation of further tunable ultraviolet (UV) light by nonlinear processes. In both cases, two features of the radiation which determine its suitability for a particular application are the spectral purity and power. The various systems for pumping dye lasers give a wide variety of possible values for these quantities. Systems currently available commercially are continuous wave (cw) ion lasers, commonly argon ion, pulsed flashlamps containing moderate pressure xenon, nitrogen TEA lasers giving pulsed UV, pulsed Nd:YAG lasers which are frequency doubled or frequency tripled for dye laser pumping and excimer lasers, whose UV pulses can operate at wavelengths below 200nm. Commercially, the xenon ion laser is not available.

The cw ion laser is characterised by low powers in the output beam, commonly a few watts at best, but with very good spectral purity with a resolution which can be as low as 1MHz ($\simeq 10^{-6}$ nm). Mode locking techniques have enabled such systems to generate pulsed outputs with powers of the order of kilowatts in 10ps pulses, though inevitably the cost is prohibitavely high.

In the case of pulsed systems, the factor limiting the spectral purity is the pulse duration. The lowest possible frequency bandwidth $\Delta\nu$ for a pulse of length Δt is given by the approximation:

$$\Delta\nu \, \Delta t \simeq 1$$

This means that with the highest quality laser, the resolution of a pulse of duration 1ns is limited to about 1GHz, and for a 100μs pulse, the limit is about 100kHz.

Flashlamp dye lasers operate with pulses of the order 10μs long, but because of their construction, operate only at a low pulse rate and at comparatively low powers of a few kilowatts. Their reliability is also poor due to the short lifetime of the flashlamps. Thus despite their better spectral purity than other pulsed systems, they have little to recommend them if alternatives are available.

Nitrogen TEA lasers have provided cheap and powerful pumps for dye lasers. The 337nm output in 100kW, 2ns pulses is very suitable for exciting most dyes, and such systems are widely used, being both reliable and relatively inexpensive. Their disadvantage lies in the resolution they can achieve being limited to around 500MHz, which, despite the many kilowatts of power, is very much poorer than that of cw or flashlamp systems.

Nd:YAG and excimer pumped systems give very similar results and there is little to differentiate between them. In both cases, very large pumping powers, in excess of 1MW, are used, in the UV for excimer systems and in the visible or UV for Nd:YAG. The latter involves frequency doubling or tripling the fundamental wavelength at 1064nm before most dyes can be pumped, and even if this is carried out efficiently, up to 70% of the power may be

wasted. At the very large pumping powers involved in these systems, the photostability of the dyes can be an important factor. Intense UV powers can cause singificant photodissociation of the dye molecules even over a short operating period, and the efficiency is reduced rapidly. This problem occurs to a much lesser extent with cw and flashlamp pumped systems due to the pumping being mainly from the visible and at lower total energies, and to a small extent with nitrogen pumped lasers due to the lower powers and shorter pulses. In terms of spectral resolution, the 10ns pulses from Nd:YAG or excimer pumped dye lasers still only allow an ultimate resolution of 100MHz and few systems have come within an order of magnitude of this figure.

Reference to the details of the various systems given in Table 4-1 shows that at one extreme, cw pumping gives high resolution but fairly low power light, while most of the pulsed systems certainly offer very much higher powers but at the expense of resolution in the output.

To some extent, the wide gaps in power and resolution are filled by flashlamp pumping, but the reliability and expense are often important factors. The xenon ion laser, however, offers a very versatile and efficient pumping system for pulses in the 100ns to 1μs range with powers up to a few kilowatts. The laser is one of the few which can be made at low cost without special equipment, and gives a powerful output in the green-blue region of the visible and also in the near UV. The lower power than for other pulsed systems is compensated by the the longer pulse and the ability to pump most dyes without

Table 4-1 Features of the xenon ion laser compared with other types.

Property	CW	Flashlamp	Xenon	Excimer	Nd:YAG	Nitrogen
Pumping power to dye	10W	1MW	10kW	40MW	100MW	12MW
Pumping power from dye	2W	100kW	1kW	1MW	10MW	100kW
Pulse length		10μs	0.1-1μs	10ns	5ns	1-10ns
Pump wavelength	visible & UV	broadband visible	visible & UV	UV	IR,visible & UV	UV
Typical pulse rate	cw	1Hz	20Hz	100Hz	30Hz	100Hz
Typical dye resolution (visible)	10^{-5} nm 10MHz	10^{-3} nm 1GHz	10^{-5} nm 30MHz	10^{-3} nm 1GHz	$2x10^{-3}$ nm 1GHz	10^{-3} nm 1GHz
Theoretical resolution limit		100kHz	1-10MHz	100MHz	200MHz	500MHz
Resolution using special techniques	10GHz modelocked			150MHz [19]	17MHz [20]	60MHz [21]
Power in this case	400W			5MW	20kW	100kW
Commercial cost [full system] (£k)	25-30	8-10	N/A	20-25	15-25	10-15

photodissociation problems. In the case of the commonest laser dye, Rhodamine 6G (Rh6G), the visible output of the xenon ion laser corresponds almost exactly with the maximum absorption of the dye, a feature unique to the pulsed systems discussed. Efficiencies in the dye system of up to 40% are thus possible.

The long pulse duration of the xenon system is of benefit in that spectral purities of better than 10MHz are obtained in the dye output. The beam within the dye cavity makes several hundred circuits before emerging and this allows a good Gaussian intensity profile to be built up, which is of great value if nonlinear processes are to be studied.

Thus for the particular purpose of operating a Rh6G dye laser with intracavity frequency doubling, the xenon ion laser offers an ideal pump source.

4-2 Development of the xenon system

4-2-1 Background

The xenon laser has been available since the early 1960s, with laser action being reported at an increasing number of wavelengths by Gordon, Labuda and Bridges [1], Bridges and Chester [2], Dahlquist [3], Hoffman and Toschek [4] and Jarrett and Barker [5]. Some of the workers have obtained cw laser action (Bridges and Mercer [6]), but the large majority have used pulsed systems. A summary is given in Table 4-2.

Table 4-2 Reported work on xenon ion lasers.

Ref	A	b	L	V	p	λ	P	σ
8	120	4	0.1-1.5	15	5-30	431-596	4kW total 0.8kW (495 and 539nm)	2500
17,16	300	17	0.1-0.2	15-25	6	495-596	82 total	20
15	200	25	0.5	27	50 TORR	2027-3652	1.0 IR	10
13	150	2.3	0.5-5	5-10	14-28	495-526	0.15 per single line	70
3	100	6	1	5	0.5-3	406-596	0.01 total	45
7	120	4	0.45	20	5-20	431-596	0.3 total 0.15 green	25
5	150	5	50	N/R	7	535 only	0.11	25
14	90	10	0.2-0.4	23	7	365-539	1.4 total 0.38 (535nm)	35
10	80	2.5	0.08	10	10	495-596	2.0 total 1.0 blue/green	N/R
4	175	5	0.6-1.5	10	5-20	456-700	0.5 total 0.12 (539nm)	60
9	190	8	0.2	12	"several"	365 only	5.0	380

A = Active length (cm)
b = Tube bore (mm)
L = pulse length (μs)
V = Firing p.d. (kV)
p = Pressure (mtorr)
λ = wavelengths used (nm)
P = Power output (kW)
σ = Current density (A/mm^2)

The xenon laser has been used by several workers as a dye laser pump [7,8,9,10] for which the resonator lengths, gas pressures, discharge lengths, currents and output powers have covered wide ranges. A brief study of the use of a xenon ion laser for pumping a Rh6G dye laser has been reported by Ferguson [11].

Many of the possible laser wavelengths come from electronic transitions in singly ionised (XeII) or doubly ionised (XeIII) species, but the powerful green and blue-green lines, those of most use in Rh6G pumping, are believed to originate in triply ionised XeIV, although with one exception the actual electronic configurations involved do not seem to have been determined [12, pages 254-5].

4-2-2 Laser requirements

A pulsed laser system such as this has some specific practical advantages over a cw system, namely the absence of a complex and expensive cooling system for both the power supply and the laser tube, and the much lower current requirements of the power supply, offset to some extent by the need for high p.d., high current switching of capacitor banks.

The lasers reported have produced output powers in the range 10W to 80kW, with corresponding variations in gas pressures and current densities. The current density seems to be the most important factor in determining the power of the laser. In a specific study of this feature,

Simmons and Witte [13] obtained optimum current densities of 65-95A/mm^2 for the green and blue-green lines at filling pressures of 14-28mtorr. Papayoanou and Gumeiner [14] obtained values of 30A/mm^2 and 7mtorr respectively. In both cases, an increase in pressure by a factor of two did not have a marked effect on the powers produced.

Mirror reflectivities, where reported, have almost always been over 97% for the rear mirror, but have covered a large range for the output coupler. Papayoanou and Gumeiner, for example, used different front mirrors for each of the wavelengths observed, with transmissions ranging from 45% at 539nm to 18% at 431nm and with similar output powers. Harper and Gundersen [16] used broadband dielectric mirrors with transmissions of 20% and 35%, both centred at 500nm. They found little difference in the output power in the two cases, or even when using a He-Ne mirror, totally reflecting at 633nm. Lasing was even observed at 495nm with the rear (100%) mirror removed, though it must be emphasised that this did not produce significant power, and, more importantly that the volume of the active medium was many times larger than in the majority of the other lasers considered. Simmons and Witte used a broadband output coupler of 12% transmission, but did not attempt to optimise this figure. The consensus among those few workers who have addressed the matter, is that the reflectivity of the output coupler is not by any means a critical feature of the laser design. The only mirror of suitable size and wavelength range available to us had a transmission of only 2.5%. This is probably rather too low, but at present is unavoidable.

It can be seen from Table 4-2 that with the exception of [15] the lasers all operate at pressures of a few millitorr and have discharge tubes of the order of 1-2 metres in length and a few millimetres bore. The pulse lengths almost all cover a good proportion of the range 0.1-2.0μs.

In designing our laser, we chose to follow the general guidelines of a 1μs pulse from a p.d. of 12kV, to give current densities of around 80A/mm^2, with a resonator length of less than 2m to permit easy handling.

4-3 Operation

The princple of operation of many pulsed lasers is that a capacitor is charged to a suitable p.d. and then allowed to discharge through the laser tube, either freely or via a trigger, producing excitation of the active medium and allowing stimulated emission to take place. The schematic of this is shown in Fig 4-1. The thyratron discharges the capacitor in a controlled fashion by receiving a triggering pulse to the grid G. After the discharge, the capacitor recharges at once, but the thyratron does not discharge it again until it receives another pulse on to the grid.

Two thyratrons have been used, both manufactured by the English Electric Valve Co. Ltd., models CX1164 (12kV, 350A max) and CX1570 (16kV, 3000A max). Several capacitors have been used. For p.d.s up to 12kV a bank of Dubilier "Duconel", each of 0.01μF (±15%) at 11kV rms, has been

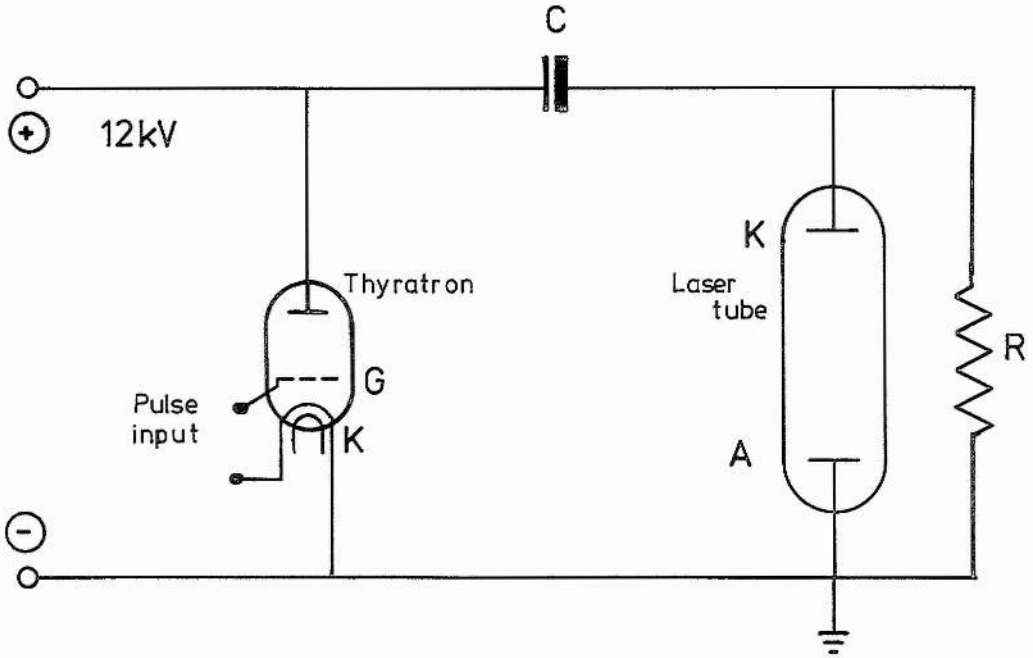

Fig 4-1: Pulsed laser electrical schematic

satisfactory. However, these were later replaced by three HML rapid discharge units of 0.1μF and 0.2μF and rated at 25kV, which are connected in either series or parallel, giving a variety of effective values with no risk of exceeding the p.d. ratings with the power supply available. These larger capacitors have allowed a considerable improvement in laser performance, although a great deal of useful information was obtained with their predecessors.

The control circuit is shown diagrammatically in Fig 4-2. A 20V pulse from a separate pulse generator is applied to the grid of the Mullard 2D21 valve, which acts as a small thyratron, discharging capacitor C and generating a pulse of approximately 600V in the pulse transformer T. This allows a pulse of 1200V to be applied to the grid of the main thyratron, which then fires the laser. The circuit has operated reliably at typical firing rates of 15-20Hz continuously for several hours.

The duration of the current pulse must be reduced as much as possible in order to increase the peak laser power. The principal factor in determining the length of the current pulse is the time constant of the discharge, and this must be as small as possible. Accordingly, the thyratron and capacitor bank are placed as close as practicable to the laser tube electrodes. A photograph of the assembly is shown in Plate 4-1.

Operational pressure of the laser is monitored by an AEI thermocouple gauge fitted between the laser and the pumping system. Since the pressures indicated are of the

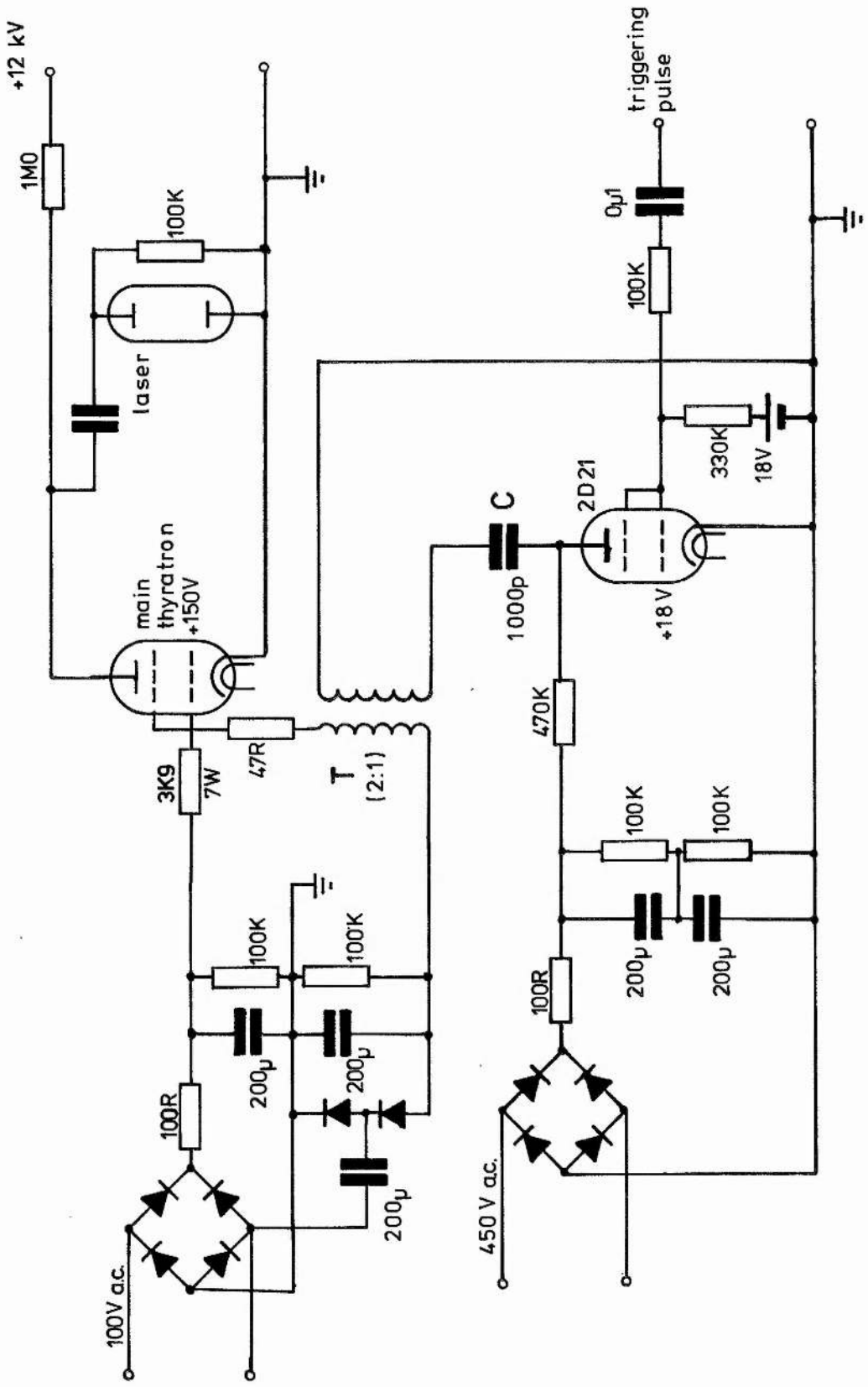

Fig 4-2: Thyratron firing circuit

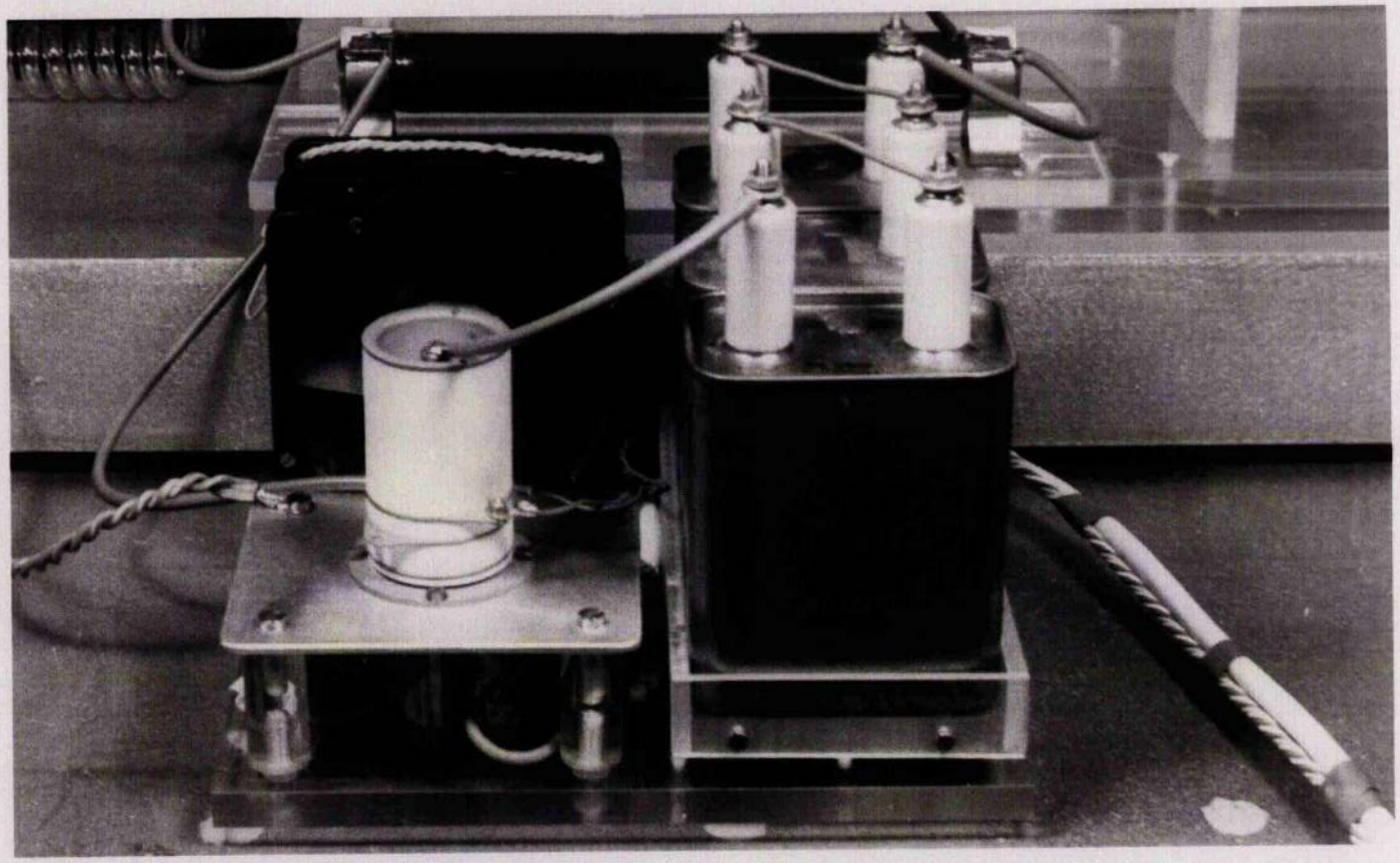

Plate 4-1

order of a few millitorr and the gauge is then operating close to its low pressure limit of scale, all scale readings are only considered accurate to ±1mtorr. The calibration of the gauge for xenon is also different from that for air and we estimate that the actual pressure is 4 to 4.5 times that indicated. This is based on the extrapolation of the calibrations for similar gauges for argon (factor 1.5) and krypton (3) using relative atomic weights. Thus pressure values quoted here must be assumed to have reading errors of ±4mtorr associated with them. The corrected pressure values also refer to filling pressures and not to the pressure within the laser tube when operating, which will be affected by the heating of the gas and possibly by gas pumping due to the intense current. The latter effect has been considered for this type of laser by Harper and Gundersen [16] who quote a formula for the pressure differential, dP/P, across the ends of the active length as

$$dP/P = 6.7 \times 10^{-10}\ ItfL/D^3$$

where I is the peak current, t the pulse length in microseconds, f the pulse repetition rate and L and D are the length and diameter of the discharge in centimetres. Typical values for our laser are: I=800A, t=0.5μs, f=15Hz, L=60cm and D=0.25cm. This gives a value for dP/P of 1.5%, which we consider small enough to be neglected.

Pressure values quoted in published results have either been filling pressures or unspecific.

4-4 Laser construction (Mark I)

Two operational versions of the laser have been built, the major difference between them being the length of the active medium. The MkII version has also included refinements to the electrodes and to the Brewster-angled windows following operational problems with the MkI.

The discharge tube of the laser is a quartz tube 50cm long with a bore of 2.5mm and a wall thickness of 1mm. The cathode and anode are held in pyrex sidearms at either end. The cathode is a hollow cylinder of aluminium*, 8cm long and 3cm inside diameter, with the discharge channelled into the inside surface of the electrode by a pyrex feedin. The anode is a short rod of tungsten projecting directly into a short sidearm beyond the narrow bore quartz tubing. The total discharge length is 80cm, the active medium length (within the resonator) being 57cm. The tube is sealed with quartz windows set at Brewster's angle to the axis of the cavity to give an output with vertical electric field polarisation. Due to problems with gas cleanup by the anode (Sec. 4-5-6) a 600cm^3 ballast tank was subsequently fitted, with connection to the tube near the anode sidearm, and this has reduced the problem considerably. The entire tube is connected to the pumping system by a 1m pyrex spiral, connecting opposite the anode, which terminates in a

---

* The aluminium alloy used is HE15TF, recommended for use in this type of laser. The alloy content is as follows:
Cu: 3.8-4.8%; Mn: 1.2%; Si: 0.9%; Mg: 0.8%
Fe: 0.7%; Ni: 0.2%; Zn: 0.2%; rest Al.

double valve system for greater control of tube pressure.

The mirrors are mounted on three-point suspension mounts, with fine thread vertical and horizontal adjustments thrusting about 8cm from the pivot, allowing very good control over optical alignment. The high reflector is of 2m radius of curvature, 25mm diameter and has a maximum reflectance at 510nm. The output coupler is from a Coherent Inc. CR3000K krypton ion laser, being the yellow-green output coupler, (ref 903-067-00), of 15m radius of curvature, 12mm diameter, with a transmission of 2.5% in the range 520.8nm to 568.2nm. The resonator length is 86cm.

The entire laser is supported on an inverted aluminium channel, with rubber feet to minimise vibration. The mirror mounts are bolted directly to the channel, but because of the high p.d.s involved (up to 25kV), the discharge tube, electrodes and other parts are mounted on a piece of 12mm thick perspex, which bolts to another identical piece which itself then bolts to the channel. This has two advantages: there is considerable insulation between all high p.d.s and the base, which will be touched by the operator and is therefore earthed, and further, the tube assembly can be removed complete from the base of the laser without removing it from its individual supports, should the need arise to make mechanical alterations, which minimises the risk of damage to the glassware. The tube and electrodes are supported 6cm above the perspex base by asbestos columns, while the ballast tank and resistor in parallel with the tube are held by spring clips. H.T. connections are by stiff wires requiring no

extra support and the earth connection is via an eyelet bolted to one of the mirror mounts, so that accidental removal is virtually impossible.

Photographs of the MkI laser appear in Plates 4-2 to 4-4.

This laser has proved an efficient dye laser pump, and is particularly to be recommended by its simple design and low cost. The powers produced have exceeded 80W in a 0.5μs pulse, comparing favourably with those already reported.

4-5 Operational results (Mark I)

It should be emphasised that we do not intend to discuss the theoretical aspects of the results reported here as much of this has been dealt with in considerable detail already [1,2,3,6,13,14], rather we wish to offer guidance to other workers who wish to construct a pump laser of this type.

4-5-1 Observed wavelengths

A total of nine wavelengths have been observed in the laser output, though no more than six have been seen at any one time as the intensities of several lasing transitions are highly dependent on gas pressures and current densities [13,14]. The wavelengths are in agreement with those already reported [2,14] and no

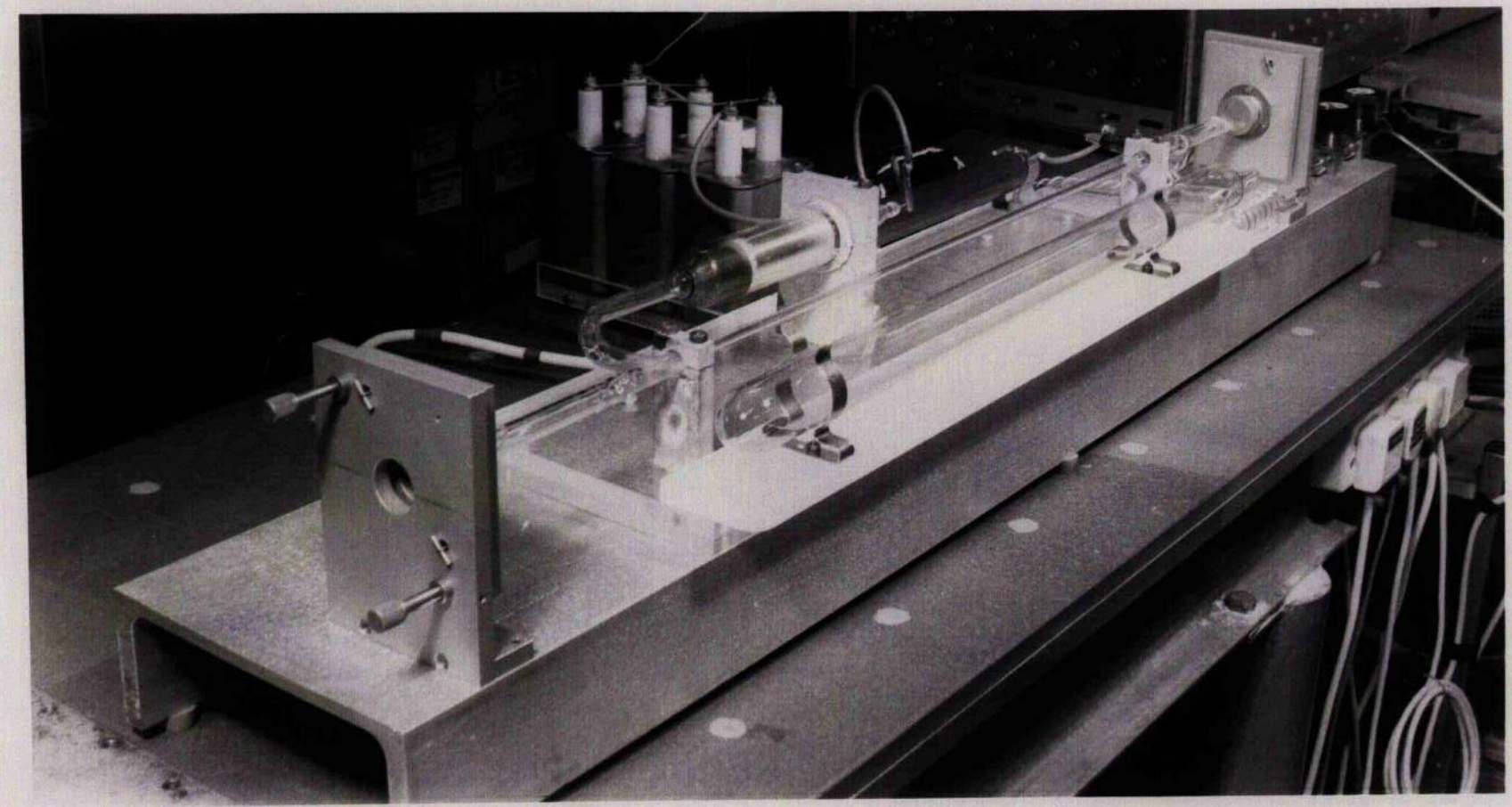

Plate 4-2

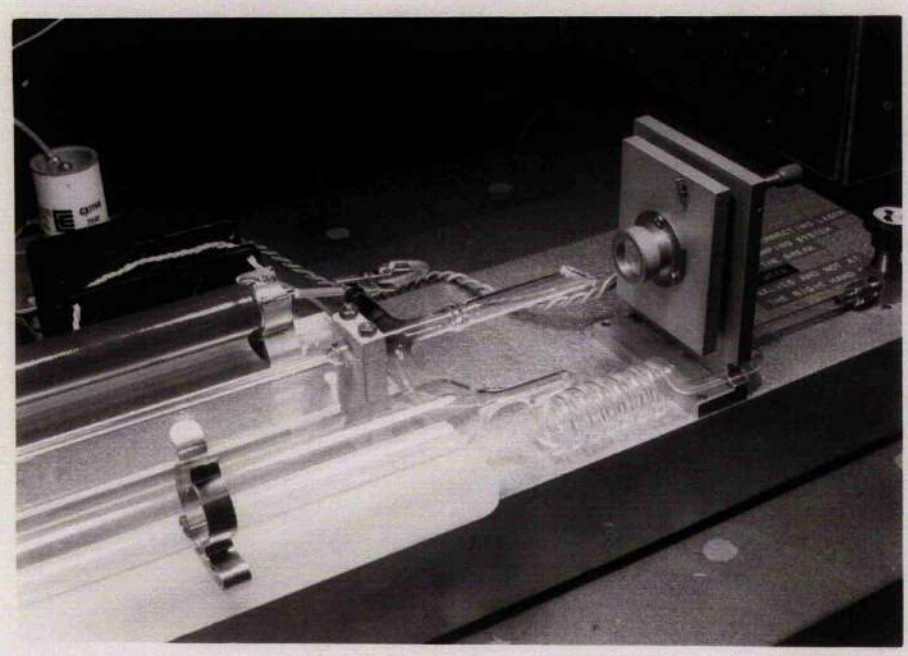

Plate 4-3

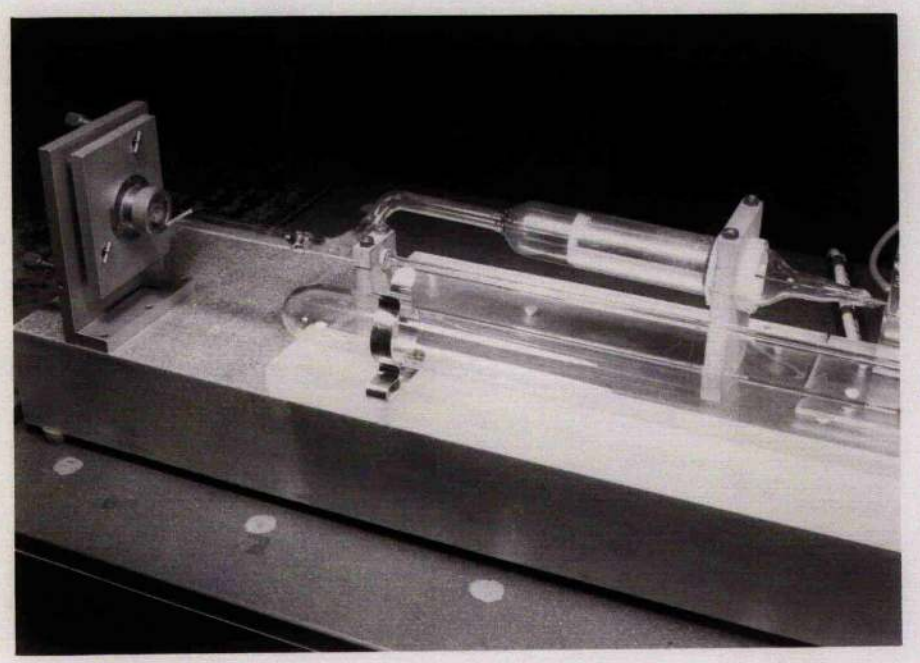

Plate 4-4

previously unobserved lines have been seen. The wavelengths are listed in Table 4-3, together with an indication of the typical intensity of each line as observed in our experiments, and the optimum discharge conditions reported, where appropriate, in [13].

The laser lines most easily obtained were those at 539nm, 535nm, 526nm and 495nm, since these seem less dependent than the rest on the discharge conditions. They are also well suited to the pumping of a Rh6G dye laser. The violet line at 431nm is quite powerful, but is only found at higher gas pressures, when the green and blue-green lines are fading, and this combined with its negligible absorption by Rh6G solution (50 times less than for 526nm) means that it is not normally used. A brief study of the effects of gas pressure, tube current and pulse repetition rate on the total power and relative line strengths has been carried out in order to choose the best operational conditions for eventual dye laser pumping.

4-5-2 Pressure

Fig 4-3 shows the relative line strengths of the six strongest lines for a range of pressures from low (≃5mtorr) to high (≃50mtorr). The pressure values are not considered accurate to ±4mtorr, as explained above, but the trend is clear. On another occasion a diffraction grating was used to separate the beam for photography (Fig 4-4) and colour photographs taken to illustrate the numerical observations. For the case of the pressure dependence illustrated in Fig 4-3, the

Table 4-3 Xenon ion laser lines observed in this work

Wavelength (nm)	Typical intensity	Optimum conditions [13] mtorr	A/mm^2	Comment
539.459	strong	28	83	) most often seen
535.289	V. strong	24	80	
526.017	strong	25	65	
523.889	V. weak	N/R		rare
515.904	moderate	14	95	
500.772	moderate	20	92	
495.410	strong	19	90	
467.373	V. weak	N/R		rare
430.577	strong if present	N/R		high threshold

[Reference 13, (Simmons and Witte), used a tube of 2.3mm radius, 4.2mm^2 c.s.a]

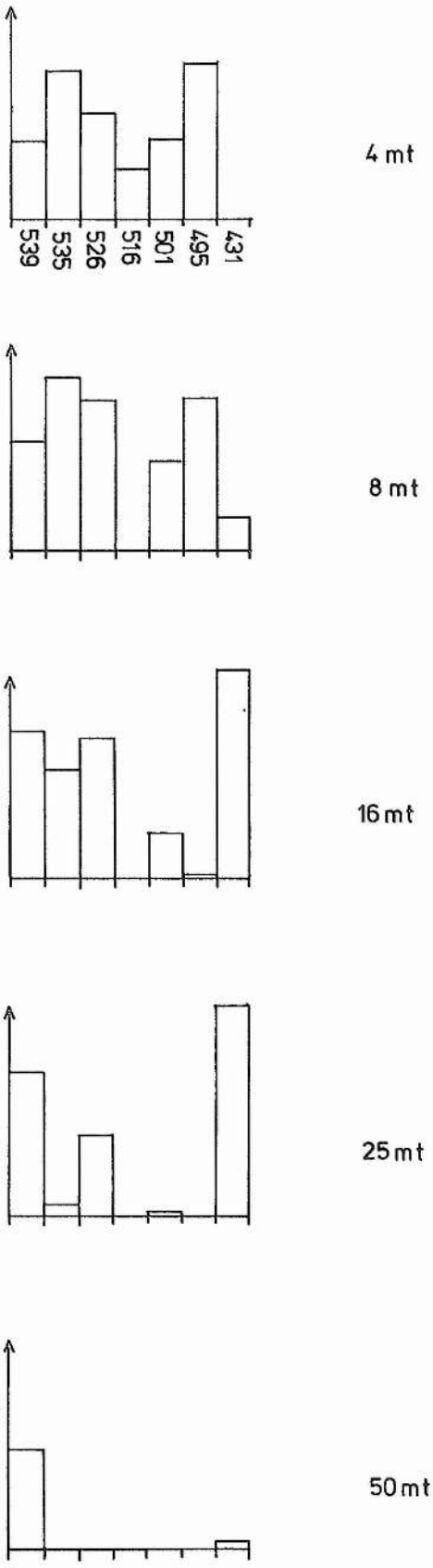

Fig 4-3: Pressure dependence of relative line strengths
(compare with Plate 4-5)

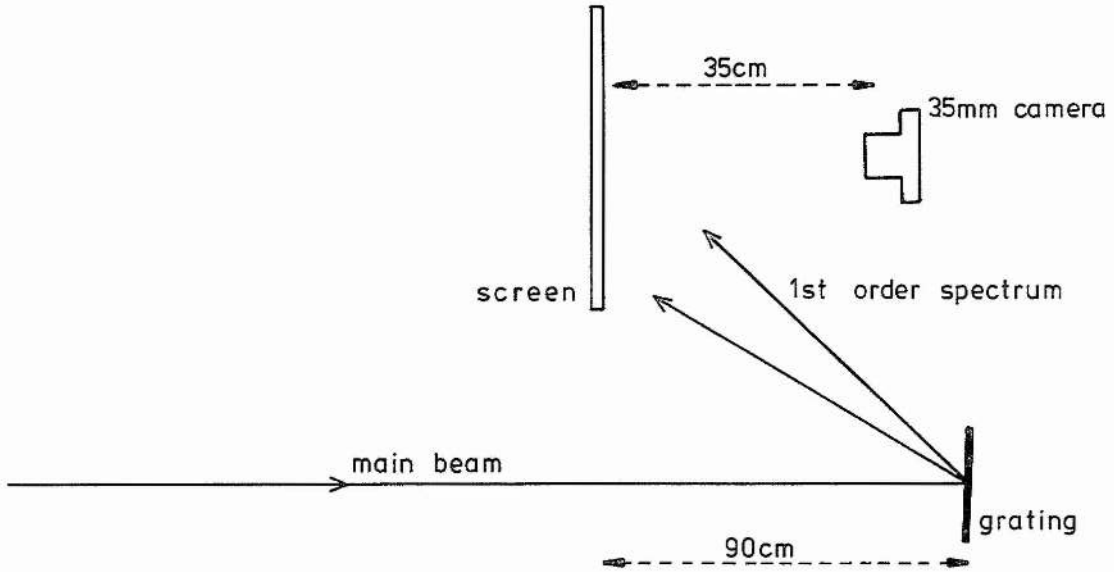

Fig 4-4: Spectrum photography

relevent photographs are shown in Plate 4-5.

The multiline energy per pulse was determined by a Laser Precision Corp. pulse energy meter, model RJP735 with a PJ7200 analyser, (by "multiline" we mean all the lines present under the conditions concerned being observed as a single beam, rather than being dispersed by a diffraction grating, and we are not actually suggesting that at any one time all nine lines are actually present). Graphs of pulse energies as a function of pressure are shown in Fig 4-5. The firing rates are chosen for each capacitor so that the discharge p.d. is approximately constant for all points shown. This is necessary so that a sensible comparison between different sets of conditions may be made. The effective discharge p.d. is 10kV, corresponding to average current densities in the tube of $40A/mm^2$, $80A/mm^2$ and $120A/mm^2$ for capacitors of 0.02μF, 0.04μF and 0.06μF respectively.

The curves of Fig 4-5 show that a current density of around $80A/mm^2$ at a filling pressure of around 10mtorr gives maximum output power. The current density of $80A/mm^2$ is in good agreement with that obtained by Simmons and Witte [13], although it is not clear why there is considerable difference between their pressure values and those obtained here.

4-5-3 Capacitance

The current in the discharge for a given p.d. and pulse duration is determined by the capacitance and the degree to which it recharges after each pulse. The recharging

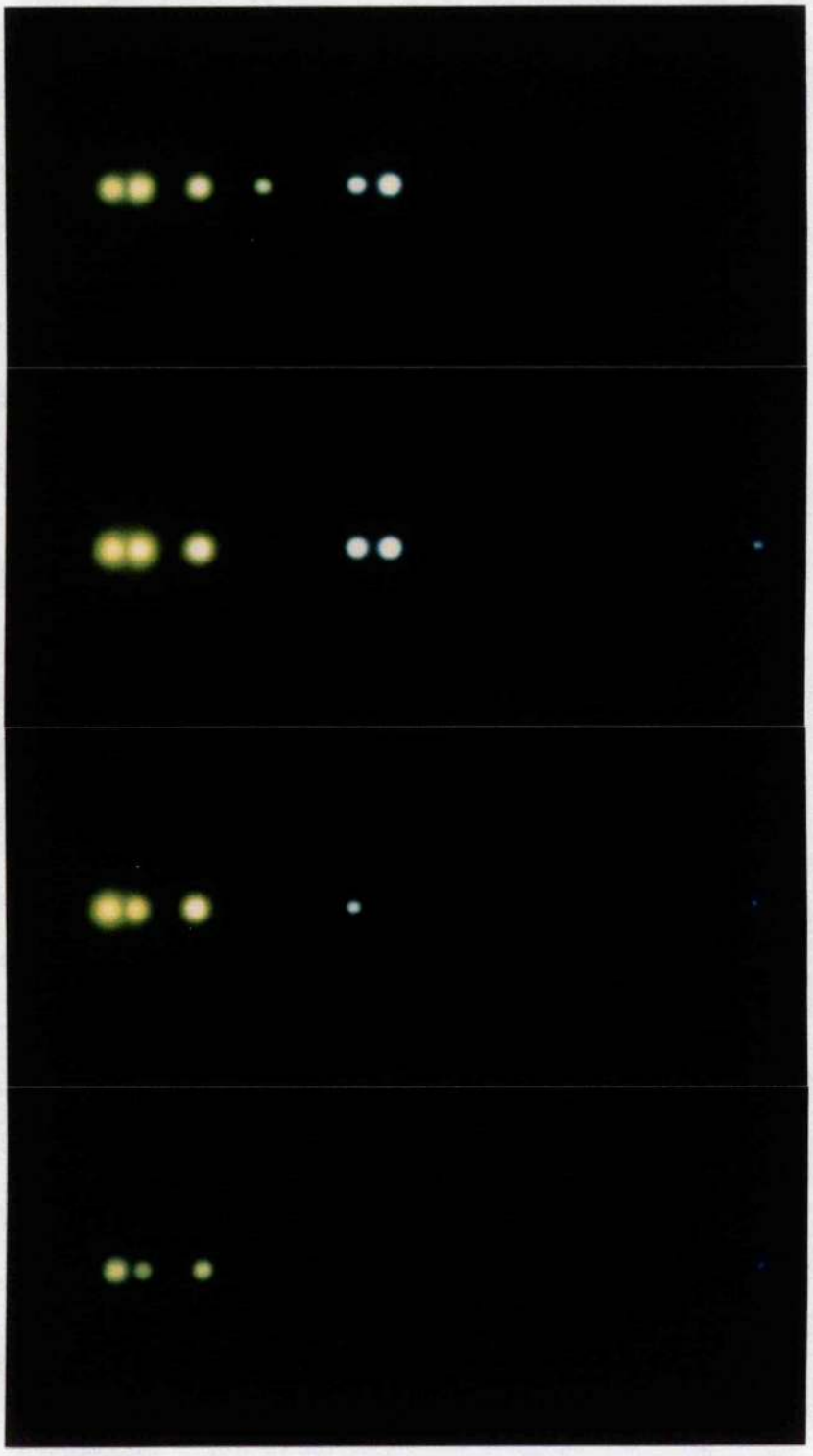

Plate 4-5

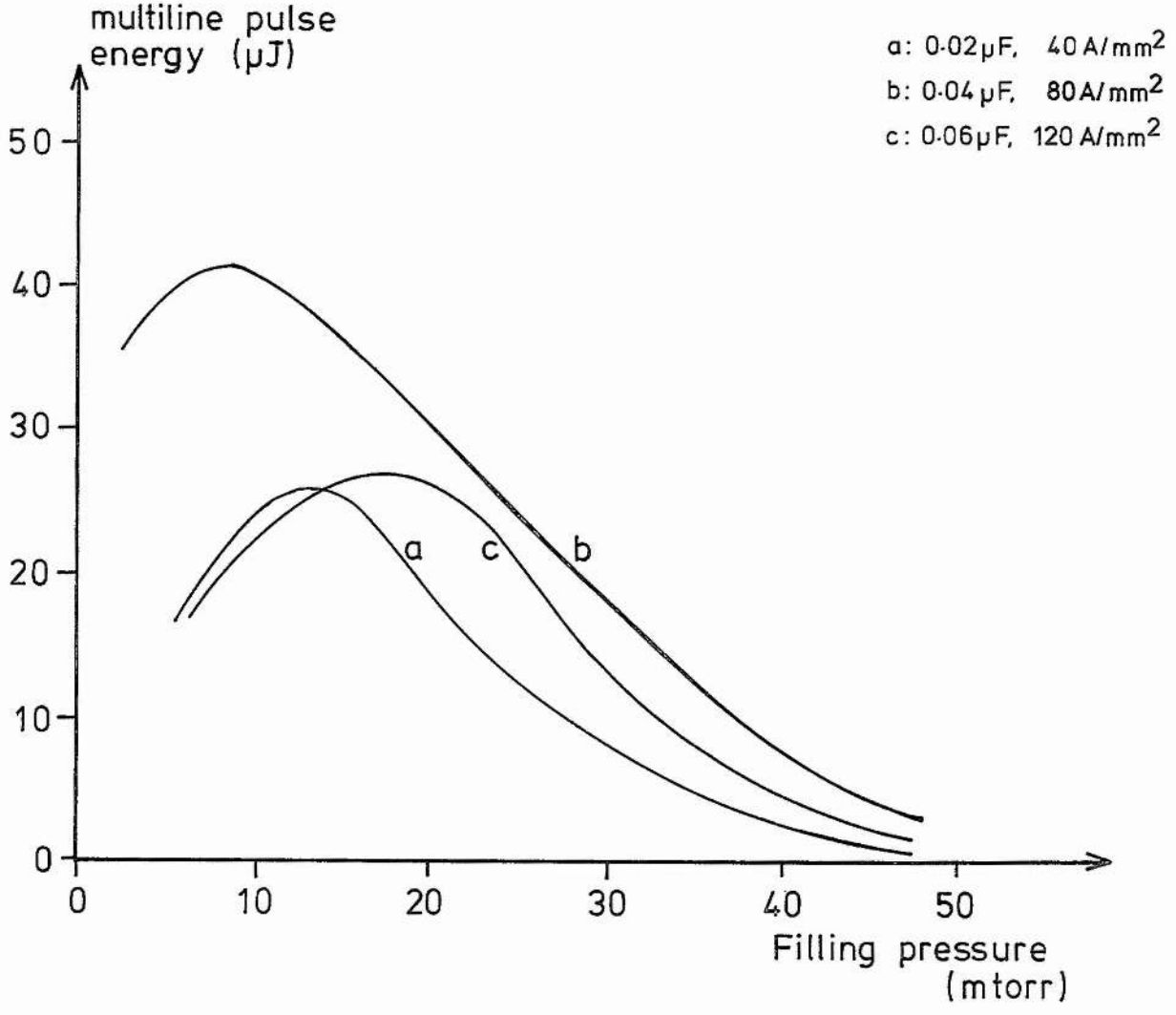

Fig 4-5: Pulse energy against firing rate for the Mk I laser with three capacitors

of the capacitor between pulses is determined by the time constant RC of the system, where R is the resistance in series with the capacitor C. After time t from the moment of discharge, the p.d. V across the capacitor is given in terms of the supply p.d. V_S by:

$$V = V_S \left(1 - e^{-t/RC}\right)$$

In our case, R=1MΩ, and C takes values of 0.02μF, 0.04μF and 0.06μF. For typical operating conditions of C=0.04μF and pulse rates of 15Hz, the time constant is 0.04s, or about half the time between pulses. This means that, at that firing rate, the p.d. across the capacitor will never reach more than 81% of the supply p.d., and for a rate of 25Hz, this value would be 63%.

This aspect must be taken into account when analysing the output power's dependence on capacitance and firing rates, which is illustrated in Fig 4-6a,b,c. Each set of axes refers to a different capacitance, and the multiline pulse energy is then plotted against firing rate. Using the above discussion, this firing rate is converted into an effective discharge p.d., given a supply p.d. of 12kV, and this effective value is also shown. The average current density in the gain region of the discharge is then determined from this effective p.d., assuming that the timescale of the complete discharge is of the order of 1μs, determined from CRO measurements.

4-5-4 Pulse duration

The pulse shape was examined for each line using a Hewlett

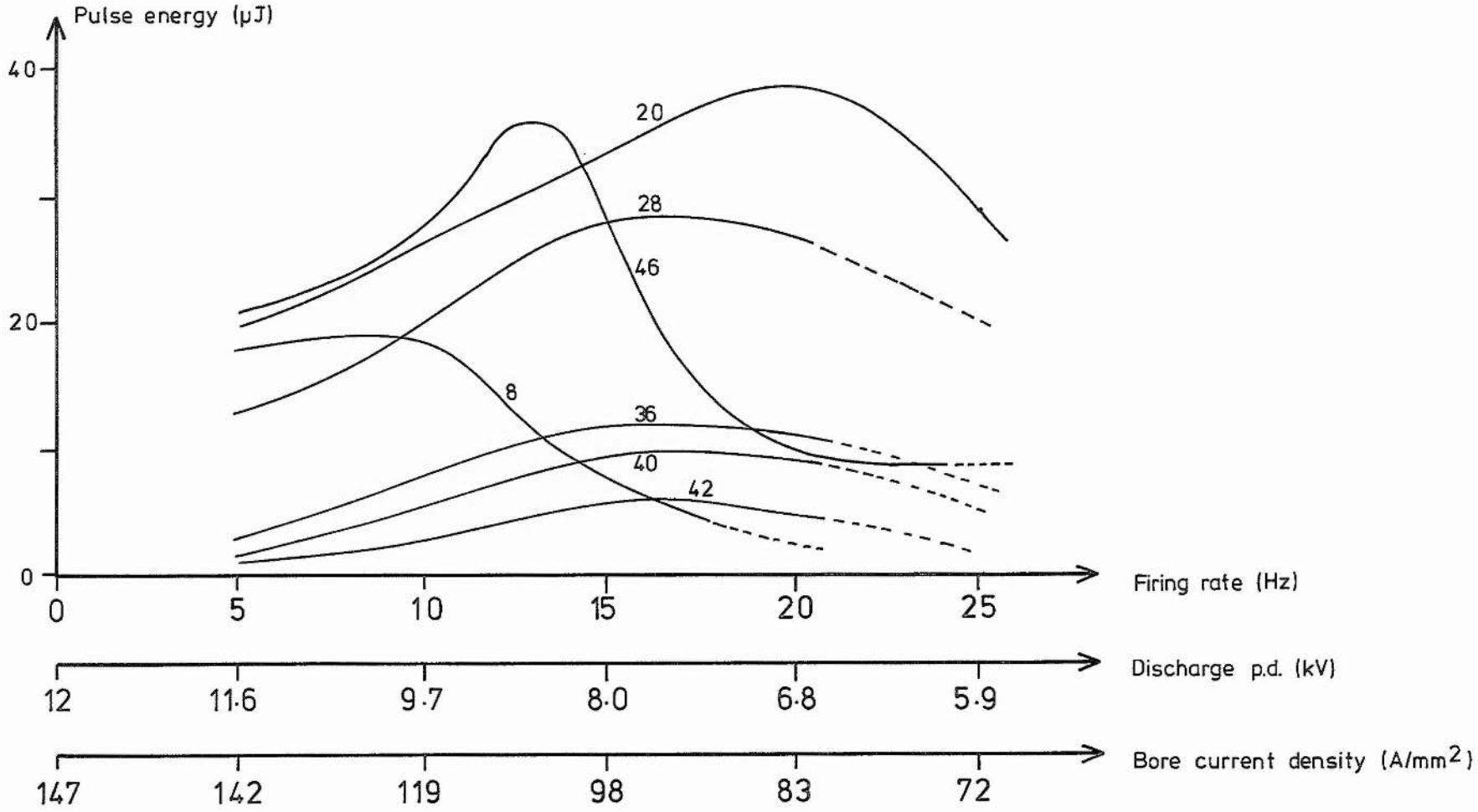

Fig 4-6a: Multiline pulse energies for C = 0·06μF

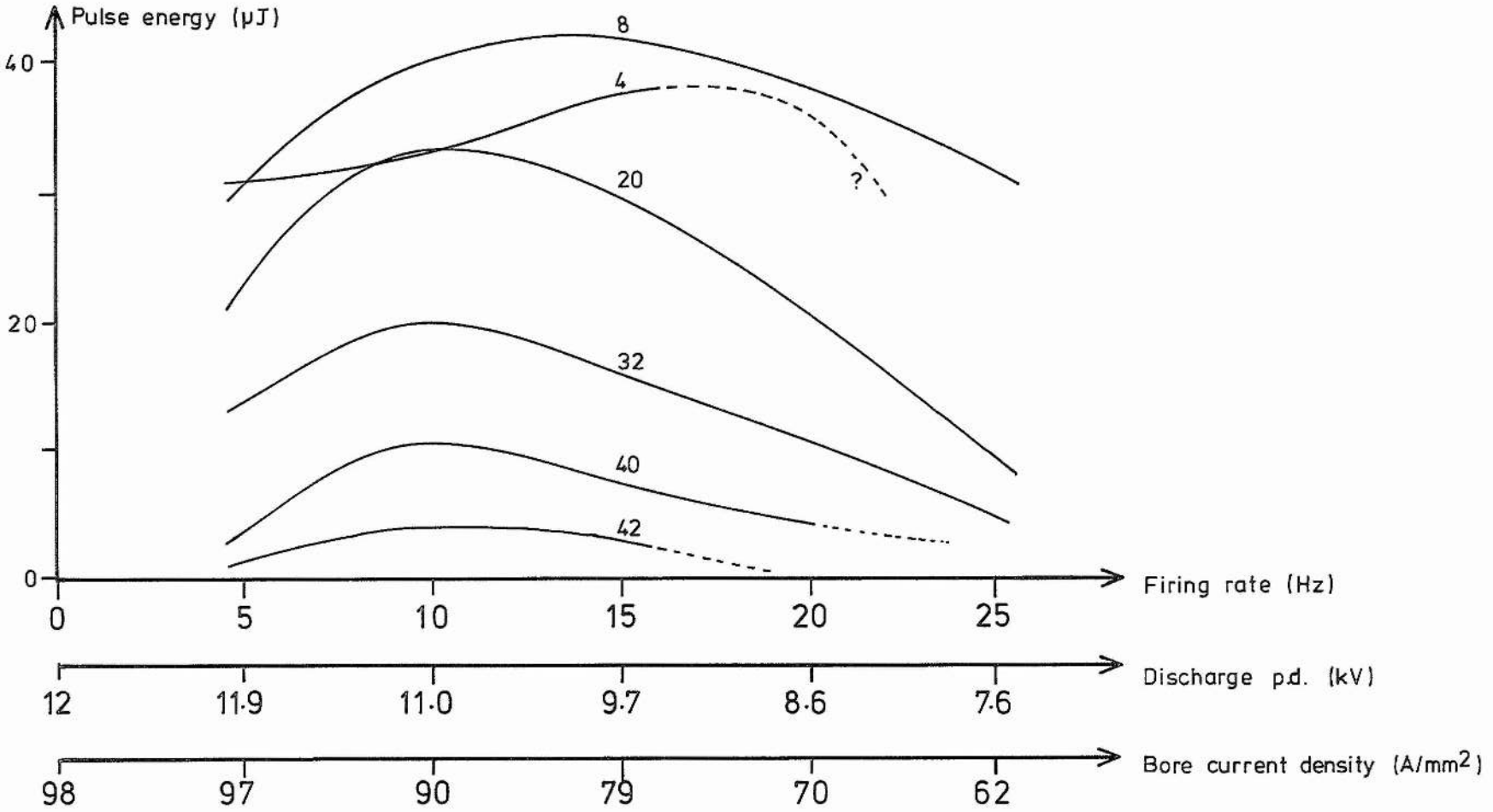

Fig 4-6b: Multiline pulse energies for C = 0·04 μF

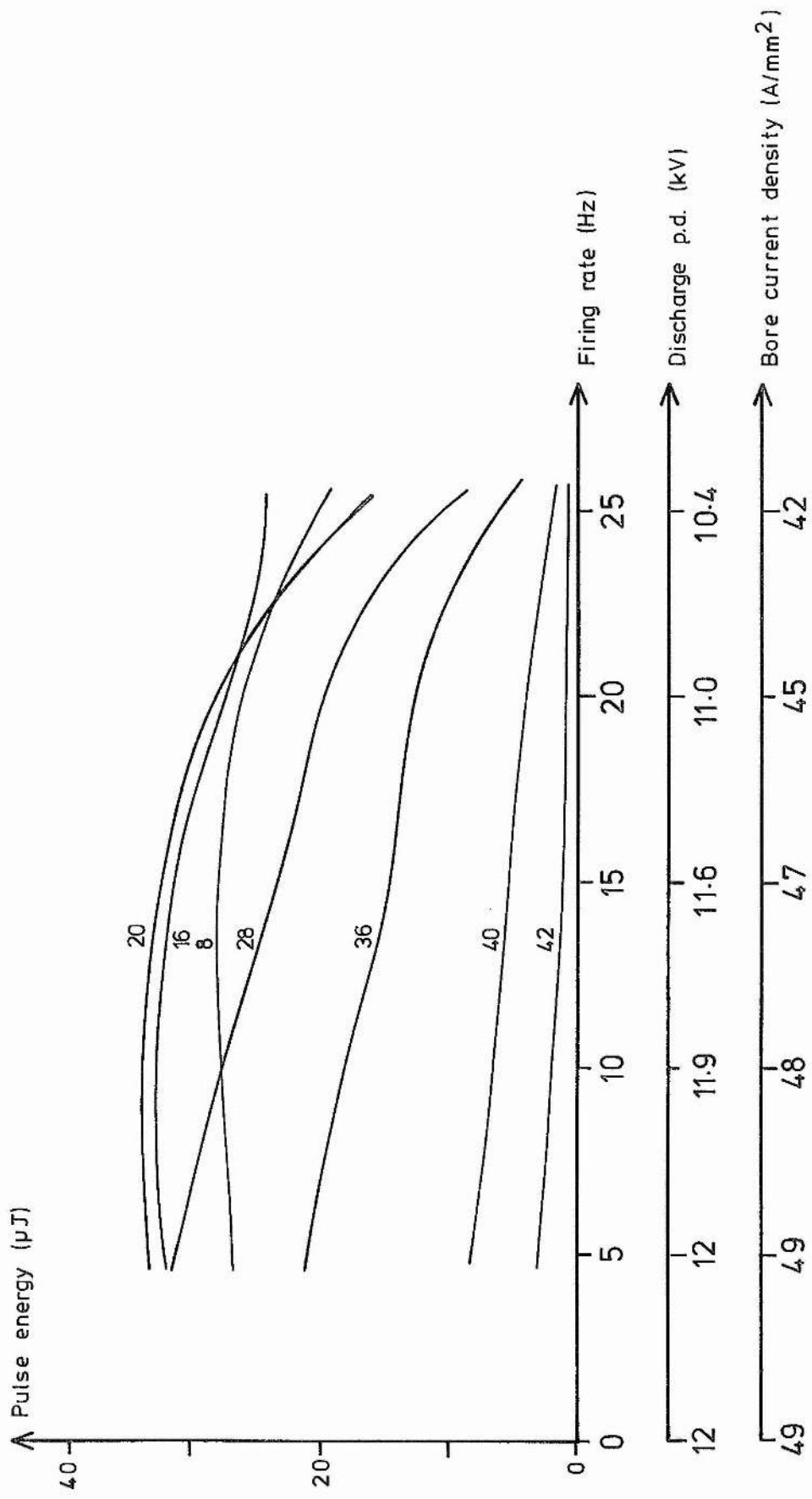

Fig 4-6c: Multiline pulse energies for C=0·02μF

Packard HPA4203 photodiode and a Tektronix 535A oscilloscope triggered from the pulse generator used to fire the laser. In most cases the pulse width was of the order of 0.5μs (FWHM) but varied slightly according to the capacitance, pulse rate and the line concerned. The most obvious feature was that for the 431nm line the pulse width was only 0.25μs, and that the most consistent results were obtained using a capacitance of 0.04μF.

4-5-5 Gain measurements

Single pass gain measurements were made for most of the laser lines. This was achieved by inserting a thin quartz plate into the cavity at an angle and rotating it about a horizontal axis, which will be normal to both the beam and its plane of polarisation. The single pass Fresnel loss at this plate is equal to $2R-R^2$, where R is the single surface Fresnel loss, given by:

$$R = \frac{\tan^2(\theta_i - \theta_t)}{\tan^2(\theta_i + \theta_t)}$$

where θ_i and θ_t are the incident and transmitted angles of the beam with respect to the surface normal at the plate, linked by the Snell formula:

$$\text{refractivity} = \frac{\sin\theta_i}{\sin\theta_t}$$

which in this case has the value $1.462 \pm 0.2\%$.

A summary of the results showing the angles of tilt at which the various lines extinguished, the corresponding

losses, and how these were affected by pressure, is given in Table 4-4. Comparison with Fig 4-3 shows that while most of the lines extinguish in the order corresponding to their line strengths at a particular pressure, the 431nm line in particular has a high lasing threshold, since it is not seen with the quartz plate in the cavity, even at Brewster's angle.

4-5-6 Operational problems

A major difficulty with the MkI laser became obvious only after some time. This was damage to the anode, which was breaking up, due presumably to the very large surface current densities. Pieces of the electrode up to 1mm across were found adhering to the walls of the discharge tube, with many several centimetres away, their motion aided by the acoustic shockwaves produced in the gas at each pulse. This alone was not a severe problem, as the rate of damage was small, but, due to their proximity, the inner surfaces of the Brewster windows were rapidly becoming covered in a fine tungsten dust, causing a considerable reduction in laser power. The problem was not confined to the window near the anode; that at the other end was almost as severely affected, and the obvious need for removable Brewster windows was a major incentive for the construction of a MkII laser.

Probably also a consequence of the damage to the anode was the cleanup of the xenon gas over a period of a few minutes, in a manner similar to the gettering of a thermionic valve, resulting in a excessive reduction in

Table 4-4 Single pass losses for a quartz plate at angle θ to the intracavity beam, and the corresponding extinctions of xenon lasing lines.

θ (deg)	Loss %	Lines extinguishing (Pressures in millitorr) high >25	medium 10-25	low <10
61.0	0.75			516
62.0	1.11		506	
63.0	1.57	495		
67.0	4.60			526
70.0	8.63	526 539		
70.5	9.50	535		
71.0	10.0		539	
72.0	12.5		526	535
73.5	16.1		535	
79.0	36.8		495	495

Lines not listed were not present at that pressure with the quartz plate in the cavity at Brewster's angle.

tube pressure, a tendency to arc and a greatly reduced power output. The cleanup was not reversible, at least in the short term, and so a large ballast volume was fitted to the tube, increasing the total gas volume by a factor of ten. Cleanup was still observed, of course, but now took much longer to have a significant effect on the laser power. Similar effects were reported by Harper and Gundersen [16].

4-6 Laser powers

The multiline output power of the MkI laser had a pulse duration of approximately 0.5µs providing that at least one of the green lines was present, which was usually the case, and pulse energies of 42µJ per pulse, (Fig 4-6b). This gives an approximate power of 84W multiline, which, in the case of the gas pressures concerned, means mainly the green and blue lines, with only a very small contribution from the 431nm line, and powers in excess of 70W could usually be obtained with a roughly equal mixture of the six strongest lines, 539nm, 535nm, 526nm, 516nm, 501nm and 495nm. This power is acceptable for dye laser pumping, but perhaps could be increased with a more transmitting front mirror. The decrease in power due to window degradation meant that dye laser pumping eventually became impossible.

The output beam normally appeared as a bright central spot, approximately 1.5mm diameter at the output mirror, surrounded by an irregular halo roughly 5mm diameter. The shape of this halo varied according to the mirror

alignment and was probably caused by the intracavity beam striking the wall of the discharge tube. The full angle beam divergance was of the order of 1mrad.

4-7 Mark II laser

Having obtained much useful information regarding the best operational conditions with the MkI laser, we rebuilt an old laser assembly to provide a much more powerful and versatile MkII.

4-7-1 Modifications to Mark I

The principal modifications made in the production of MkII were a larger discharge active length, an anode of identical size and material to the cathode and held in a long sidearm clear of the Brewster windows, removable windows which could therefore be cleaned and an X-Y alignment adjustment for the discharge tube at its midpoint. The bore of the tube was also increased slightly from 2.5mm to 3.5mm diameter due to problems with the availability of suitable quartz. Unchanged were the mirror mounts and mirrors which were transferred from the MkI, pressure, capacitance, firing rate, p.d. and power supply. Constructional details which were modified were mainly the result of the existing hardware, such as the Brewster windows, which are ultra-high vacuum stainless steel assemblies with gold O-ring seals, allowing the steel Brewster surface carrying the window to be removed without affecting the existing structure.

The quartz windows were originally sealed to the steel surfaces with rubber O-rings, but this rather defeated the object of the gold seals elsewhere, so the windows were later glued to the steel with epoxy adhesive. No outgassing seems to take place, as the glue, being some distance from the discharge, remains at approximately room temperature. The windows are therefore not easily removed for cleaning, but if cleaning of the inner surface is necessary, then the window would probably need replacing rather than mere cleaning and so the permanence of the adhesive has not been a problem. Such maintainance would only be necessary after several months operation.

A summary of the variations between the two lasers is given in Table 4-5.

4-7-2 Performance

The output power from the MkII laser was 185W multiline, and very much more suited to dye laser pumping.

Table 4-6 compares the performance, sizes and electrical parameters of the various laser recently reported and of both our versions. In all cases where sufficient data is given, the efficiency per percentage output coupling, per unit volume of active medium is shown in the last column. This represents the quality of the laser in terms of physical size as well as electrical and optical characteristics, and the various lasers are analysed in

Table 4-5 Summary of the MkI and MkII xenon ion lasers.

Feature	MkI	MkII
Discharge length	80cm	148cm
Active length	57cm	103cm
Cathode	hollow Al	hollow Al
Anode	W rod	hollow Al
Resonator length	86cm	158cm
Ballast volume	590cm^3	1040cm^3
Tube bore	2.5mm	3.5mm
Windows	quartz, 1cm diam, sealed to quartz tube	quartz, 2.5cm diam, glued to S/steel mounts
Peak power multiline	84W	185W

Table 4-6: Comparison of physical, electrical and optical features of various Xenon ion lasers

Ref	L cm	ϕ mm	vol cm^3	C µF	V kV	E_{in} J	P W	t µs	E_{out} J	E_{out}/E_{in}	(E_{out}/E_{in})/vol cm^{-3}	P_{out}/vol W/cm^3	% trans	Eff/vol/% cm^{-3}
Schearer [8]	120	4	15.1	0.2	12.5	15.6	3000	0.2	6×10^{-4}	3.8×10^{-5}	2.5×10^{-6}	199	20	1.25×10^{-7}
Harper and Gundersen [16,17]	300	17	681	0.25	25	78.1	82000	0.11	9×10^{-3}	1.2×10^{-4}	1.7×10^{-7}	120	20-35	$8.5-4.9\times10^{-9}$
Schwartz and de Temple [15]	200	25	982	0.02	27	7.29	1000	0.5	5×10^{-4}	6.9×10^{-5}	7×10^{-8}	1	NR	-
Simmons and Witte [13]	150	2.3	6.23	0.4	10	20	900	2.5	2.3×10^{-3}	1.1×10^{-4}	1.8×10^{-5}	144	12	1.5×10^{-6}
Dahlquist [3]	100	6	28.3	0.1	5	1.25	10	1.0	1×10^{-5}	8×10^{-6}	2.8×10^{-7}	0.35	NR	-
Hansch et al [7]	120	4	15.1	0.45	20	90	300	0.45	1.4×10^{-4}	1.5×10^{-6}	1.0×10^{-7}	20	20	5×10^{-9}
Gallardo et al [10]	80	2.5	3.9	NR	10	0.8	2000	0.08	1.6×10^{-5}	2×10^{-5}	5×10^{-5}	254	NR	-
Papayoanou and Gumeiner [14]	90	10	71	0.026	25	8.1	1700	0.4	6.8×10^{-4}	8.4×10^{-5}	1.2×10^{-6}	24	18-45	$6.7-2.7\times10^{-8}$
Fahey and Schearer [9]	190	8	96	0.3	12	21.6	5000	0.2	1×10^{-3}	4.6×10^{-5}	4.8×10^{-7}	52	NR	-
Jarrett and Barker [5]	150	5	30	NR	NR	-	110	NR	-	-	-	3.7	NR	-
Hoffmann and Toschek [4]	175	5	34	NR	10	-	390	1.5	5.9×10^{-4}	-	-	11	NR	-
Bridges and Mercer [6]	46	2.3	1.9	-	-	-	10	cw	-	-	-	5	NR	-
This work MkI	80	2.5	3.9	0.04	10	2	84	0.5	4.2×10^{-5}	2.1×10^{-5}	5.3×10^{-6}	21	2.5	2.1×10^{-6}
MkII	148	3.5	7.3	0.04	10	2	185	0.5	9.3×10^{-5}	4.7×10^{-5}	6.4×10^{-6}	25	2.5	2.6×10^{-6}

this way to provide fair comparison among many different machines. It will be seen that in terms of efficiency per unit volume alone, both our lasers are highly placed, being bettered only by that of Simmons and Witte. Their laser was almost exactly a cross between our two designs, but with capacitors a factor of ten larger. More significantly, however, is the transmission of the output mirror. That used by Simmons and Witte, over 540nm to 480nm, had a transmission of 12%, whereas both our lasers used an output coupler of only 2.5% transmission, over 521nm to 568nm. Outside this range the transmission is unlikely to vary by more than a factor of two for an extension of ±25nm. Even if the variation is greater than this, over the range of the green and blue-green xenon lines our mirror transmits only about a quarter of that used by Simmons and Witte.

The performance of both our lasers is therefore comparible (in terms of efficiency per percentage output coupling per unit volume) with the best so far reported, and uses a smaller electrical input than the majority. As discussed already in Chapter 1 (Sec. 1-6-5), there is an optimum output coupling for any laser, which depends partly on the size of the laser, and partly on the laser transition involved. We have considered this optimum transmission for both the xenon lasers described, using the gain measurements discussed in Section 4-5-5 and the results presented in Table 4-4.

The small signal gain of the medium is found by taking the total losses at the point where the tilted quartz plate just extinguished a particular lasing line. These

positions are different for each line, so we take an average of 16% per pass. The output coupler used here adds a loss of 2.5% to this figure, and we then add a chosen parasitic loss to select one of the chosen curves in Fig 1-6 of Chapter 1. We may find the saturation intensity of the beam from the power equation:

$$P = A\beta_m I_s \left(\frac{\alpha_o}{\beta_m + \beta_p} - 1 \right)$$

as given in Chapter 1, by assuming that the first term in the bracket dominates.

Applying the above equation to the Mk I laser, which gave 84W with a 2.5% output coupler and output principally on the green and blue-green lines at 539nm, 535nm, 526nm and 495nm, we obtain an optimum output coupling of 7.2% at which point the maximum power will be 136W. For the Mk II laser, the maximum output will be 300W at 7.3% output coupling, and we feel that this represents a reasonable improvement in the lasers available for pumping pulsed Rh6G dye lasers.

4-8 Use in dye laser pumping

Both our xenon ion lasers have been used for pumping a Rh6G dye laser in which intracavity frequency doubling has been carried out, the details of which are discussed in Chapter 5. Our MkII laser operating at around 180W has enabled such a dye laser containing an intracavity ADA crystal to generate tunable UV in 300mW pulses, which is greater than that which would be obtainable by extracavity doubling using any of the xenon-dye combinations reported

[7,8,10], unless pumping powers of 20kW were used [18]. This also appears to be the first occasion on which a detailed study has been made of the use of a xenon ion laser to pump a dye laser containing any kind of frequency doubling element.

REFERENCES CHAPTER 4

1 Gordon EI, Labuda EF, Bridges WB; Appl Phys Lett, 4 178-80 (1964)

2 Bridges WB, Chester AN; Appl Opt, 4 573-80 (1965)

3 Dahlquist JA; Appl Phys Lett 6 193-4 (1965)

4 Hoffmann V, Toschek P; IEEE J Quant Electr QE-6 757-8 (1970)

5 Jarrett SM, Barker GC; IEEE J Quant Electr QE-5 166 (1969)

6 Bridges WB, Mercer GN; IEEE J Quant Electr QE-5 476-7 (1969)

7 Hansch TW, Schawlow AW, Toschek P; IEEE J Quant Electr QE-9 553-4 (1973)

8 Schearer LD; IEEE J Quant Electr QE-11 935-7 (1975)

9 Fahey DW, Schearer LD; IEEE J Quant Electr QE-14 220-1 (1978)

10 Gallardo M, et al; IEEE J Quant Electr QE-15 541-2 (1979)

11 Ferguson AI; PhD thesis, Univ. St Andrews (1977)

12 Bridges WB, Chester AN; "Ionised gas lasers", in Handbook of lasers ed Singh S (1974)

13 Simmons WW, Witte RS; IEEE J Quant Electr QE-6 466-9 (1970)

14 Papayoanou A, Gumeiner I; Appl Phys Lett 16 5-8 (1970)

15 Schwartz SE, DeTemple TA, Targ R; Appl Phys Lett 17 305-6 (1970)

16 Harper CD, Gundersen M; Rev Sci Instrum 45 400-2 (1974)

17 Gundersen M, Harper CD; IEEE J Quant Electr QE-9 1160 (1973)

18 Levenson MD, Eesley GL; IEEE J Quant Electr QE-12 259-60 (1976)

19 Hohla KL; Laser Focus 18-June 67-74 (1982)

20 Eesley GL, et al; IEEE J Quant Electr QE-16 113-5 (1980)

21 Salour M; Opt Commun 22 202-6 (1977)

CHAPTER 5: A pulsed Rh6G dye laser, with frequency doubling using ADA, pumped by a xenon ion laser.

5-1 Pulsed dye laser systems

Pulsed dye lasers are characterised by rather lower costs and simpler construction than their cw counterparts. The commonest system, and the simplest to produce, uses a nitrogen laser as the pumping source and a sealed cell containing the dye solution. Other systems are flashlamp or Nd:YAG laser pumped, normally with flowing dye and excimer laser pumped, again with flowing dye. These however, are much less common than the nitrogen laser pumped system. The merits of the various pump lasers have already been discussed in Chapter 4.

5-1-1 Nitrogen pumped dye lasers

One of the earliest uses of the nitrogen laser to pump a dye laser was by Myer et al [1] who obtained efficiencies of 12% in Rh6G dye at 575nm in a 4ns pulse. This yielded a dye output of about 14kW at a pulse rate of 100pps. No linewidth measurements were made. Subsequently, Capelle and Phillips [2] obtained 1kW pulses with a linewidth of 0.3nm using a rather more sophisticated dye cavity than in [1], with a correspondingly lower efficiency of 1%.

The most thorough work on the nitrogen pumped dye system was by Hansch [3] who obtained linewidths of 0.001nm, in order to undertake narrow band spectroscopy of sodium vapour. Using a Fabry Perot etalon and an Echelle grating within the cavity, the linewidth was reduced to around 10^{-5}nm in a 30ns pulse of only a few watts peak power. This illustrates clearly the drawback of the

nitrogen laser pumped system: due to the very short pulse duration, the beam from the stimulated emission has time for only a very few round trips of the cavity before the excitation of the dye ceases, and thus a large number of frequency selecting elements have to be included in the cavity, increasing losses and reducing the output power considerably.

5-1-2 Xenon ion pumped dye lasers

Such problems as described for the nitrogen pumped laser apply far less to xenon pumped systems, which have pulse lengths of the order of 1μs. Early work on this type of laser was done by Hansch, Schawlow and Toschek [4], whose dye laser design was based on that for a cw system, with coaxial pumping and a 1mm dye cell at Brewster's angle in an astigmatically compensated three-mirror cavity. No tuning element was included, and it was Schearer [5] who obtained narrow linewidths (0.025nm) with a similar laser using off-axis pumping and a reflection grating for tuning purposes. Powers of around 50W in the dye output were obtained for a 1.6kW pump power. Gallardo et al [6] used an open stream dye laser, a commercial Spectra Physics Inc model, and obtained linewidths of 0.2nm, but with a pulse duration of only 80ns, more closely resembling the pulses from a nitrogen pumped dye laser than the microsecond pulses more commonly found with the xenon systems. No power was reported for the dye output in this case.

The previous examples all used the blue and green outputs from the xenon ion laser to pump dyes which fluoresce in

the yellow and red spectral regions, commonly Rhodamine 6G. Fahey and Schearer [7] extended this type of work to cover the blue-green dyes, such as diphenylstilbene and the coumarins, by using the UV output from the xenon laser at 364.5nm. The dye cavity was of the same three-mirror configuration as used by Hansch et al [4] though pumping was off-axis and the dye was flowed through a 1mm thick optical cell. A birefringent filter and etalon were used to narrow the linewidth to 0.05nm with powers of 600W from a 5kW pump power. The pulse width was 120ns.

None of the published work with xenon ion lasers pumping dye lasers has been reported as extending to frequency doubling of any kind, either intracavity or extracavity.

5-1-3 Other systems and special techniques

The inherently large linewidth of a puled laser may be reduced by a technique known as "injection locking", in which a narrow band beam from a cw laser is injected into the resonator of a pulsed dye laser and causes the dye to lase preferentially at the wavelength of the injected beam, with the power lost from the other wavelengths being concentrated into the narrow linewidth pulse. Carney, Fahey and Schearer [8], for example, have injection locked a xenon pumped dye laser with the 632.8nm line from a He-Ne laser, to give a peak power of 400W with a linewidth of 1.5GHz (approximately 10^{-3} nm at this wavelength). This is more than an order of magnitude better than previously obtained with a xenon pumped dye, and two orders of magnitude better in power than the narrower

linewidth pulse from the nitrogen pumped laser of Hansch [3]. Thus this type of system would seem to be a prime candidate for the generation of second harmonic radiation, at least extracavity, but none has been reported.

The only known work where a xenon ion laser has been used to pump a frequency doubled dye laser was by Ferguson [9]. No detailed results were reported, the only figures quoted being a UV power of 1W using a pumping power of 750W. The dye laser used ADP as the nonlinear material, and full coma and astigmatism compensation was not achieved in the cavity.

5-2 The Rh6G frequency doubled laser

The dye laser used in this investigation is very similar to that used with the coumarin dye and LFM as described in Chapter 3. The main differences lie in the crystal housing and tuning elements. A summary of the design is given here for convenience.

5-2-1 Laser design

The dye laser is a double focus, astigmatically compensated cavity of the design subsequently developed from his initial work on intracavity frequency doubling by Ferguson [9] and later extended by Wagstaff et al [10]. A schematic diagram is given in Fig 3-4 of Chapter 3. The difference between the LFM laser and that used here is that firstly the ADA crystal must be held in a temperature

stabilised oven and secondly that the UV is obtained via the plane mirror R_5 and not by reflection off a quartz plate. The dye, of course, fluoresces in the yellow and so different mirrors are needed in this case, though in terms of cavity geometry they are identical to the coumarin mirrors. The gain of Rh6G is rather larger than that of C102, so the frequency selective elements must be more discriminating.

5-2-2 Rh6G dye properties

The structure, and absorption and fluorescence curves of Rh6G are shown in Figs 5-1 and 5-2, derived from Drexhage [11]. It will be seen that for the wavelengths present in the xenon pumping beam, principally the green and blue lines from 539nm to 495nm, the dye absorption is very great and the peak at 531nm is straddled by the three most powerful lines. Thus the overall efficiency of Rh6G is high and ideally suited to pumping by the xenon laser.

Thermal and photochemical degradation of Rh6G is also very small. In our case, the dye was flowed as a jet, but even were it in a sealed cell, only 0.14J/min of energy is supplied by the 185W pumping beam operating at 25pps. If fully absorbed, this would cause a temperature increase of much less than 0.01 $^{\circ}C/min/cm^3$ of dye solution. Although with tight focusing of the beam, the heated volume would be much smaller than this, thermal agitation of the dye and solvent molecules themselves serves to distribute the energy sufficiently. This has been found to be the case with pumping powers of up to 4kW, by Schearer [5], who

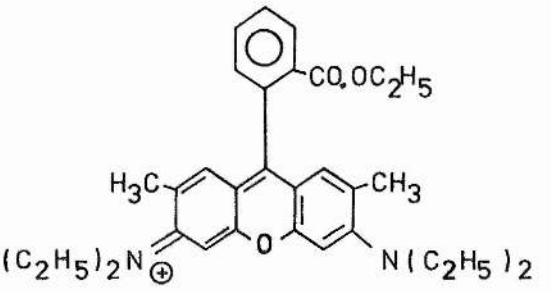

Fig 5-1: The structure of Rhodamine 6G

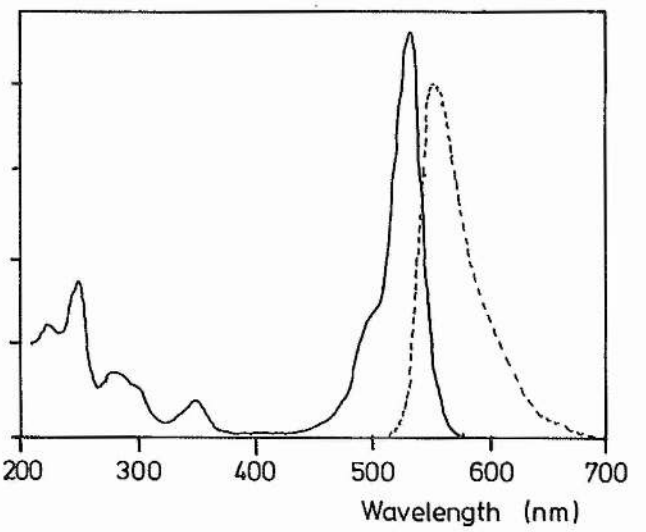

Fig 5-2: Absorption and fluorescence spectra for Rhodamine 6G (from Drexhage [11])

used a sealed cell of 1mm thickness with no observed thermochemical effects. Thermal lensing effects within the dye jet are considered in Section 5-2-7. Rh6G is also much more stable photochemically than most other dyes, and appears not to be affected significantly by the high power pulsed excitation from the xenon laser. This is not necessarily true for the very much higher powers from a nitrogen laser, for example.

The dye concentration required for pulsed operation is sometimes taken as higher than that for cw operation, in order to ensure the full absorption of the much greater laser energy within the active volume, this being particularly necessary in the case of nitrogen laser pumping. The recommended maximum concentration of Rh6G for a cw laser is about 5×10^{-3} M [12], but, according to manufacturer, this recommendation can range down to 2×10^{-3} M [6]. In practice, we have found no need to use a concentration any greater than 2.5×10^{-3} M, and that changes in this by up to 50% have only a very small effect on the laser power, as also observed by several others [1,3,5,6].

5-2-3 Optics

The mirrors used in this dye laser in the jet region are similar to those supplied for commercial dye lasers such as the Coherent Inc CR490. Those mirrors which focus the beam into the crystal (ie R_3 and R_4) are manufactured by CVI Inc, have a radius of curvature of 10cm and reflect 99.5% in the visible and 80% in the UV, in both cases at an angle of incidence of 15°. The plane mirror R_5 is

also from CVI, and reflects 99.5% in the visible and transmits 80% in the UV, in this case at normal incidence. Thus around 65% of the UV emerging from the crystal cell is obtained via R_5. A three-plate birefringent filter and a 0.5mm 30% coated solid etalon are both used to tune the laser, and the visible linewidth is reduced to 0.2nm by these operating together.

The xenon pumping beam is focused into the jet by a mirror of 10cm radius of curvature by Spectra Physics Inc, as is used in their dye lasers for focusing the 488nm and 514.5nm lines from an argon ion laser. The focusing is thus to a beam waist radius of about 20μm, close to the spot size of the dye cavity [10].

5-2-4 ADA crystal

As discussed in Chapter 2 (Section 2-2-3), ADA will undergo noncritical phasematching over the tuning range of the Rh6G dye by varying the temperature from 15°C to 80°C. The fundamental is an ordinary ray, polarised at 90° to the Z-axis and propagates in the XY plane at 45° to both axes. Our crystal is cut so that the beam enters the end of the crystal at Brewster's angle and then travels parallel to the geometric axis of the crystal. Thus the sides of the square-section crystal are also at 45° to the X- and Y-axes. This is termed a "45° Z-cut" and is the commonest for ADA when used in a frequency doubled laser. The second harmonic is an extraordinary ray and is polarised parallel to the Z-axis.

As the crystal is 90° phasematched (at the correct temperature), there is zero walkoff between the fundamental and second harmonic, and the two beams emerge from the crystal collinear. This has the considerable advantage that the two beams also emerge collinear from R_5, which is helpful in beam alignment in, for example, spectroscopic applications.

Diagrams of the optical path through the crystal are given in Figs 5-3 and 5-4. The crystal is 15mm long and 5mm square in section, with Brewster surfaces polished to $\lambda/4$ flatness. In order to set and control the temperature of the crystal to an accuracy of $\pm$0.05°C or better as already discussed (Chapter 2, Section 2-1-5-4), the crystal cell is enclosed in a temperature stabilised oven as described by Ferguson [9]. The control system for this oven stabilises the temperature by means of a thermistor close to the crystal cell, which is set in one arm of a bridge circuit, with a 10-turn potentiometer in another arm. Any imbalance current in the bridge is then used to control the heating coil. The coil itself is wrapped around the crystal cell which is of aluminium and stainless steel, (unlike that for LFM which is entirely of stainless steel). This allows both rapid heat transfer to the crystal and good temporal stability, and the control system maintains a given temperature to an accuracy of $\pm$0.01°C, rather better than that actually required. A photograph of the crystal cell and oven assembly is shown in Plate 5-1.

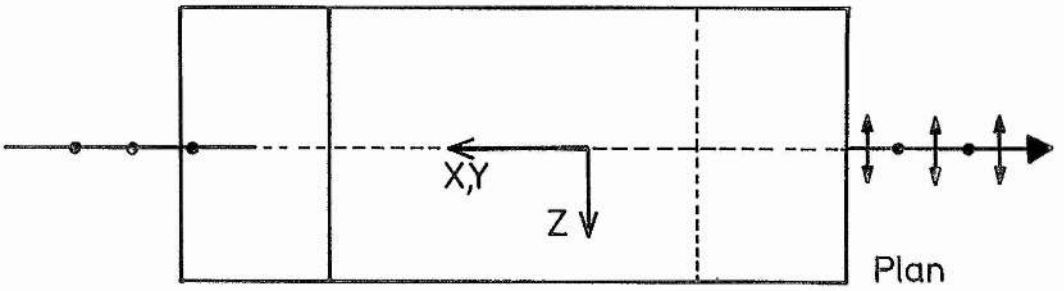

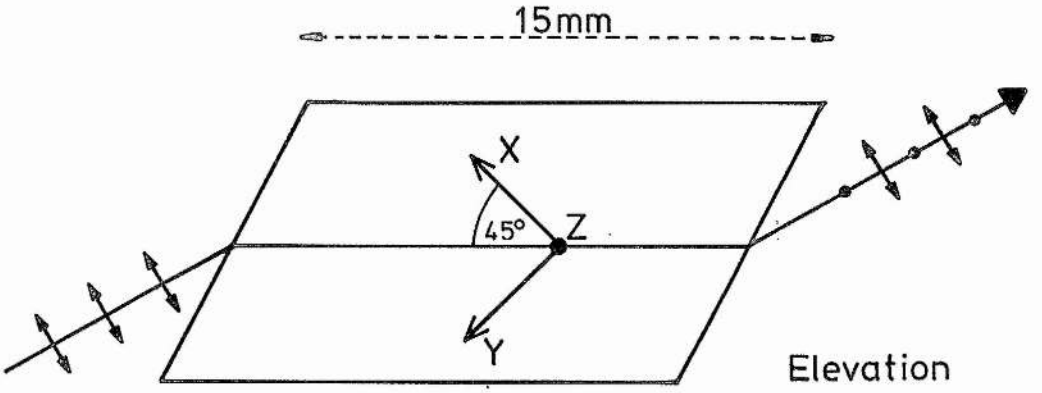

Fig 5-3: ADA crystal design showing visible and UV polarisations

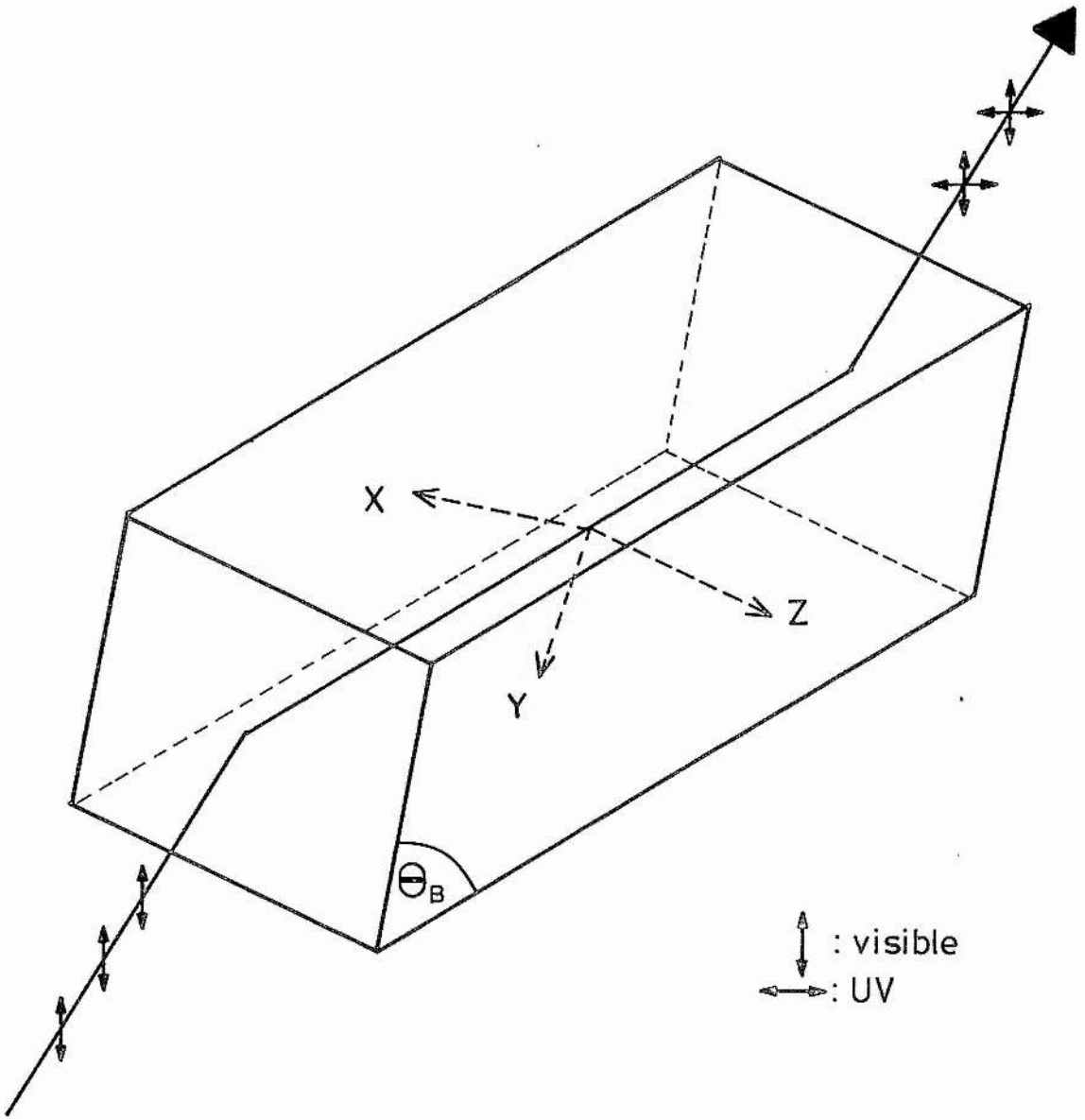

Fig 5-4: Optical arrangement of the ADA crystal

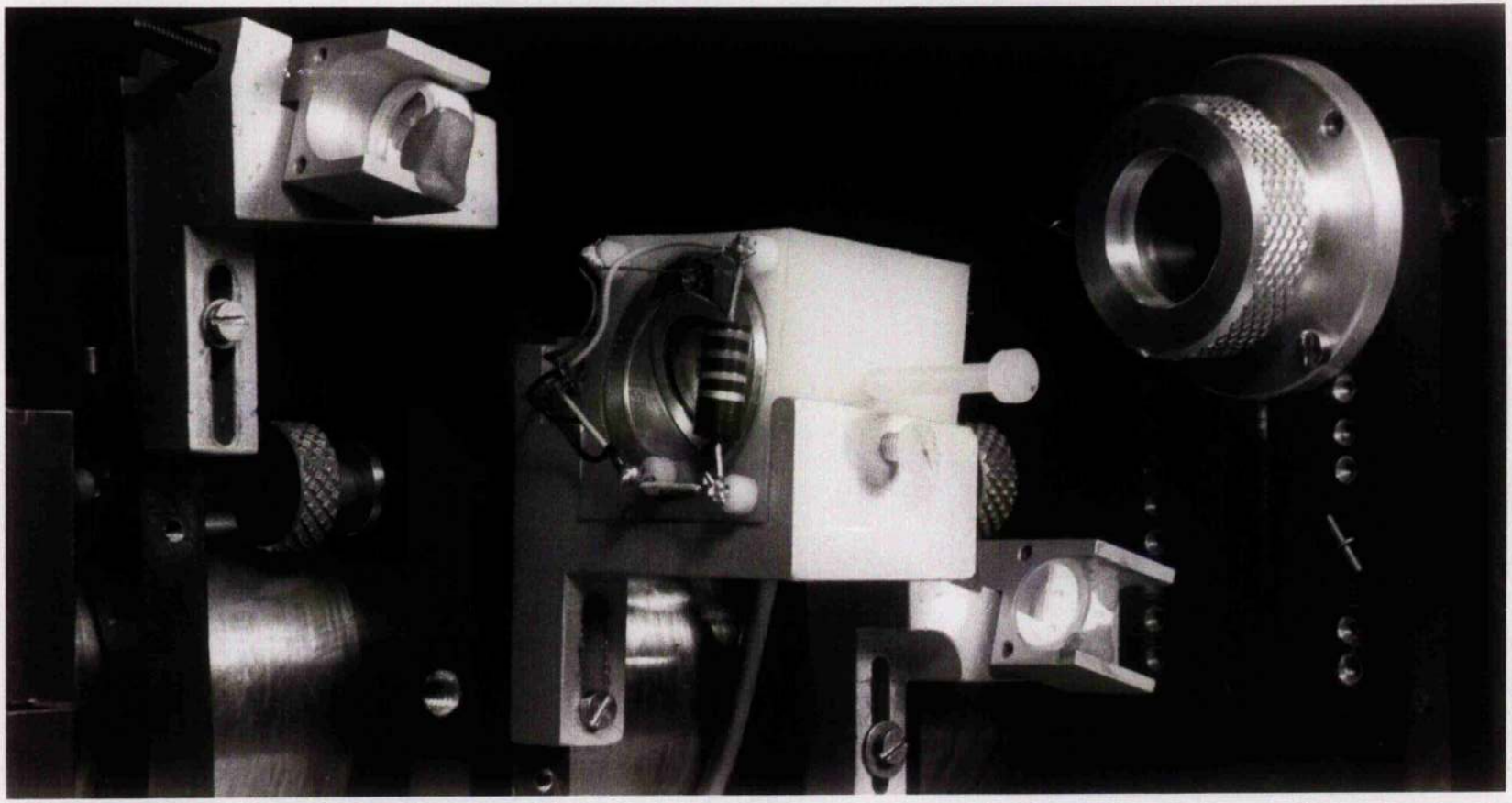

Plate 5-1

5-2-5 Powers obtained

Both the intracavity visible and UV powers were monitored by a PIN10UV photodiode placed beyond R_5. This was calibrated and fitted with visible blocking filters (Corning 9863) for UV measurements.

The intracavity visible power was measured as 55W at 590nm. This was obtained with both the birefringent filter and coated etalon in the cavity. At the same time, a UV power of about 100mW was obtained at the photodiode. These figures are in fair agreement with those of Ferguson and Dunn [13] for a cw laser using the same crystal, when their results are extrapolated to the powers used here.

With each end of the crystal cell fitted with quartz windows, there is a 29% Fresnel reflection loss for the UV. At these wavelengths, mirror R_4 reflects about 80% and R_5 transmits about 80%, as does the Corning 9863 filter over the photodiode. Thus overall, only about 36% of the UV leaving the crystal itself reaches the detector, showing that about 280mW was generated in the ADA. A larger power would be obtained beyond R_5 only with improved mirror coatings and a low-loss index matching fluid between the crystal and the quartz windows.

The tuning range was 291nm to 297nm in the UV, with the quoted powers being maintained for most of this range.

5-2-6 Linewidths

Using a Rank Monospex 1000 monochromator the visible and UV linewidths have been measured for the laser operating in a variety of configurations. With a three-plate birefringent filter and no etalon, the linewidth was 0.5nm in the visible and 0.15nm in the UV. The addition of the etalon reduced these figures to 0.12nm in the visible and 0.06nm in the UV, at optimum. The values in the absence of the etalon show clearly that in this case only about 80% of the available visible power was being used to generate second harmonic, (ie that within a 0.3nm band), verified by the increase of about 20% in the UV power obtained when the etalon was inserted and properly aligned.

5-2-7 Pulse widths and lasing delay

The pulse widths of the dye laser emission and the generated UV were measured photographically by connecting the photodiode beyond R_5 to a CRO. The dye pulse was found to have a width, at half peak power, of 0.38μs, and the UV pulse a width of 0.2μs. This is not unexpected, since the UV generation depends quadratically on the visible power within the crystal, so the UV pulse will rise to its peak and fall from it much more rapidly than will the visible pulse, and thus the time width at half

the peak value will be considerably smaller. If the visible pulse has an approximately triangular waveform, the UV pulse width would be smaller by a factor of 1.71. Within the limits of error in measurement from CRO photographs, we have obtained a pulse width ratio of 1.73.

A similar analysis for the Xenon pumping pulse compared with the dye lasing pulse is more complex, however. In this case, the dye lasing pulse does not begin at the same moment as the pumping pulse, for two reasons. The first is that the intensity of the pumping beam must rise above the threshold pumping of the dye cavity before any dye output will be obtained. The threshold of the dye cavity may be of the order of 10W, and this introduces a few tens of nanoseconds delay between the start of the pumping pulse and the start of dye lasing. Once threshold has been exceeded, there is a further delay as the dye lasing beam must be generated from the fluorescence and build up its intensity above the general luminescence.

For a cw Rh6G laser, the output coupling is about 5%, and so allowing for other losses, the gain per round trip of the cavity is about 10%, with a pumping power of about 5W. We assume that there is a linear relationship between gain and pumping power, that a Xenon beam is focused to the same size as the cw beam and that this focusing is matched to that of the dye cavity. If these conditions are met, then the round trip gain for pulsed pumping of the Rh6G laser will be of the order of 170% for a pumping power of 84W. The intensity, I, after n round trips of the cavity is given by:

$$I = I_o . (gain)^n$$

where I_o is the initial intensity of the light propagating along the axis of the cavity. Such light would come from the general fluorescence of the dye.

We must now consider the number of round trips that the beam must make before its intensity is sufficiently large to generate significant output. At this point the signal to noise ratio, I/I_o, may be of the order 10^{10} [14], though this value is not particularly critical to within an order of magnitude. Hence for the Xenon pumped dye laser, we get $10^{10} = (1.7)^n$, and so n, the number of round trips required to build up a significant signal, is about 40.

In the case of this cavity, the round trip time is about 2.7ns, and so we expect a delay of 0.11μs between the pumping threshold being exceeded and the onset of dye lasing. This is supported by the photographic observations, which are shown in Fig 5-5. It is seen that the onset of dye lasing occurs approximately 0.13μs after the start of the pumping pulse, in good agreement with expectations.

5-2-8 Thermal lensing

For the case of the standing wave laser in multiline

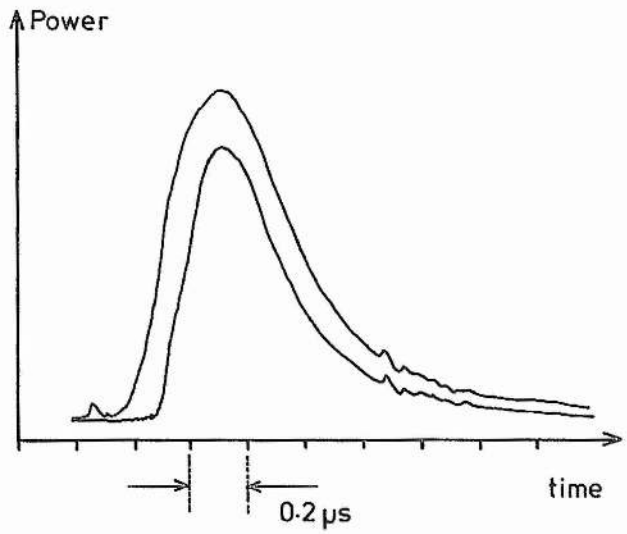

Outer trace : xenon pumping pulse

Inner trace : dye lasing pulse

Fig 5-5: Comparison of pumping and lasing pulses

pumping, Ferguson [9] found that at pump powers of the order of 20W, thermal variations of refractivity of the dye jet caused defocusing of the dye lasing beam, and at higher powers these effects were serious enough to destroy the stability of the cavity and prevent lasing. The effect was even more serious in single line pumping, where the useful limit was 6.5W, since the spot size of the focused beam was smaller. The effect was reduced by increasing the flow rate of the dye, to a maximum speed of the order of 10m/s. For a beam focused within the dye to a spot diameter of the order of 20μm, the onset of thermal lensing can thus be seen to occur if a particular region of the dye solution is exposed to the pumping radiation for more than about 2μs, at 20W pumping power.

In the case of the Xenon pumped dye laser, using a pumping power of 185W and a pulse width of about 0.5μs, more than twice the energy needed to cause thermal lensing would be deposited in the dye at each pulse, regardless of the flow rate. We would therefore expect a thermal lens to be set up and the cavity stability to be altered to take this into account. This is supported by our observaton that when a cavity set for maximum power in pulsed pumping is pumped instead by a cw argon ion laser, very little power is generated in the dye, even allowing for the reduced pumping power. Alteration of the focusing in the jet, however, restores the stability of the cavity, and the laser then behaves as expected for cw pumping.

The only way in which this thermal lensing could be

D3 minimised without reducing the xenon pumping power or reducing the degree of focusing in the jet is by increasing the rate of flow of the dye, so that the dye was swept clear of the focused spot from the pumping beam in at least the duration of the pulse. For a 0.5μs pulse focused to even 10μm diameter, a flow rate of 20m/s would be required. Apart from the much higher pressures then needed in the dye circulator unit, the flow in the jet becomes turbulent at speeds very much less than this value, making the lensing effect irrelevent. Hence it is unrealistic to consider minimising the thermal lensing problem in this type of pulsed laser.

As discussed in Chapter 2, Section 2-1-6-3, thermal effects in the actual crystal can be neglected for lasers having a duty cycle of well below 1:50, even with visible intracavity powers in excess of several hundred watts. For this laser, with the visible power at the crystal being 55W and a duty cycle of around 1:40000, no thermal effects are expected at the crystal and none has been observed.

5-3 Comparison of intracavity and extracavity frequency doubling

As in the case of the cw coumarin laser discussed in Chapter 3, the pulsed Rh6G laser has been compared as a frequency doubling system in both intracavity and extracavity configurations.

The changeover technique is exactly as was described in

Section 3-3, with an additional Rh6G output coupler from a CR490 laser being placed between the birefringent filter and the lower crystal focusing mirror, and referred to as R_6 (see Fig 3-14b). The UV power is again monitored beyond R_5 by the PIN10UV photodiode fitted with a Corning 9863 filter. In the absence of an etalon in the R_1-R_2-R_6 cavity, a visible power of 4.6W at the crystal was deduced, having a linewidth of 0.55nm. No UV was observed. With the 0.5mm etalon in the cavity, the linewidth was reduced to 0.15nm, with much the same power at the crystal. A very small amount of UV was detected, but reliable measurements could not be made above the background "noise". Consideration of the visible power at the crystal predicts that UV powers of the order of 1mW should be obtained. These powers would yield a signal of 0.03V from the photodiode used, and the typical background noise signal was 0.05V.

The power figures quoted do not agree with those of Ferguson and Dunn [13] who obtained just over 2mW of UV from an intracavity power of 4.6W in the cw laser. This discrepancy is probably due to the focusing at the crystal being different in the two cases considered as a result of the different stability conditions of the two cavities. As discussed in Chapter 3, the maximum output from the R_1-R_2-R_6 cavity is only obtained by moving R_2 from its original position before R_6 was inserted. This then alters the size of the focused spot in the crystal, an effect that cannot be compensated except by changing mirror R_3.

Clearly this comparison between intracavity and

extracavity doubling is not immediately conclusive, but the power of 4.6W from the non-doubled cavity probably represents the best power available from a laser of this size with a 185W pumping pulse and a narrow linewidth output. Schearer [5], using about 8.5 times the pumping power obtained about 50W of dye output, in the much narrower linewidth of 0.025nm. On the basis of the observations of pulse lengths of pumping and of dye lasing beams, we have suggested a thermally induced nonlinear dependence of dye power with pumping power. In the case of our laser here compared with that of Schearer, and making the same asumptions about thermal lensing, we could expect that with his laser operating at the same linewidth as ours, an output power of the order of 300W would result. His observation of 50W at around one sixth of the linewidth is therefore not inconsistent.

We consider that our dye system is near to optimum in the visible region. Considering the powers available extracavity, of four to five watts, we see that by inserting a frequency doubling crystal into the cavity we obtain more than an order of magnitude increase in the visible power at the crystal and thus at least two orders of magnitude increase in the generated UV power. In the case of intracavity generation, of course, the UV losses at at least two cavity mirrors must be allowed for before direct comparison may be made. In this case, the UV obtained beyond R_5 (with R_6 removed) is 65% of that emerging from the crystal cell, but even with this loss applied, the UV powers are 70 to 80 times those available extracavity from this system.

06 We thus regard this system as extremely suitable for applications such as the saturation spectroscopy of gases and vapours, for example in extending the work of Wagstaff and Dunn on mercury [15] to other elements.

REF1

REFERENCES CHAPTER 5

1 Myer JA, Johnson CL, Kiersted E, Sharma RD, Itzkan I; Appl Phys Lett 16 3-5 (1970)

2 Capelle G, Phillips D; Appl Optics 9 2742-5 (1970)

3 Hansch TW; Appl Optics 11 895-8 (1972)

4 Hansch TW, Schawlow AL, Toschek P; IEEE J Quant Electr QE-9 553-4 (1973)

5 Schearer LD; IEEE J Quant Electr QE-11 935-7 (1975)

6 Gallardo M, et al; IEEE J Quant Electr QE-15 541-2 (1979)

7 Fahey DW, Schearer LD; IEEE J Quant Electr QE-14 220-1 (1978)

8 Carney ER, Fahey DW, Schearer LD; IEEE J Quant Electr QE-16 9-10 (1980)

9 Ferguson AI; PhD thesis, Univ St Andrews (1977)

10 Wagstaff CE, Dunn MH, Ferguson AI, Bastow SJ; Opt Commun 25 379-83 (1978)

11 Drexhage KH; "Structures and properties of laser dyes", in Topics in Applied Physics, 1-Dye lasers, ed Schafer FP, Springer-Verlag, Berlin, 1977

12 Dye data sheets, as supplied by Coherent, Inc.

13 Ferguson AI, Dunn MH; Opt Commum 23 177-82 (1977)

14 Shimoda K; "Introduction to Laser Physics", (Sec. 6-3) Springer-Verlag, Berlin, 1984

15 Wagstaff CE, Dunn MH; Opt Commum 35 353-8 (1980)

Chapter 6: The development of a crystal growing system, its application in preparing single crystals of Urea for use in S.H.G., and their subsequent testing.

6-1 Introduction

As has been illustrated in Chapter 2, there is considerable variety in the materials available to those wishing to undertake second harmonic generation from the visible spectrum. Materials such as ADA, ADP, KDP and others are well established, and there is increasing interest in Urea, LFM and KB5 for use at shorter wavelengths.

Materials with an established use, the commonest being ADA, are also widely available, if not in the UK then at least from the USA at reasonable cost. However, the less common materials such as Urea, while readily available in powder form, are not commercially available as single crystals as far as we know anywhere on a regular basis. Those crystals which have been seen have been rather small, of poor optical quality, and, for their benefit in SHG, very expensive.

Not surprisingly, in view of the very limited market for such crystals, those few firms and University departments able to grow crystals of laser quality are rarely able to offer anything but the most sought-after materials, and are reluctant even to consider committing their equipment to several months use unless the return is worthwhile. Furthermore, high optical quality in a crystal is almost impossible to guarantee, being largely a matter of luck once the skills have been mastered, and thus the expectation of a saleable crystal is low and the price high.

Consequently, we chose to investigate the possibility of setting up our own growing system, with particular interest in obtaining a good single crystal of Urea, though with the long term prospect of extending the techniques to other water based crystals such as LFM, KB5 and others if the need arose.

This Chapter considers the initial work on the crystal growing systen as carried out by S.J.Bastow. Mention is then made of the subsequent development work carried out by Departmental technician Mr.F.Ackerboom, who eventually grew the crystals which were later used and tested in SHG. It is necessary to include a summary of Mr.Ackerboom's work to provide a complete view of the problems associated with this type of project, and to enable the problems to be discussed fully.

The final sections of the Chapter discuss some of the crystals obtained and their testing for use within a second harmonic laser.

6-2 Crystal growing systems

6-2-1 General crystal requirements

For use within a laser, a crystal of, say, Urea, must firstly be of sufficient size for the geometry of the Z-fold frequency doubling region and secondly of good optical quality on both the large and small scales. This latter requirement will usually mean that no defect in the path of the intracavity beam may be larger than one tenth

of the wavelength of light. If this is not the case, then phase changes will be introduced into either the fundamental or SH beams which will be sufficient to reduce the overall efficiency of the phasematching. Generally speaking, if a crystal has a defect large enough to matter, then by the nature of the crystal growth it will have many of them, and the combined effect of these is what is significant.

Additionally, in order to maximise the intracavity power of the fundamental beam, there must be very few reflective or scattering losses, and this means not only that large-scale transparency of the crystal is required, but also that the surfaces of the cut crystal must be able to sustain polishing, again to $\lambda/10$ flatness. Such surfaces of most crystals will be cut to meet the incoming beam at Brewster's angle, and this combined with the required orientation of the crystal for proper phasematching means that the polished faces lie across all three crystalline axes, making polishing even more difficult.

6-2-2 Growth methods

All methods of crystal growth involve the seeding of a supersaturated solution, followed by the maintainance of the supersaturation in a controlled fashion as more material is deposited out of solution on to the seed. The degree of control needed to produce a good crystal is very considerable indeed, and the quality of the final product is highly dependent upon the quality of control.

The methods of maintaining supersaturation in a largely water based growing system are: (a) temperature lowering, (b) constant temperature differential, and (c) solvent evaporation. The first of these maintains a constant degree of supersaturation by lowering the temperature at a suitable rate which depends on the solubility-temperature curve of the material. The second often involves the flowing of a saturated solution over a growing seed and maintaining a constant temperature difference and thus a constant degree of supersaturation and rate of deposition. The third method involves a controlled evaporation of the solvent, perhaps by pressure reduction of the vapour.

The choice of one of these methods, or a refined version of them, is dependent on the shape of the solubility curve and the magnitude of the solubility. By far the easiest to control is the temperature lowering method and it was this which was chosen for use with Urea. Normally the method would be considered difficult to use with such an highly soluble material as Urea, but other methods have further problems related to the solubility gradient, and so the temperature lowering method was chosen as that most likely to succeed. Nothing further will be said about the other methods available; a thorough discussion of all aspects of crystal growth is given in [1].

The requirements of growth by temperature lowering are that the temperature in the growing bath must be maintained to a stability of better than 0.001K over long periods, superimposed on a controlled reduction of 0.1K to 1K per day, dependent on the solubility and the solubility gradient. In the case of Urea, both of these values are

large: at 303K the solubility in water is 1335g/l and changes at a rate of 12.5g/l/K. Thus at this temperature (30°C) a fall of 0.1K per day would yield a crystal around $1cm^3$ in volume in 24 hours. This is far too rapid a growth rate for the production of a good quality crystal, though this fact was not obvious at first. Other factors besides a slower fall of temperature can improve the growth of the crystal, however. For example, many additional crystals growing randomly on the base of the growing tank can allow a high overall growth rate (in terms of grammes per day), while maintaining a small rate of deposition for the crystal of interest, and thus a much more uniform growth is achieved, hopefully giving high optical quality.

The rate of lowering of temperature may be controlled by a driven contact thermometer with electronic or electromechanical control of the contact point movement, and the same thermometer may of course be used as the thermostat. Providing that the rate input of heat is the same as the rate of loss from the growing tank, a duty cycle of 50% is readily achieved, and with good insulation, this gives the required long term stability.

The crystal shape or "habit" can be modified by either a variation of the solvent or by the addition of small quantities of impurity to the growing solution. In the case of a solvent change, this will also affect the solubility and solubility gradient, and allowance must be made for this. In the case of Urea, the solubility in methanol is only 70.5g/l at 30°C, and by a suitable choice of mixture of methanol and water, the solubility can be

chosen to have any value between this and that of 1335g/l for pure water. In this case, no habit modification takes place, but the addition of ammonium chloride or ammonium bromide in small quantities (to either the pure or mixed solvent) does alter the crystal structure, without itself being absorbed into the structure [2].

In the case of the Urea growth attemped here, a mixture of methanol and water was used as the solvent, but no habit modification was attempted. The choice of this solvent is discussed later (Sec 6-2-5).

6-2-3 Growing system for Urea

A technique for growing small Urea crystals for use in NMR studies had already been established in this department [2], but high purity crystals of the type needed for laser work had not been obtained, and the system did not have the refinements incorporated in this work. The equipment had also been dismantled and we considered that any new work undertaken was best begun from the start.

During the development, much work progressed very rapidly, with changes being made daily, and so only a summary of the final version is offered here, with comments on the underlying problems.

6-2-3-1 Water bath

The water bath is a rectangular stainless steel box, with

perspex windows on each vertical side, and an axle passing through the centre of the base. This axle carries a motor car cooling fan, and the axle is driven from outside the tank by a geared mains motor. The rotation rate is about 50rpm and gives a very thorough agitation of the water. The water volume is around 50 litres, and with the steel walls considered the whole assembly has a thermal capacity of around 200 000J/K. Initially, the tank was neither covered nor insulated, but observations of the temperature variations in the room suggested that the required temperature stability would not be achieved without extensive lagging. The tank now carries [3]* around 3cm of expanded polystyrene insulation on all sides, except for two of the windows which are left clear for observing the progress of the growth. A view of the unlagged tank, with the thermometer in place is shown in Plate 6-1. Also seen in this view is the water filter and pump. In order to minimise the growth of algae in the warm water ($\simeq$35°C), the water was circulated through a 20μm filter using an old pump and filter assembly from a dye laser. This, combined with an algae inhibitor (from a pet shop) has kept the water clean for several months at a time. We have not found any heat loss problems due to the unlagged connecting pipes on this system.

6-2-3-2 Thermometer

The thermometer used was a mercury-in-glass contact thermometer, with a scale of approximately 1°C per

---

* Work thus referenced is by Mr.Ackerboom.

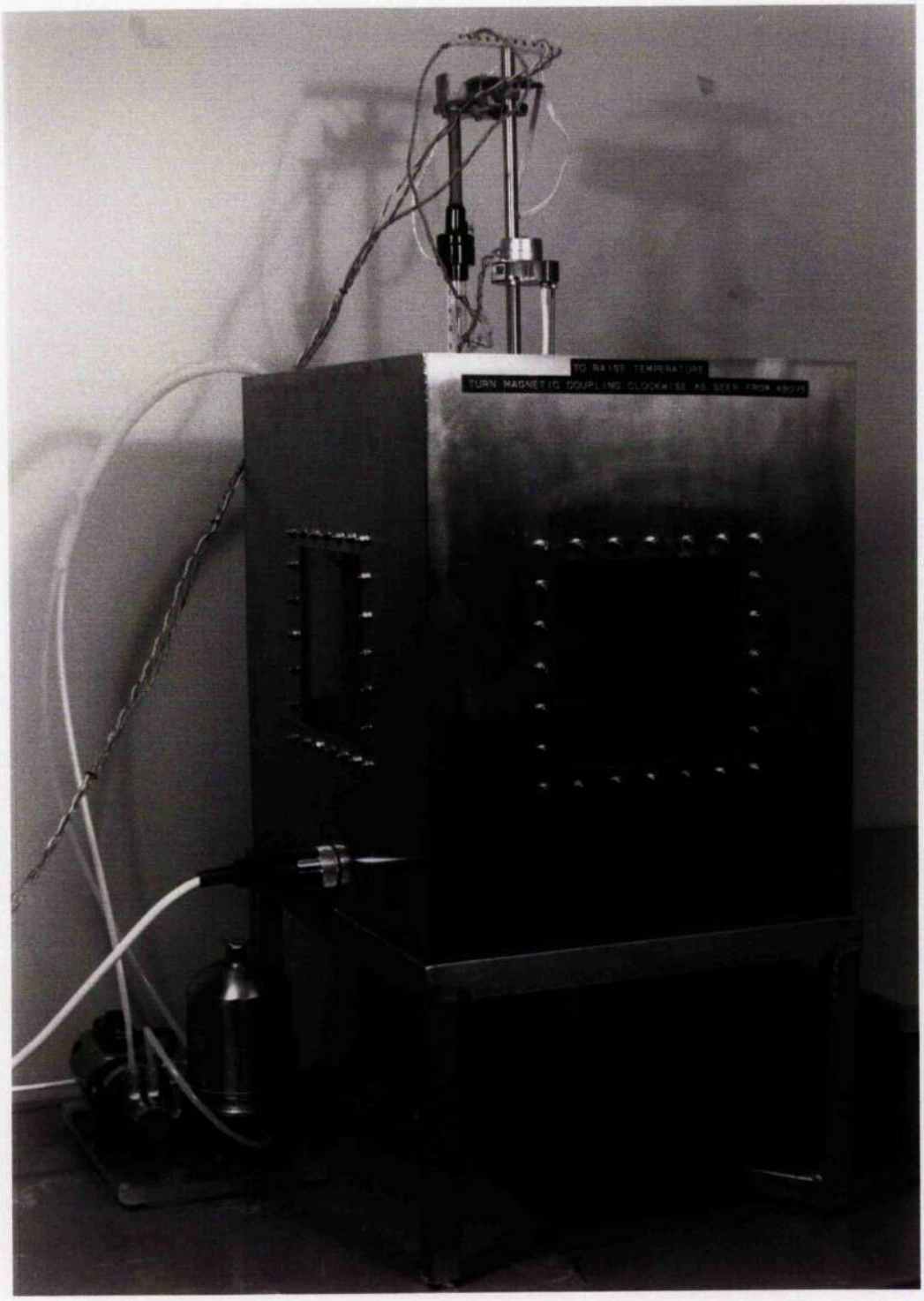

Plate 6-1

millimetre. The range covered was about 10°C to 70°C. Such thermometers are commercially available in a variety of ranges and sensitivities. The contact was driven by a rotating magnetic coupling acting on an BBA screwed rod whose pitch was 0.43mm.

Initial experiments suggested that a temperature lowering rate of 0.25K/day would probably be sufficient, and this would be achieved by a one-pulse-per-hour operation of a ratchet relay driving the magnetic coupling around. Accordingly a circuit was built base on a 50Hz clock drive mechanism which closed a microswitch once per revolution, the microswitch then operating the relay. The drawback of this sytem was that as it stood only a fixed rate of lowering could be accommodated. Subsequent development [3] has involved the use of a variable frequency pulse circuit so that temperature lowering rates can be much more easily altered.

The contacts on the thermometer were connected to an RS Componemts resistance sensing relay (ref 349-822) which then operated the heater when the thermometer contacts were opened. The heater was a standard 3kW (at 240V) kettle element, but only operated at around 55V at a power of 180W. This was predetermined by observing the cooling rate of the tank at 35°C. The p.d. required to maintain a 50% duty cycle varies with temperature, so a 0-240V "variac" was added to the heater circuit, and the control circuit modified accordingly to provide isolation of the sensing relay from any inductive pulses when the variac switched on or off. The control circuit then used is shown in Fig 6-1, and has operated most reliably.

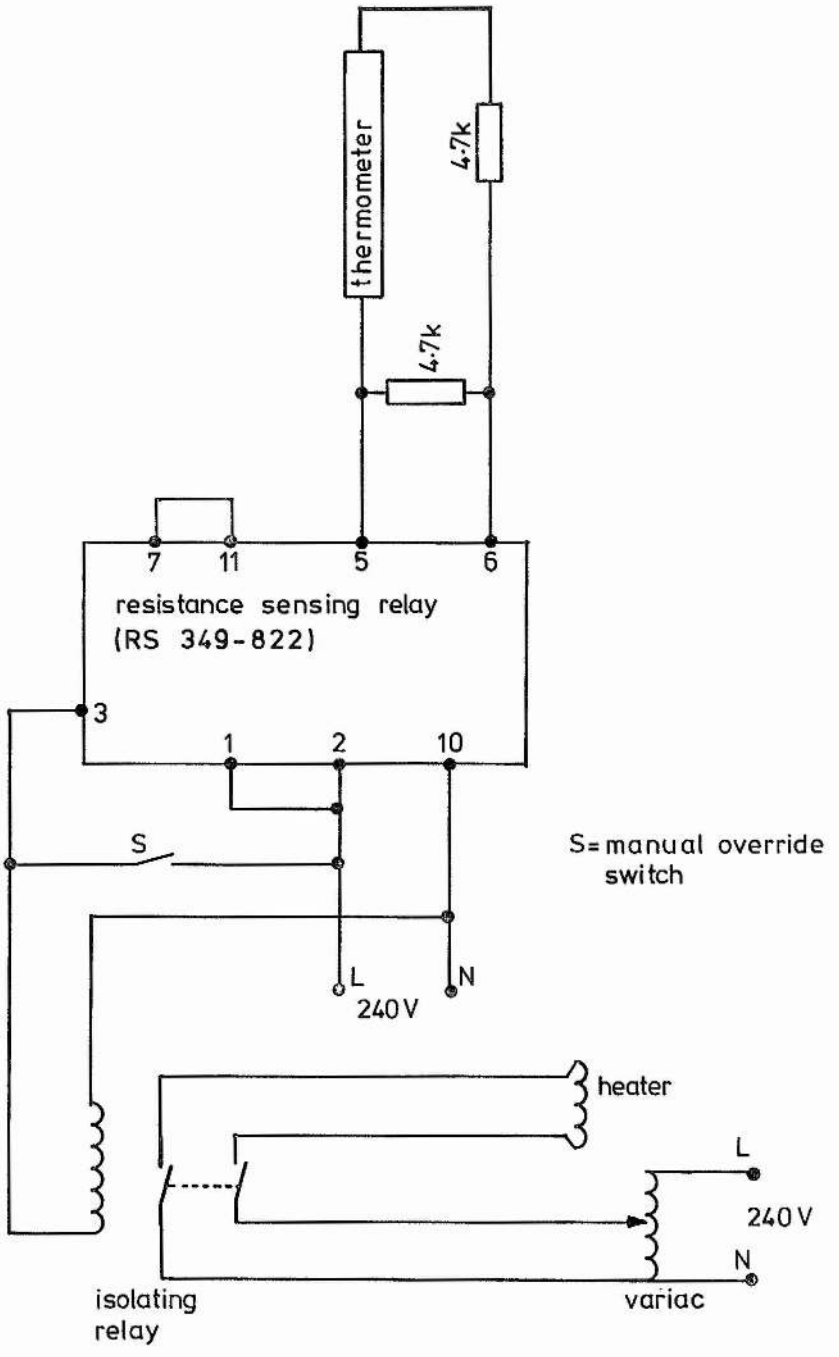

Fig 6-1: Thermostat and heater control circuit

6-2-3-3 Growing jar

The requirement of the growing jar was that it would be easily supported in the water bath, airtight to prevent solvent evaporation, and wide-necked to allow easy removal of any crystals grown. We believed there also had to be provision for rotating the crystals while growing so as to prevent local changes in the solvent supersaturation affecting the growth of the crystal.

The most suitable device available seemed to be a 1 litre "Kilner" jar as used for food preserving. The neck was about 8cm in diameter, with a screw top which would ensure a firm airtight seal with rubber O-rings. The glass top was replaced by a nylon cap on to which was screwed a motor giving a 10rpm rotation to the seed holder. The (mains operated) motor was held about 15cm above the jar to minimise the risk of contact with water. Despite recommendations from various workers [1,2] we eventually found that if the temperature lowering rate was slow enough, stirring of the growing solution was not necessary, indeed, it could lead to irregular growth at times. This would presumably be due to very small crystals or microscopic dust being circulated and adhering to the growing crystal. This would then affect future growth, but only become obvious after several days.

Eventually [3] the rotation mechanism was removed and the Kilner jar replaced with a 1 litre "Quikfit" flask, which was sealed with "Vaseline" at the neck after a single fine thread holding the seed had been inserted.

6-2-3-4 Seed holder

The seeds were held by fine strands of various materials, as discussed below. Initially the strands were suspended from the four corners of a 3cm square PTFE sheet, which had a flat paddle assembly below. The whole thing was mounted at the end of a 3mm diameter stainless steel axle, passing though the cap to the motor, whose motion was reversed every 30s or so. Views of the entire growing jar and seed holder assembly are shown in Plates 6-2 and 6-3.

Various methods were attempted for fixing the seeds into position for growing. These included glueing on to nylon wire with epoxy resin, tying with copper or gold wire and wrapping with platinum ribbon. None was successful. The epoxy resin glue softened after a few hours in the growing solution, probably due to the action of the warm methanol, and the seeds, which were only glued end-on to the nylon strands, then fell off. Copper wire tied around the seed seemed most promising, as very fine wire from high-flexibility electric flex could be used. A small amount of growth was observed, and then within an hour of each other all four seed crystals fell off. The reason seemed to be that the copper wire had dissolved into the growing solution, giving it a faint bluish colouration. In an attempt to minimise this problem, gold and platimum were used in place of the copper, but holding the seeds was then a problem as the available wire was much thicker than the copper strands.

Other workers [1,2] have suggested drilling the seeds and

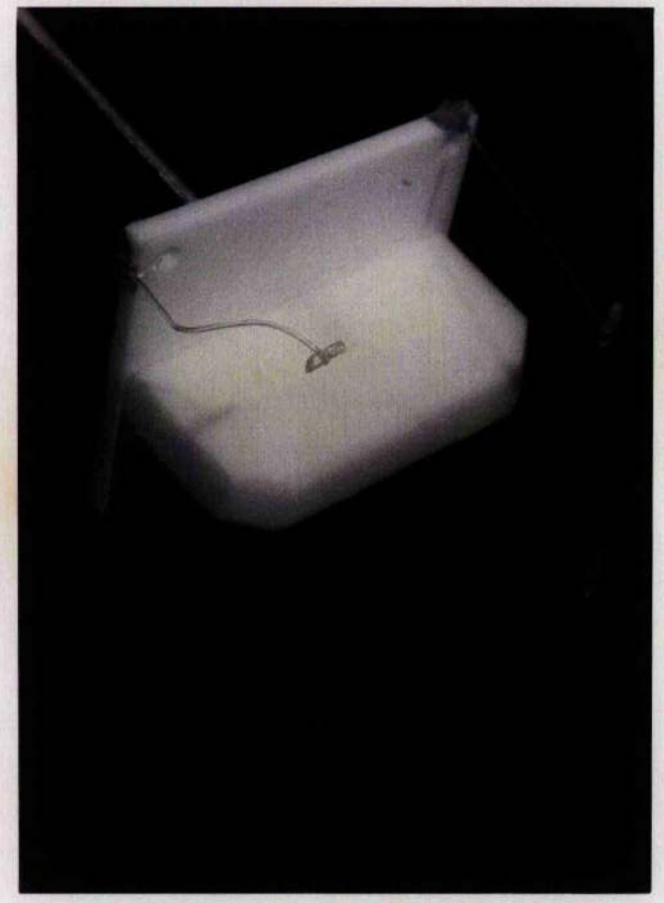

Plate 6-2

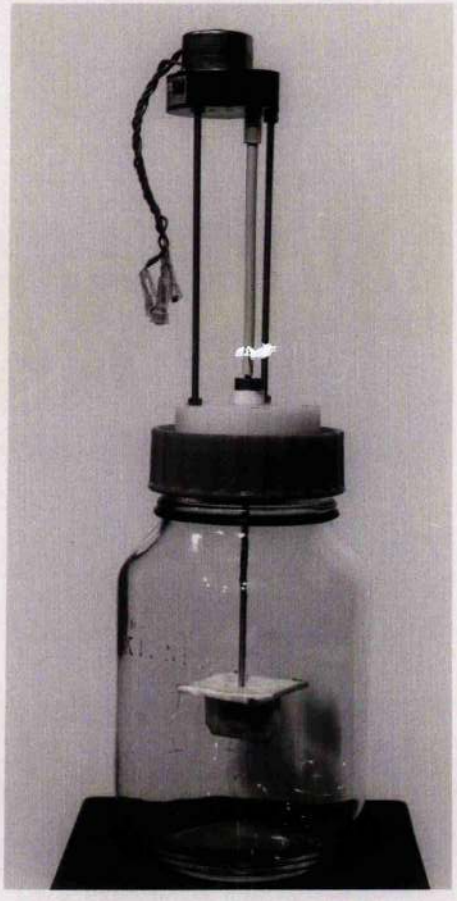

Plate 6-3

mounting them on stainless steel pins, but our seeds were only around 1mm thick, which we considered too thin for this approach to be used successfully.

Subsequent work [3] has shown that human hair offers an excellent choice of material for suspending a seed. It is simply tied around the seed and no glue of any kind is used. Chemical attack from the growing solution seems negligible.

6-2-4 Choice of seeds

The careful selection of seeds is very important if a good crystal is to be grown. Seeds may be obtained by one of several methods: a solution of Urea may be left to evaporate in an open dish, a small number of seeds may be grown on a rough wire held in a slowly cooling solution or, more usefully, they may be obtained from the base of the main growing jar.

The seeds obtained by open dish evaporation are often not of good quality, as they are usually very brittle and highly elongated. This will lead to problems when attempting to grow them because of the large side area, which encourages growth there rather than uniformly over all surfaces.

Seed growth in small numbers on strands of cotton or wire can give good results providing the temperature is lowered slowly enough. Growth on the base of the main jar is probably the best source of seeds, and the majority of

D2 those used here have been from this source.

The final choice of seed should be governed by its shape and surface quality and not necessarily by its transparency. this latter feature is irrelevant as far as a laser crystal is concerned, as the central region of the final crystal will probably not be used anyway. Good growth at a uniform rate can be expected from a short squat seed, with more or less equal surface areas at sides and ends. This is because growth favours larger areas, and if the seed is too long, the sides grow at a much faster rate than the ends, leading to a highly irregular structure of the final result. A typical size of seed would be 5mm long by 2mm square, and growth over several weeks would yield a final crystal of perhaps ten times these dimensions.

6-2-5 Choice of solvent

The choice of the appropriate solvent for Urea was governed partly by previous workers' experience [2] and partly by the desire to avoid habit modifications.

The solubility curve for Urea in water is shown in Fig 6-2, after data in [2]. Full data for Urea in methanol has not been published, although at 30°C the solubility is about ten times less than in water and changes at about one sixth of the rate. The initial choice of solvent was designed to allow a reasonable quantity of Urea to crystallise out of solution and to achieve this over a period of a few weeks. For example, suppose a crystal of

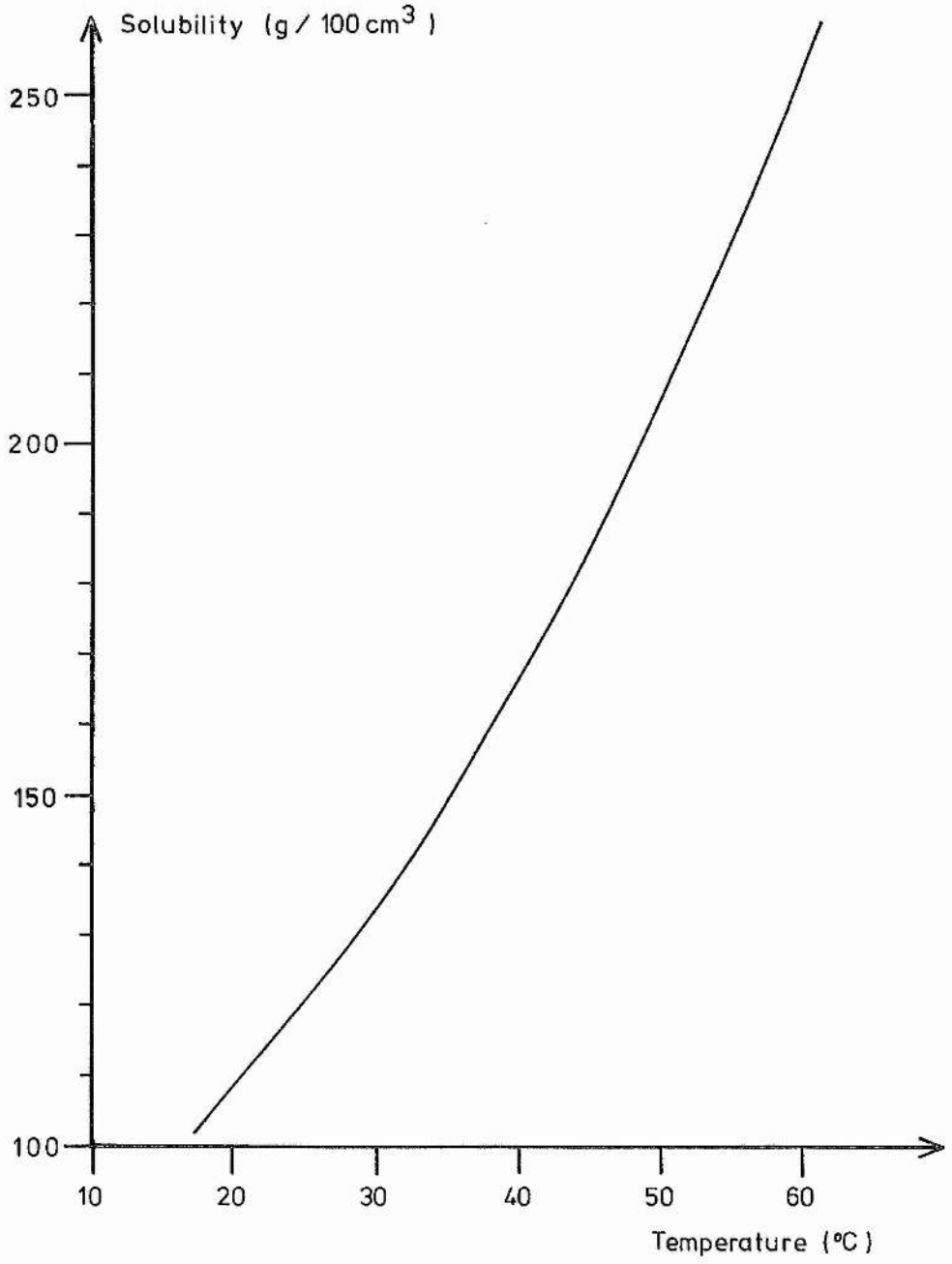

Fig 6-2: Solubility curve of Urea in water
(from data in Hyndman [2])

D3 dimensions 3cm x 1cm x 1cm is to be grown in one month at a temperature lowering rate of 0.05°C per day. We assume also that at least as much volume of crystal grows randomly on the base of the jar as does on the seed itself. This is justified by experimental observation. After one month, the temperature has fallen by 1.5°C and a volume of about 6cm^3 of Urea has crystallised out. This has a mass of about 7.8g, giving a required solubility gradient for the solution of about 5g/K. The usual volume of growth solution was 1 litre, and this gradient of 5g/l/K can be obtained by a mixed solvent of approximately 70% methanol and 30% water. This was the mixture initially chosen.

6-3 Crystals grown

Over the course of several months, many hundreds of crystals were obtained from the base of the growing jar. Many of these were too large for use as seeds, but exhibited many of the growth features likely to be found, and to be avoided, in growing large crystals.

6-3-1 Examples of growth faults

The photographs of crystals in Plates 6-4 to 6-6 illustrate the range of defects observed. In most cases, the crystals are found to have some areas which are clear, and larger areas where there are many hundreds of small cracks or other distortions. Plates 6-4a and 6-4b show a crystal 7cm x 1.5cm x 0.7cm which is typical of those

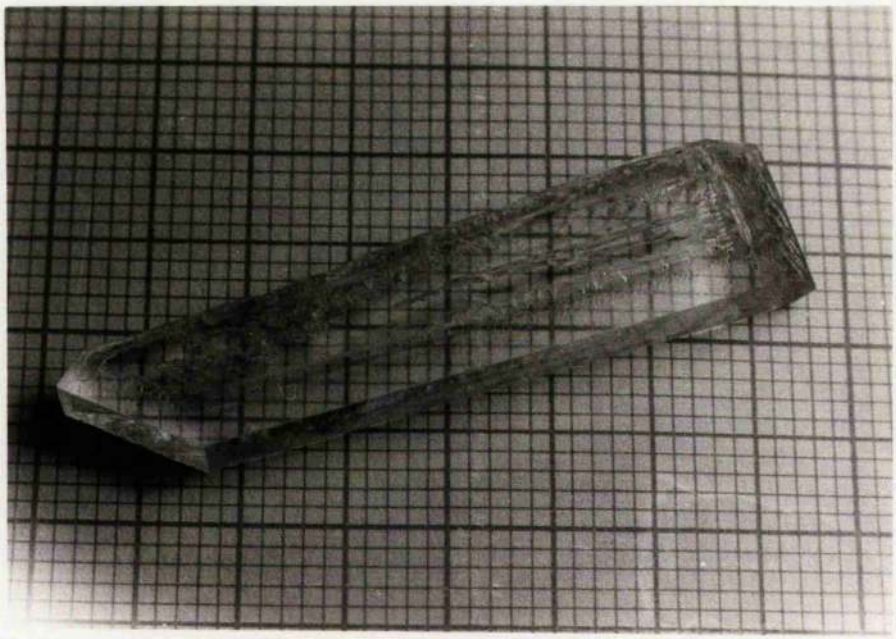

a

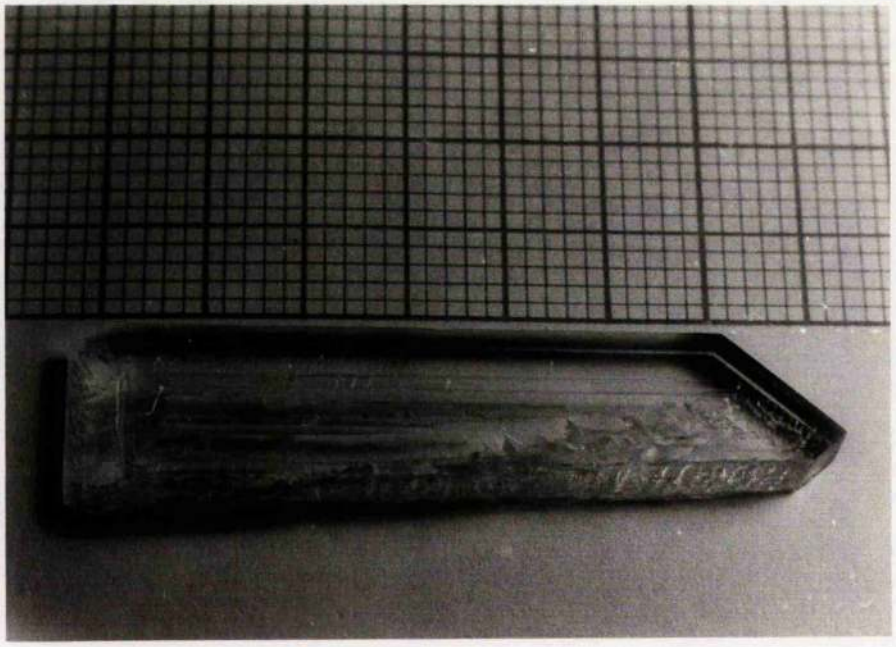

b

Plate 6-4

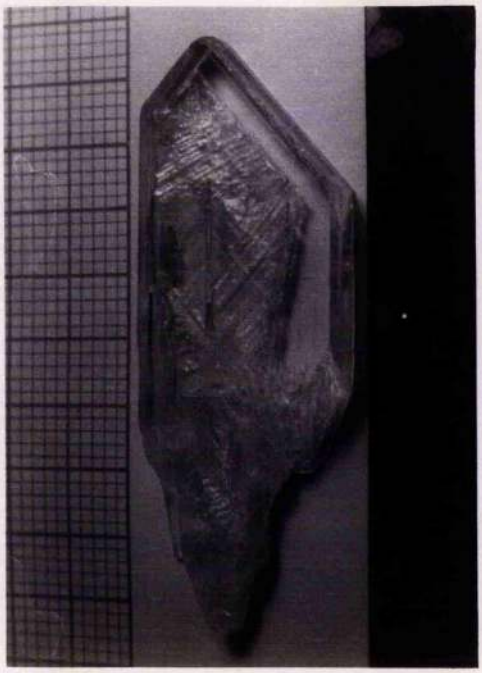

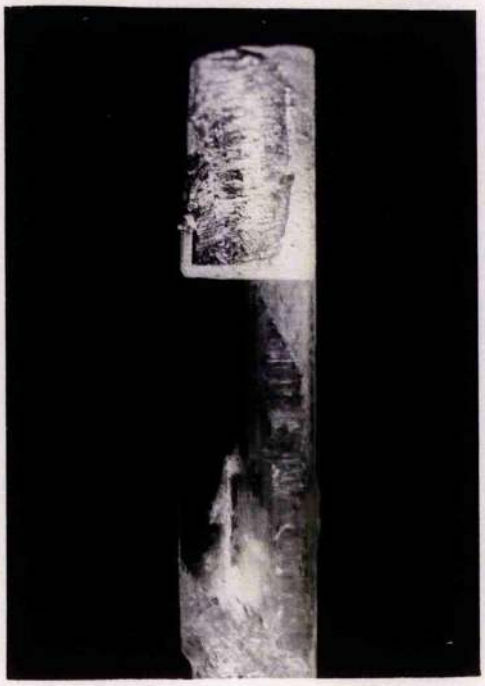

Plate 6-5

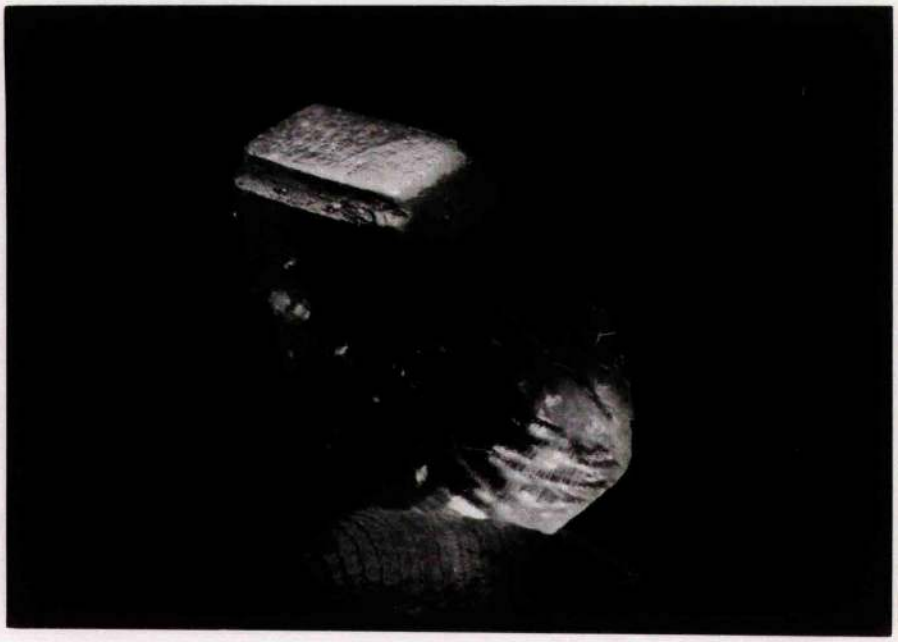

a

b

Plate 6-6

which grow elongated along the Z-axis. There is a large clear volume running along one side for almost the entire length, which would be uppermost when the crystal grew on the base of the tank. The surface of this region is not perfectly smooth, but this is not significant as the crystal would be cut at 45° to the natural faces anyway. Were this crystal rather larger, and remained clear, it would be a prime choice for cutting to a laser crystal.

A wider, flatter crystal is shown in Plate 6-5, with four views of the clear region. These illustrate how sharply defined a region of good growth will often be. This is not unexpected, since once uniform growth becomes established over a large surface, only fine particular deposits on the surface, from impurities in the solution, are likely to disturb the regularity of the growth. In this example, the clear region has a volume approximately 3cm x 0.5cm x 0.5cm. This would be satisfactory for use in a dye laser, except for the need to cut at 45° to the natural faces, which reduces the useful thickness to only about 2mm if sufficient area is to be left for entry and exit of the beam.

Plate 6-6 shows two smaller crystals with growth defects leading to a stepped surface, in case (a) a large single step about 2mm high, and in (b) a series of much smaller steps. This latter effect is more likely to cause regions of poor growth than is a single step, as there are many more irregularities on which new growth tends to concentrate.

6-3-2 Selection and cutting of a crystal for laser use

The requirements for optimising UV generation in Urea were discussed in Chapter 2, Section 2-2-2, in which it was shown that for Type I phasematching the fundamental beam is an extraordinary ray propagating in the ZX or ZY planes. The natural morphology of Urea has the Z-axis parallel to the long crystal axis and the X- and Y-axes at 45° to the side faces. Thus any plates for use in a laser frequency doubling system must be cut parallel to the natural diagonal of the crystal, (Fig 6-3), with the beam to propagate in a plane normal to the cut surface.

The angle of cut with respect to the Z-axis depends on the wavelength to be used and the Brewster angle at this wavelength. Consider Urea at 590nm. The phasematch angle (for Type I in the ZX plane) is found from equations 24 and 45 of Chapter 2, as approximately 48°, and the Brewster angle is 57°. As shown in Fig 6-4, this requires the plate to be cut at an angle of about 10° to the Z-axis. This allows a ray to enter at Brewster's angle and then propagate at the correct phasematching angle to the Z-axis and in the ZX plane.

Ideally such a plate would be cut to lie along the diagonal of the natural crystal, as shown in Fig 6-3. In practice, there are irregularities in all crystals along their centrelines due to the original seed, and a better result is likely to be obtained by cutting between the centreline and one edge, as shown in Fig 6-5.

Accordingly, a crystal was selected that would allow this

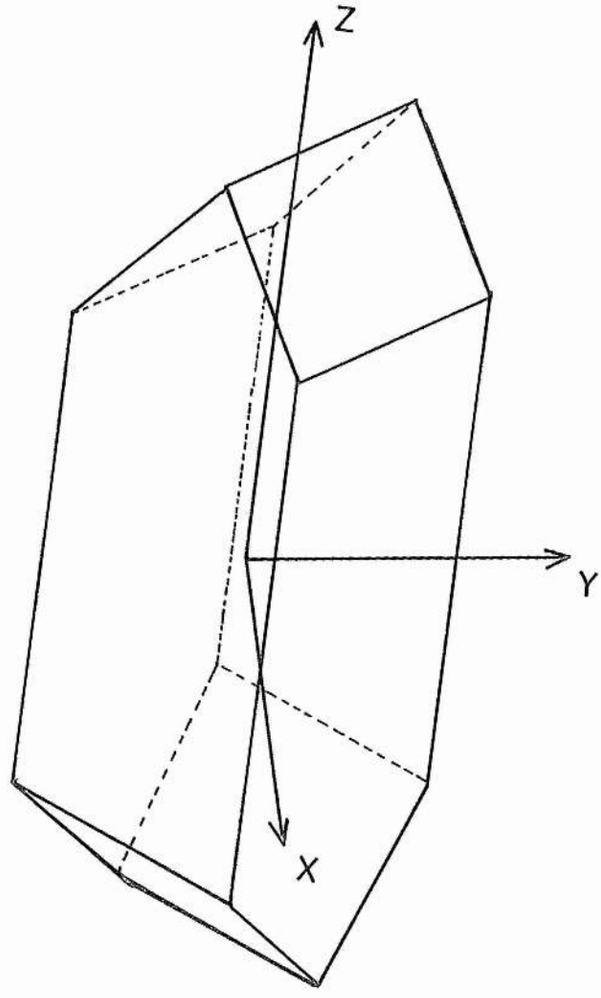

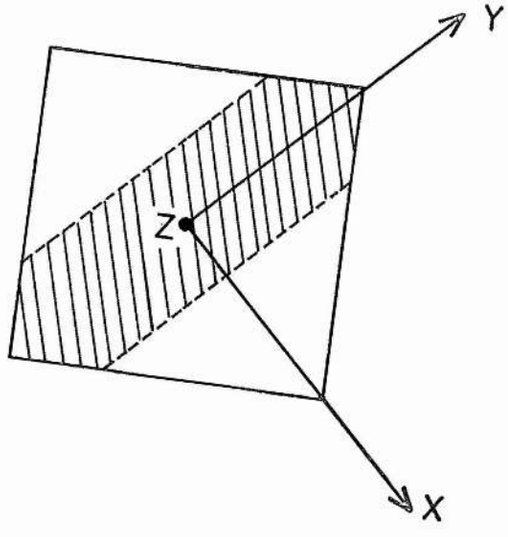

||| = plate to be cut

Fig 6-3: Urea crystal morphology

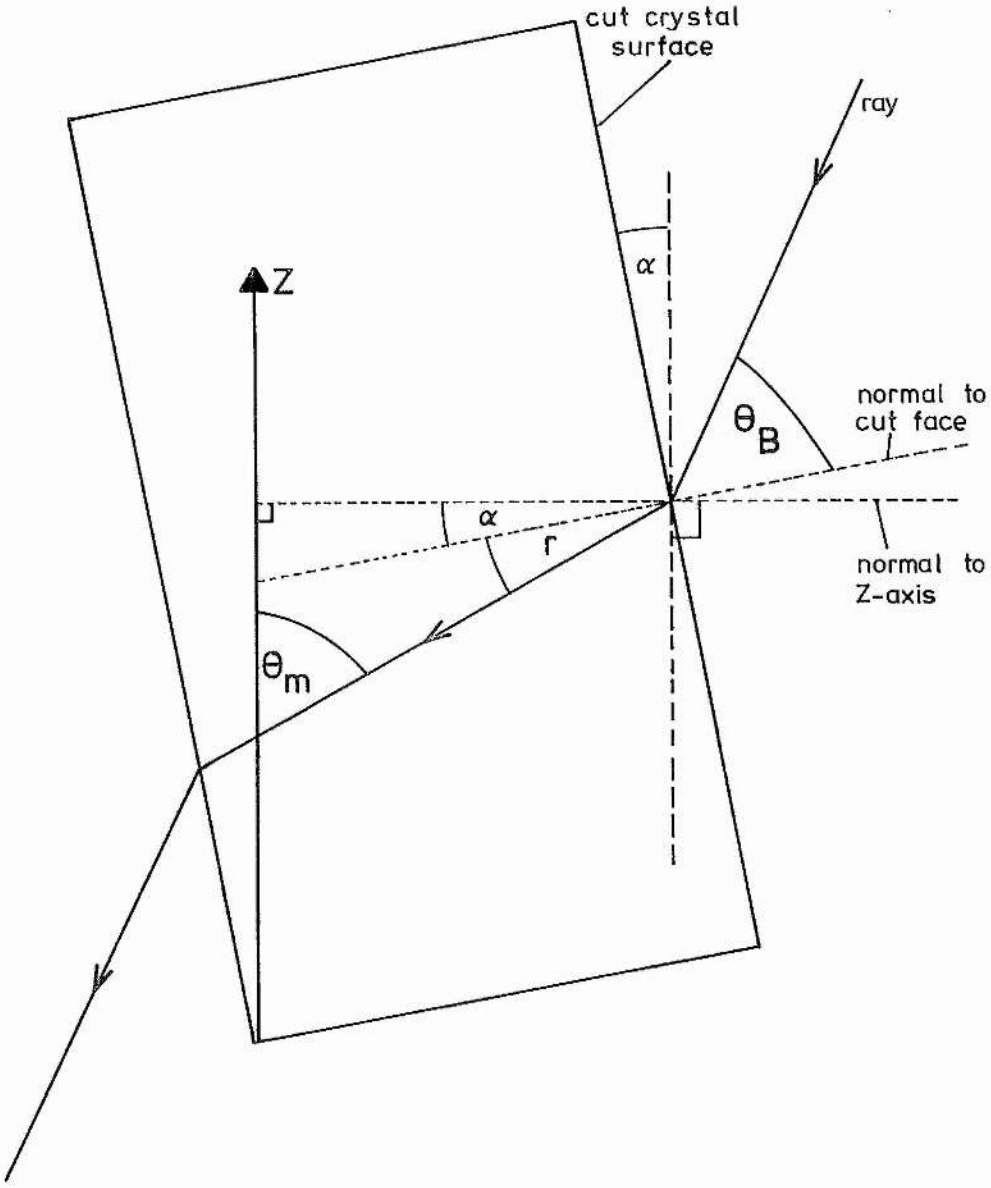

$$\theta_m + r + \alpha = 90^\circ$$

$$\theta_B = \arctan[n(\theta_m)]$$

$$r = \arcsin\left(\frac{\sin(\theta_B)}{n(\theta_m)}\right)$$

Fig 6-4: Geometry of cutting the plate

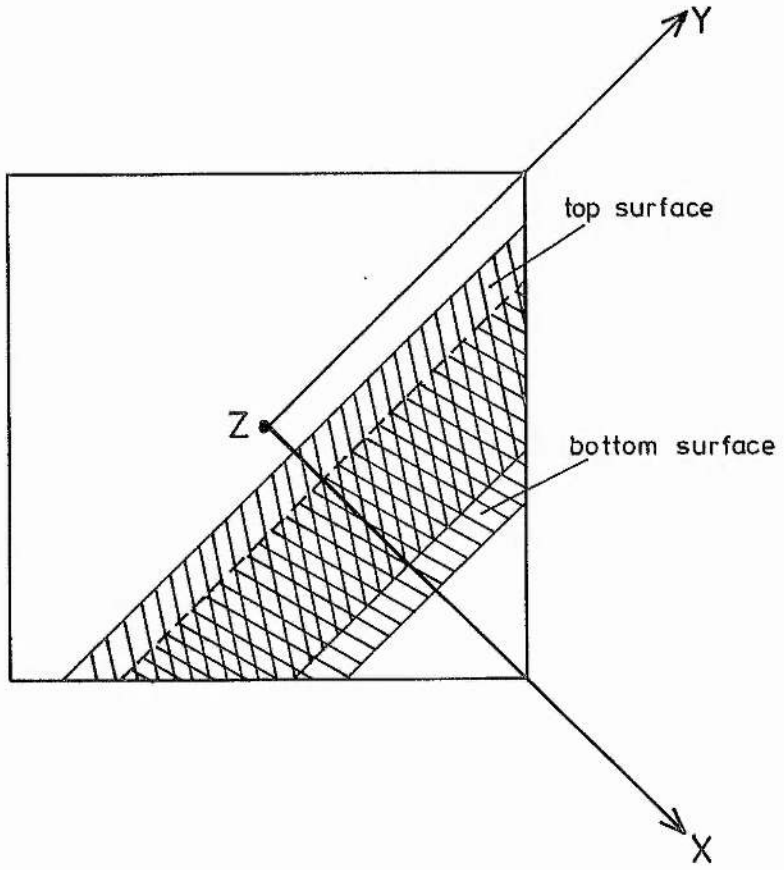

Fig 6-5: View down the Z-axis, showing the plate location

cut to be made and leave a reasonable size of cut plate. The crystal was 49mm long and roughly 11mm square. It had been grown over a period of about two months from a seed about 6mm long and 2mm square. During growth, this crystal was the only one in the growing jar apart from those on the base of the jar and was not rotated nor the growing solution stirred. The clear regions are shown in Fig 6-6. The crystal plate was cut and polished by Messrs. Electro-Optic Developments Ltd., of Basildon, Essex.

It was hoped that the resulting plate would be clear enough to allow its use in a dye laser, using Rh6G dye to make comparision between Urea and ADA. Difficulties in cutting and polishing, however, prevented a laser quality surface polish being produced. In order to test the internal quality of the crystal, it was decided to attach quartz windows to the surfaces with UV transparent index matching fluid (Bayer "Baysilone M 10000"), even at the risk of unknown damage due to the fluid. On doing so, only a few transparent regions in the bulk of the plate were visible, and the idea of incorporating the plate within a laser cavity abandoned. Rather than attempt UV generation at 295nm by using the output of a Rh6G dye laser, we decided to use the beam from an argon ion laser, whose power would be between 1.3W and 7.0W, depending on wavelength, compared with only 0.5W at best (extracavity) from the dye laser with sufficiently narrow linewidth. This would provide the same order of magnitude of power that would be expected at the crystal had it been placed within a dye laser.

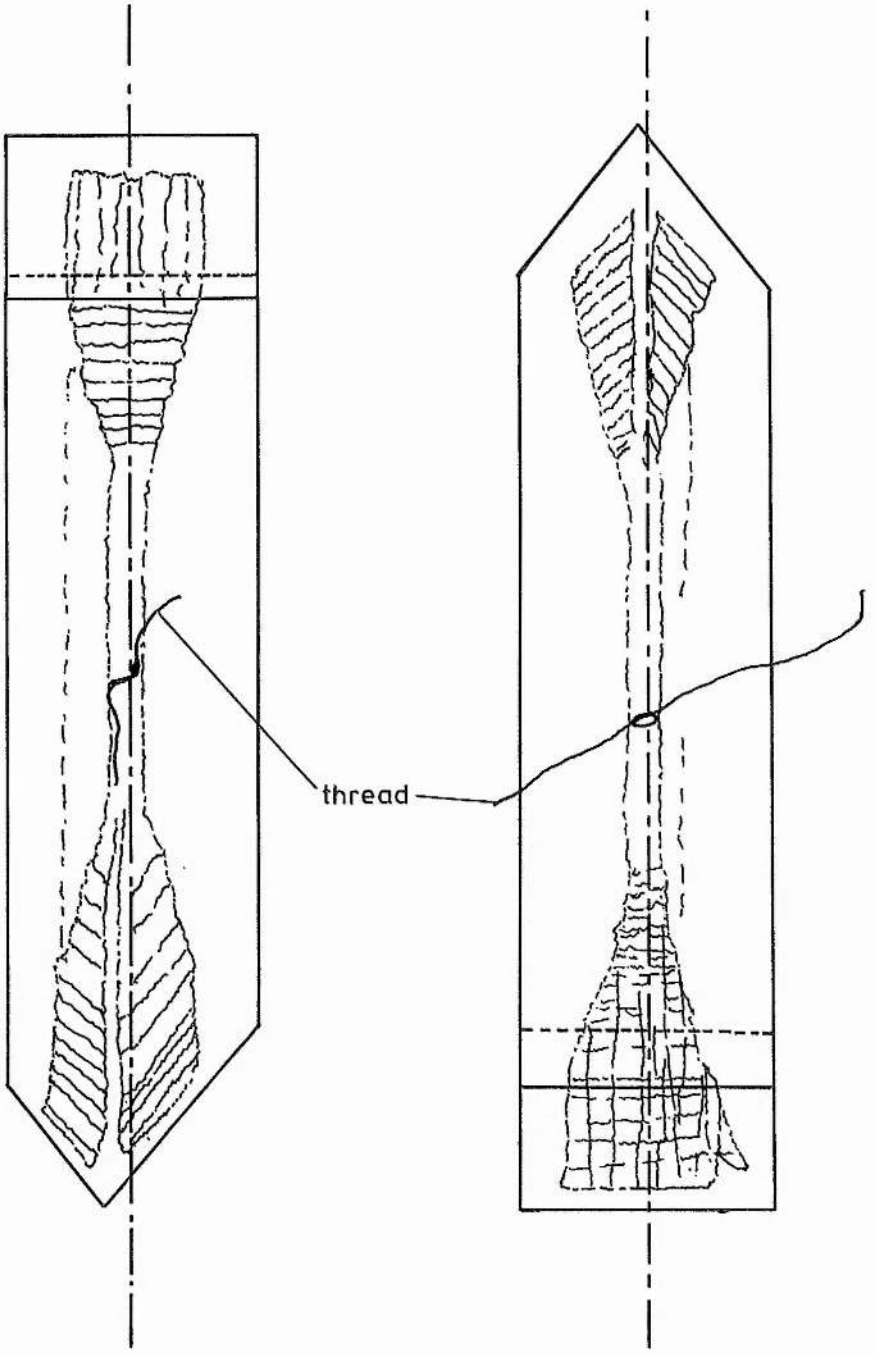

scale : actual size x 3

Fig 6-6: Urea crystal before cutting

6-3-3 Performance of crystal plate

The crystal plate was set up between the argon laser and a UV100 photodiode. The visible beam was focused into the crystal by means of a quartz lens, and the output beams then focused on to the detector, again by a quartz lens. The detector was covered by two Schott UG5 filters and had been calibrated at 300nm. For the UV wavelengths generated (248nm to 264nm), the photodiode is about 30% less sensitive. The transmission of each of the UG5 filters has been measured as 82% at 260nm, falling to 75% at 257nm.

UV powers were measured for generation from each of four lines from the argon laser, at 528.7nm, 514.5nm, 501.7nm and 496.5nm. The UV power emerging from the crystal (with the quartz windows in place) is then deduced by allowing for scattering and reflective losses and for absorption by the filters. The nonlinear coefficient d_{14} is then found (for zero UV absorption by the crystal) from equation 33 of Chapter 2, to be:

$$P_2 = \frac{\omega_1^2 d_{eff}^2 L P_1^2 h_{mm}}{\varepsilon_o n_1 n_2 c^3 \lambda_1}$$

Here, we have:

$d_{eff} = d_{14} \sin(2\theta_m) \cos(2\phi)$

$\phi = 0$ as the beam is in the ZX plane

$n_1 = n_e(\lambda)$

$n_2 = n_o(\lambda/2)$

$c = \omega_1 \lambda_1 / 2\pi$, the speed of light

and h_{mm} is determined for each wavelength via B and ξ as explained in Chapter 2. In fact the focusing is not

quite optimised, but the value of ξ varies only slowly with B and so the resulting error is small.

The crystal length L is about 5mm, but the aperture length l_a varies between 1.64mm and 4.43mm for the range of wavelengths concerned due to the variation of SH walkoff, [See Table 6-1].

The expression for d_{14} is then:

$$d_{14} = \sqrt{\frac{P_2 \varepsilon_o n_1 n_2 \lambda_1^3 c}{4\pi^2 L\, h_{mm}\, P_1^2 \sin^2(2\theta_m)}}$$

Values of all variable quantities, and of the coefficient d_{14} are shown in Table 6-1.

Although there is some variation in the value of d_{14}, the mean value of 0.90pm/V is near to the value reported by Halbout et al [4] and others when using single crystals, but lower than that of 7.0pm/V reported for powder measurements by Kurtz and Perry [5].

The implication of this figure is that the SHG is probably approaching its most efficient in our crystal, and this in turn implies that the crystal is of reasonable quality. Although we do not claim that all crystals grown by the methods described are likely to be this good, the results are most encouraging. Additionally, we have observed no damage to the Urea crystal by the index matching fluid, at least over a period of 8 months.

Table 6-1: UV powers and values for finding d_{14}

λ (nm)	528.7	514.5	501.7	496.5
P_1 (W)	1.9	6.8	1.3	2.2
P_2 (mW)	0.11	1.0	0.10	0.22
n_1	1.59590	1.59696	1.59800	1.59846
n_2	1.56538	1.57272	1.58018	1.58348
h_{mm}	0.28	0.36	0.46	0.61
l_a (mm)	1.64	2.25	3.46	4.43
θ_m (deg)	58.8	62.6	66.9	68.9
d_{14} (pm/V)	0.83	0.43	1.05	0.83

6-4: Future developments

Future work must concentrate upon the elimination of growth defects in large crystals. There appear to be two princpal causes of such defects, temperature instability and solvent impurity. The latter problem has largely been eliminated by not stirring the growing solution, allowing solid impurities to settle after a few days, during which time the growth is small. The temperature stability, however, is a more complex problem. The stability required is clearly better than $\pm$0.001K, or about 3×10^{-3} %. For the total volume of water concerned, with a thermal capacity of about 200 000J/K, this represents a limit on the power loss (or gain) of about 6W. Consideration of the total area of the tank (0.8m^2), the typical conductivity of foam polystyrene (0.035W/m/K) and taking the temperature difference between the tank and room as 10°C, we find that this heat loss is achieved with about 5cm of insulation on all sides. As these figures refer to the present stability of 0.001K, any improvement must involve either a smaller temperature differential or thicker insulation. There is little to be gained by using an alternative insulation material, as the conductivity of expanded polystyrene is as small as available from other materials [6].

Significantly thicker insulation, by perhaps a factor of five, would render the apparatus rather too large and almost impossible to control in terms of monitoring the progress of the crystal growth, which at present requires that apertures are left in the insulation for observation. Such apertures must inevitably increase the heat loss by

both convection and conduction. Elimination of this problem could be achieved by use of a small periscope system or fibre optics, though both would require use outside the water bath to avoid problems with algae deposition on optical surfaces.

To some extent, the reduction of temperature differential between tank and room has already been partially addressed, by housing the growing system in a screened area at a higher temperature than the main room and thermostatically air conditioned. Problems still arise, however when entering or leaving the area. A doubly screened area would improve matters, but effectively complete elimination of the problem will probably be impossible. Taking reasonable further steps to improve losses, however, an order of magnitude improvement in temperature stability could probably be achieved.

Finally there remains the randomness of the crystal growth itself, which cannot be altered, is ultimately consequential upon the thermal motions of the solvent molecules and will set a limit on the uniformity of the final product.

REF1

REFERENCES CHAPTER 6

1 "Crystal Growth", ed. Pamplin B, Pergamon Press, London, 1979; Chapter 10

2 Hyndman D; PhD thesis, Univ St Andrews (1955)

3 Work thus referenced is by Mr. Ackerboom

4 Halbout J-M, Blit S, Donaldson W, Tang CL; IEEE J Quant Electr QE-15 1176-9 (1979)

5 Kurtz SK, Perry TT; J Appl Phys 39 3798 (1968)

6 Kaye GWC, Laby TH; "Tables of Physical and Chemical Constants", 14th Edition, Longman (1973)